STRESS AND STRAIN IN A SHALLOW ELASTIC CALOTTE SHELL

STRESS AND STRAIN IN A SHALLOW ELASTIC CALOTTE SHELL

by

GLENN RILEY, B.ENG.

A Thesis

Submitted to the Faculty of Graduate Studies

in Partial Fulfilment of the Requirements

for the Degree

Master of Engineering

McMaster University

September 1964

MASTER OF ENGINEERING (1964) McMASTER UNIVERSITY
(Civil Engineering) Hamilton, Ontario.

TITLE: Stress and Strain in a Shallow Elastic Calotte Shell

AUTHOR: Glenn Riley, B.Eng. (McMaster University)

SUPERVISOR: Professor G. Æ. Oravas

NUMBER OF PAGES: viii, 118

SCOPE AND CONTENTS:

This thesis describes the experimental and theoretical analysis of a shallow spherical calotte shell of hexagonal plan. Installation of strain gauges in the circumferential and radial directions enabled the measurement of the direct and flexural strains, from which the corresponding stress resultants and stress couples could be evaluated. In the theoretical analysis, an approximate solution utilizing the collocation procedure for satisfaction of boundary conditions is used.

ACKNOWLEDGEMENTS

The writer wishes to express sincere gratitude to his research supervisor, Dr. G. Æ. Oravas, for his invaluable guidance in the experimental and theoretical analysis. His indebtedness to Professor J. N. Siddall for his assistance in the execution of this investigation is acknowledged.

Sincere thanks are also due to the National Research Council of Canada, whose award made it possible for the author to carry out this study.

TABLE OF CONTENTS

NOMENCLATURE

A_1, A_2	Fundamental Magnitudes of first order for middle surface of shell or LAMÉ coefficients.
$ber_n(x), bei_n(x), ker_n(x), kei_n(x)$	KELVIN Functions of argument x
ds_i	Infinitesimal line segment along parametric co-ordinate α_i
D	Flexural rigidity of shell
E	Modulus of elasticity
$\bar{e}_s$	Unit vector in the surface of shell tangent to shell's boundary
$\bar{e}_r, \bar{e}_\theta, \bar{e}_n$	Unit base vectors to middle surface of shell
$F_{rr}(\sigma), F_{\theta\theta}(\sigma)$	Components of direct middle surface stress resultants
$F_{r\theta}(\sigma), F_{\theta r}(\sigma)$	Components of shear stress resultants in middle surface
$F_{rn}(\sigma), F_{\theta n}(\sigma)$	Transverse shear stress resultant components
$\bar{F}_1(\sigma), \bar{F}_2(\sigma)$	Stress resultants per unit length of parametric lines in middle surface
h	Shell thickness
$i = \sqrt{-1}$	Imaginary unit
$\bar{\bar{1}} = \bar{e}_i \bar{e}_i$	Idemfactor or Identity Tensor
$I_n(x)$	Modified BESSEL Function of First Kind
$J_n(x)$	BESSEL Function of First Kind
$K_n(x)$	Modified BESSEL Function of Second Kind
$M_{r\theta}(\sigma), M_{\theta r}(\sigma)$	Components of flexural stress couples
$M_{rr}(\sigma), M_{\theta\theta}(\sigma)$	Components of torsional stress couples
$\bar{M}_1(\sigma), \bar{M}_2(\sigma)$	Stress Couples per unit length of parametric lines in middle surface

$\overline{\overline{M}}(\sigma)$	Moment tensor
$\bar{n}$	Unit vector in the surface of shell normal to shell's boundary
p_n	Loading intensity normal to middle surface of shell
$\bar{p}$	Load intensity per unit area of middle surface
r	Radial parametric co-ordinate of shell
$\bar{r} = \bar{r}_o + \bar{\rho}$	Radius vector to arbitrary point in shell
$\bar{r}_o$	Radius vector to middle surface of shell
$\bar{\rho} = \bar{r} - \bar{r}_o$	Radius vector of arbitrary point in shell relative to middle surface
R	Radius of middle surface of spherical shell
u_n	Normal Displacement Function
$V = V_o + V_1 + V_2$	Complex solution of two fundamental differential equations
α_n	Parametric co-ordinate normal to middle surface
α_1, α_2	Parametric co-ordinates in the middle surface
$\delta\kappa_1^{(t)}, \delta\kappa_2^{(t)}$	Variations in torsion of middle surface about parametric co-ordinate lines α_1, α_2
$\delta\kappa_r, \delta\kappa_\theta$	Kinematic curvature variation of the surface about co-ordinate lines r, θ
$\epsilon_{rr}^{(d)}, \epsilon_{\theta\theta}^{(d)}$	Direct middle surface strains
$\epsilon^{(f)}\left(\frac{h}{2}\right), \epsilon_{\theta\theta}^{(f)}\left(\frac{h}{2}\right)$	Flexural strains in the upper surface of shell
ϵ_{ss}	Middle surface strain parallel to shell's boundary
$\overline{\overline{\epsilon}} = \bar{e}_i \bar{\epsilon}_j = \epsilon_{ij} \bar{e}_i \bar{e}_j$	Strain Tensor
$\epsilon_I = \overline{\overline{\epsilon}} : \overline{\overline{1}}$	First Scalar Strain Invariant
$K_2^{(n)}, K_1^{(n)}$	Normal kinematic curvatures of parametric co-ordinate lines defined by α_1, α_2 in the primitive configuration of shell's middle surface
$\hat{\lambda}, \hat{\mu}$	CAUCHY-LAMÉ Elastic Constants

ν	POISSON's Ratio
$\sigma_{rr}^{(f)}(+\frac{h}{2}), \sigma_{\theta\theta}^{(f)}(+\frac{h}{2})$	Flexural stresses in the upper surface of shell
$\sigma_{rr}^{(d)}, \sigma_{\theta\theta}^{(d)}$	Direct stresses acting in middle surface of shell
$\sigma_{rr}(\pm\frac{h}{2}), \sigma_{\theta\theta}(\pm\frac{h}{2})$	Composite or total stresses in the external surfaces of shell
$\overline{\overline{\sigma}} = \overline{e}_i \sigma_i = \sigma_{ij} \overline{e}_i \overline{e}_j$	Stress Tensor
$\sigma_I = \overline{\overline{\sigma}} : \overline{\overline{1}}$	First Scalar Stress Invariant
$\underline{\Phi}$	VLASOV's Force Function
$\nabla^2 \equiv \frac{d}{d\overline{r}_o} \cdot \frac{d}{d\overline{r}_o}$	EULER-LAPLACE Operator

DIRECT TENSOR ALGEBRA

A Tensor of the second order is defined by

$$\bar{T} = T_{ij}\bar{e}_i\bar{e}_j$$

where $\bar{e}_\kappa$ denotes the rectangular unit base vectors, and

$$T_{ij}$$

designates the rectangular components of the tensor. The direct, or dot product of a Tensor $\bar{\bar{T}}$ and a vector $\bar{v}$ is defined by

$$\bar{\bar{T}}\cdot\bar{v} = T_{ij}\,\bar{e}_i(\bar{e}_j\cdot\bar{v})$$

The Double Direct Product, or double dot product between two tensors of the second order $\bar{\bar{T}}$ and $\bar{\bar{D}}$ is defined by

$$\bar{\bar{T}}:\bar{\bar{D}} = (T_{ij}\bar{e}_i\bar{e}_j):(D_{\kappa l}\bar{e}_\kappa\bar{e}_l) = T_{ij}D_{\kappa l}(\bar{e}_i\cdot\bar{e}_\kappa)(\bar{e}_j\cdot\bar{e}_l)$$

$$= T_{ij}D_{\kappa l}\delta_{i\kappa}\delta_{jl}$$

$$= T_{ij}D_{ij}$$

where δ_{rs} denotes KRONECKER Delta. For further references see WEATHERBURN in 1924.

CHAPTER I

INTRODUCTION

Many stress analyses of segmental shells, such as those by DISCHINGER in 1935*, PUCHER in 1939 and CSONKA in 1955 have been carried out by means of analytical methods which disregard the transverse flexural stiffness of the shell. The present study was undertaken for the purpose of carrying out an experimental and analytical investigation of a thin shallow calotte shell over hexagonal base.

The aluminum shell of spherical middle surface was supported on members forming a hexagonal boundary which was free to expand in its own plane under applied forces. The external impressed loading represented a rotationally symmetric normal pressure applied to the upper surface of the shell. Extensive strain gauge measurements were carried out in order to evaluate the direct and flexural stress resultants at various locations on the shell surface. The effect of transverse flexure of the shell constituted the central feature of the investigation, since the stress couple determines, to a certain extent, the critical phase of the stress distribution.

Simultaneously, an analytical study of this type of shell was carried out by means of an approximate solution developed for thin segmental shells of spherical middle surface (ORAVAS in 1957). This solution is obtained from the system of fundamental differential equations formulated for shallow shells by DONNELL in 1933, MUSHTARI in 1938, MARGUERRE in 1939, and VLASOV in 1949. The particular

*References are given chronologically in the BIBLIOGRAPHY.

truncated series form of the solution is dictated by the geometric configuration of the shell boundary which does not exhibit rotational symmetry, but rather rotational periodicity. Since the boundary of the shell does not coincide with the cylindrical co-ordinate system used in the solution of the otherwise rotationally symmetric field problem, TÖLKE'S Boundary Collocation Method was employed which satisfies the imposed boundary conditions at discrete points on the boundary rather than along its entire length that is the true condition of the support (TÖLKE in 1934). This type of finite degrees of freedom solution of TÖLKE for a closed spherical shell at the apex requires a knowledge of Kelvin Functions $ber_n(x)$, $bei_n(x)$ and their derivatives for large integral orders (n) which describe the effect of the outer boundary of the shell upon the interior of the shell surface. A literature survey revealed that tabulated values for integer orders (n) greater than ten were not available (see tables by YOUNG in 1964). Therefore it was necessary to calculate the higher order KELVIN Functions using the BACKWARD RECURRENCE TECHNIQUE. The basic solution to the problem, as well as the functional calculations, were made utilizing the I.B.M. 7040 computer at McMaster University. This investigation was initiated in 1958, but it was carried to its conclusion only in 1963/64 due to the lack of suitable computer facilities.

In both the experimental and the analytical procedure, the distribution of direct stress resultants and flexural stress resultants or stress couples along the radial distance from the shell apex are graphically depicted, thus facilitating the visualization of the influence of this type of boundary disturbance upon the interior of the shell.

CHAPTER II

PHYSICAL ASSEMBLY AND TESTING PROCEDURE

II - 1 Construction of the Shell Structure

The main structure used in this experimental test was a segmental shell resting on edge beams forming a hexagonal boundary in the base plane. Such a segmental shell of double curvature represents a calotte shell. The middle surface of this calotte shell is of spherical configuration with a maximum ratio of rise to base diameter of 1/8.6 .

The shell was formed from 3/8" plate aluminum alloy 65S-T4 using a pressing process at the TORONTO IRON WORKS LTD. It was machined to a hexagonal plan shape at the McMaster University Engineering Machine Shop and then sent to AVRO AIRCRAFT LTD. to have the 2" x 6" edge beams shown in Figure 3 metal bonded to the shell. Each beam was bolted to steel supports which rested on rollers to permit freedom of lateral movement. The edge beams were not continuous since a small slit was provided at each corner of the hexagonal boundary in order to further facilitate movement of the boundary member.

The base structure consisted of three main component parts. The base ring, on which the edge beam rollers rested, was made of 1/2" steel plate and rested on six equidistant vertical legs of circular cross-section. The support ring, raised from the base ring by eighteen tie rods and flush with the outer edge of the shell, was machined to

hexagonal inner shape to allow a 1/8" gap between the shell and the ring in order to permit the shell to expand under load. The pressure head was formed from 1/8" steel plate by a spinning process and bolted in 96 locations to the support ring. A rubber diaphragm was placed over the aluminum shell before the pressure head was bolted in place. The cell space between the pressure head and the rubber diaphragm was partially filled with water to cover the shell and subsequently air pressure was applied to this cell. Figure 1, Figure 2, and Figure 7 illustrate the physical layout of the experiment.

II - 2 Strain Gauge Installation

Though the applied load was rotationally symmetric in character, the hexagonal boundary, which is rotationally periodic, brings about a certain degree of unsymmetry. The strain gauges were located in two sectors of the shell, in such a manner that at each station both the meridianal and circumferential strains could be recorded. In addition, the strain gauges were located on the upper and lower surfaces of the shell along its surface normal; this permitted the evaluation of the direct and flexural strains for various loads at each of the 84 locations in the shell shown in Figure 4. Careful installation of the strain gauges in the vicinity of the slit corner was necessary to investigate flexure in this region. Figure 5 and Figure 6 illustrate the installation of strain gauges on the surface of the shell.

Tatnall strain gauges C12-121 with a gauge factor 2.09 and with temperature compensation for aluminum were located on the shell. In total, 168 gauges were used, of which 84 were located on the upper

surface and 84 on the lower surface of the shell. Some difficulties were encountered in mounting the gauges near the slit corner of the shell, but the small gauge length of 1/4" permitted 5 gauges to be placed side by side. A detail of the corner layout of strain gauges is shown in Figure 8. The connections from the strain gauges to the external installation were made using polystrip cable containing twelve conductors side by side. These cables can be seen in Figure 5. The strain measuring assembly is shown in Figure 9 and depicts the switching unit through which the 168 gauges were connected. One of the difficulties in the operation of this unit was the corrosion of the switch contacts, which had to be silver plated in order to render consistency to the strain readings. The strains were measured using the half-bridge of the digital strain indicator (D. S. I.) with a temperature compensating gauge on 65S-T4 alloy. The strain readings were printed out on tape with a "Victormatic" print-out recorder. Using this layout, both the zero strain readings and the strain readings at various pressures were measured, as a null balancing apparatus was not available.

II - 3 Pressure Measuring Instrumentation

The applied load was measured using a MARTIN-DECKER precision test gauge with a range of 0 to 60 p.s.i., an accuracy of ± 0.15% of full scale and a sensitivity of 0.1% (see Figure 2). The seal between the pressure head and the support ring was such that only 35 p.s.i. pressure could be maintained without the leakage of water between the bolted connections. It was felt that 0-30 p.s.i. was an appropriate range of pressures to maintain linear strains throughout the shell.

II - 4 Deflection Measurements

In order to record the boundary movement of the shell under load, dial gauges of 0.001" scale division were located at each of the six boundary edges to measure the horizontal movement. This arrangement also provided an important check for the symmetry condition of the deformation of the shell.

In addition to the strain gauges, dial gauges were located as near as possible to each strain station on the radial line extending from corner to corner to record the vertical displacement of the shell. It was only possible to place the displacement indicators within 11 in. of the boundary due to the lack of space in the vicinity of the shell edge. However, a satisfactory displacement pattern could be obtained with the 5 gauges used.

II - 5 Experimental Procedure

In order to check the consistency of D.S.I. readings, several preliminary test runs were made at various pressures. Each run consisted of printing out a set of strain readings at zero load, of loading the shell to prescribed pressure and then printing out the final strain readings. The difference in strain readings represents the strain in micro-inches per inch at the prescribed pressure. In addition, another record of zero readings was taken upon unloading in order to check the drift in the indicator. It was found that certain adjustments were necessary in the D. S. I.; moreover, switch contacts had to be cleaned to yield reliable results. These preliminary runs indicated that a precision of $\pm$ one unit of strain could be achieved. Since a scale factor of four was used throughout, the precision in any strain reading

became ± four micro-inches per inch. The total time elapsed to complete a set of readings for each pressure was approximately thirty minutes. The increment of loading used in the sequence of tests was 5 p.s.i. Zero readings were initially taken with the shell unloaded, and then readings were taken in 5 p.s.i. increments from 5 p.s.i. to 30 p.s.i.

Contemporaneously, horizontal boundary movements were measured for each pressure increment using dial gauges fastened to the base ring. The dial gauges were located approximately in the middle of each of the edges and were recorded to the nearest thousandth of an inch. These measurements gave another check on the degree of symmetry of deformation that prevailed in the shell.

Also a series of more precise gauges of 0.0005" scale division were located on the lower surface of the shell, as close as physically possible to the strain gauges, in order to measure the vertical displacement of shell under load. These dial gauges were situated at the strain gauges along the radial corner to corner line, but only 5 gauges closest to the apex could be utilized because of the space requirements. Again displacement readings were recorded for each pressure from 5 p.s.i. to 30 p.s.i.

A series of tests were made to evaluate the agreement existing between experimentally observed boundary conditions and the theoretical boundary conditions in the form of zero edge rotations. Two dial gauges of 0.0005" scale division measuring horizontal displacements were located vertically above one another at a distance of 3.75" and attached by "C" clamps to the base ring. This permitted evaluation of any boundary rotation in radians by computing the difference between the readings of the two

gauges positioned above one another and dividing it by the vertical gauge length (3.75"). These tests were carried out at each terminus of the six boundary members in order to check the uniformity of rotation along the edges of the shell. Each of these measurements was carried out for the entire range of test pressures.

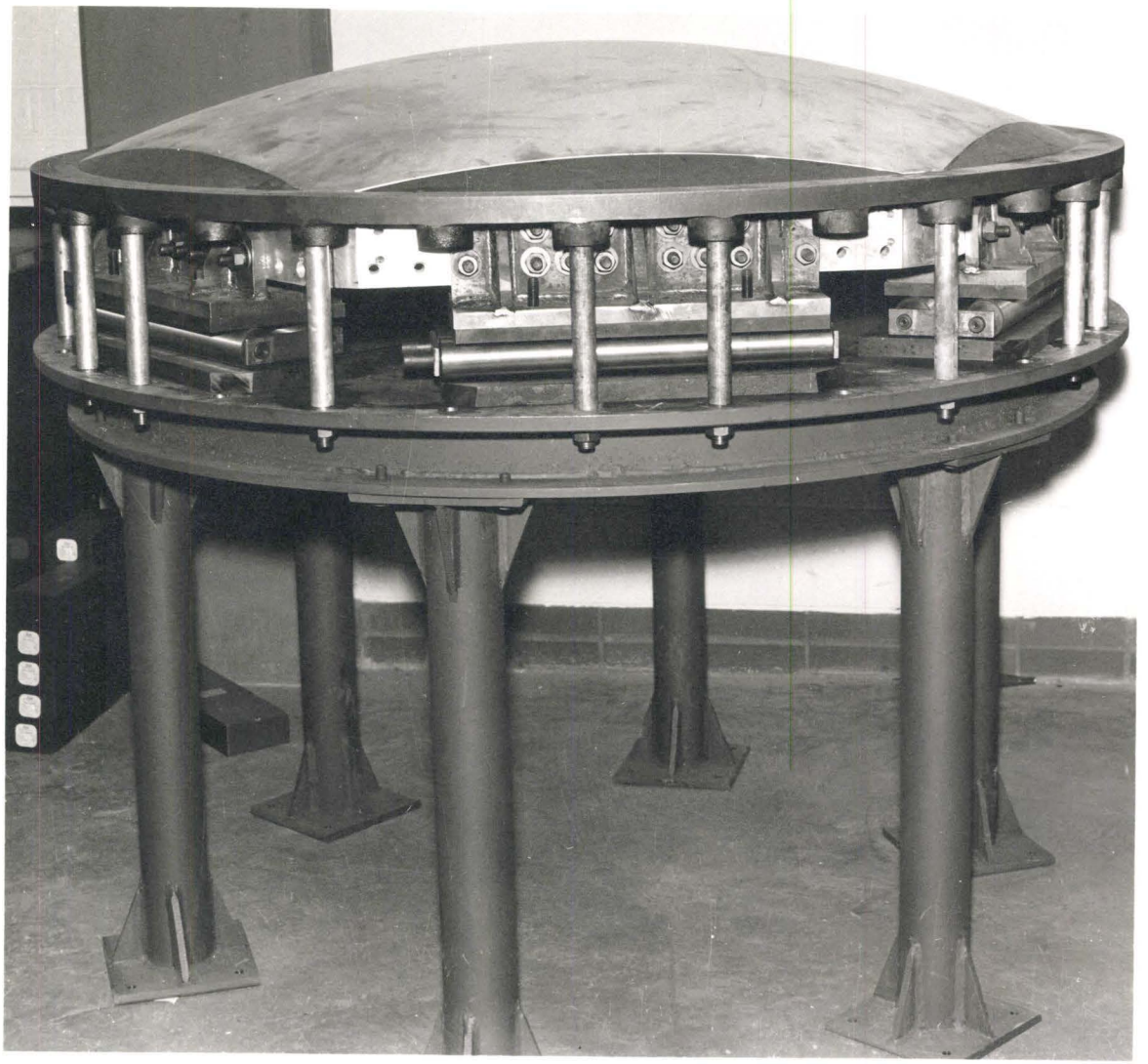

SHELL ASSEMBLY BEFORE STRAIN

GAUGING AND PRESSURE HEAD ATTACHEMENT

FIGURE 1

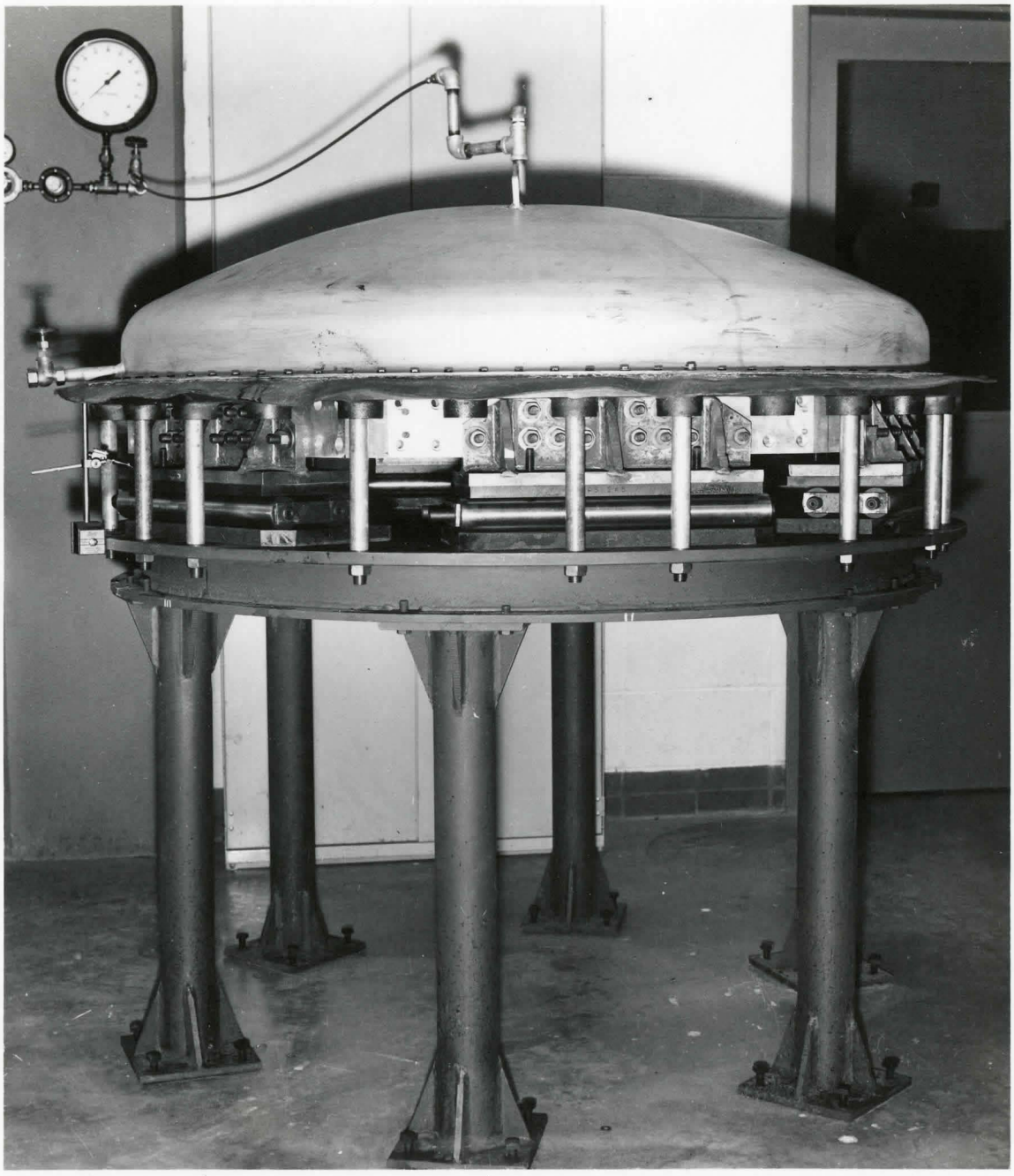

SHELL ASSEMBLY WITH PRESSURE HEAD

AND MEASURING GAUGE IN PLACE

FIGURE 2

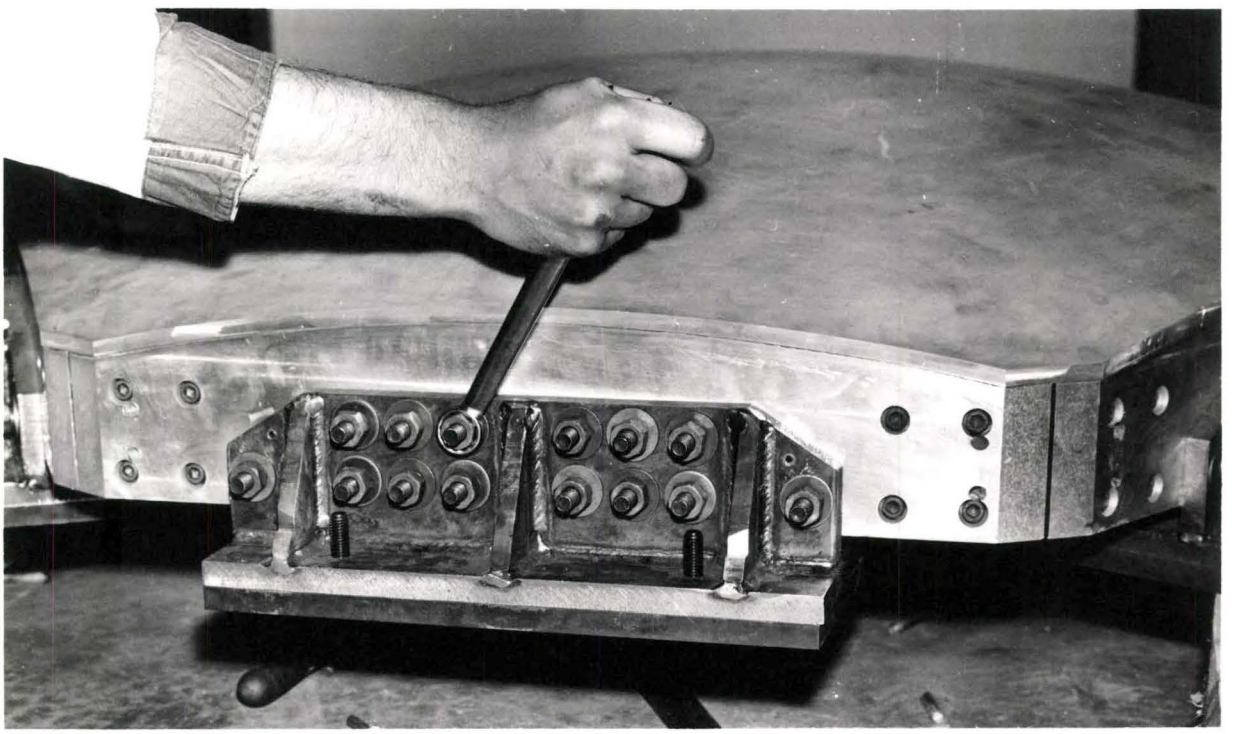

DETAIL OF BOUNDARY MEMBER, SLIT CORNER,

AND EDGE SUPPORT

FIGURE 3

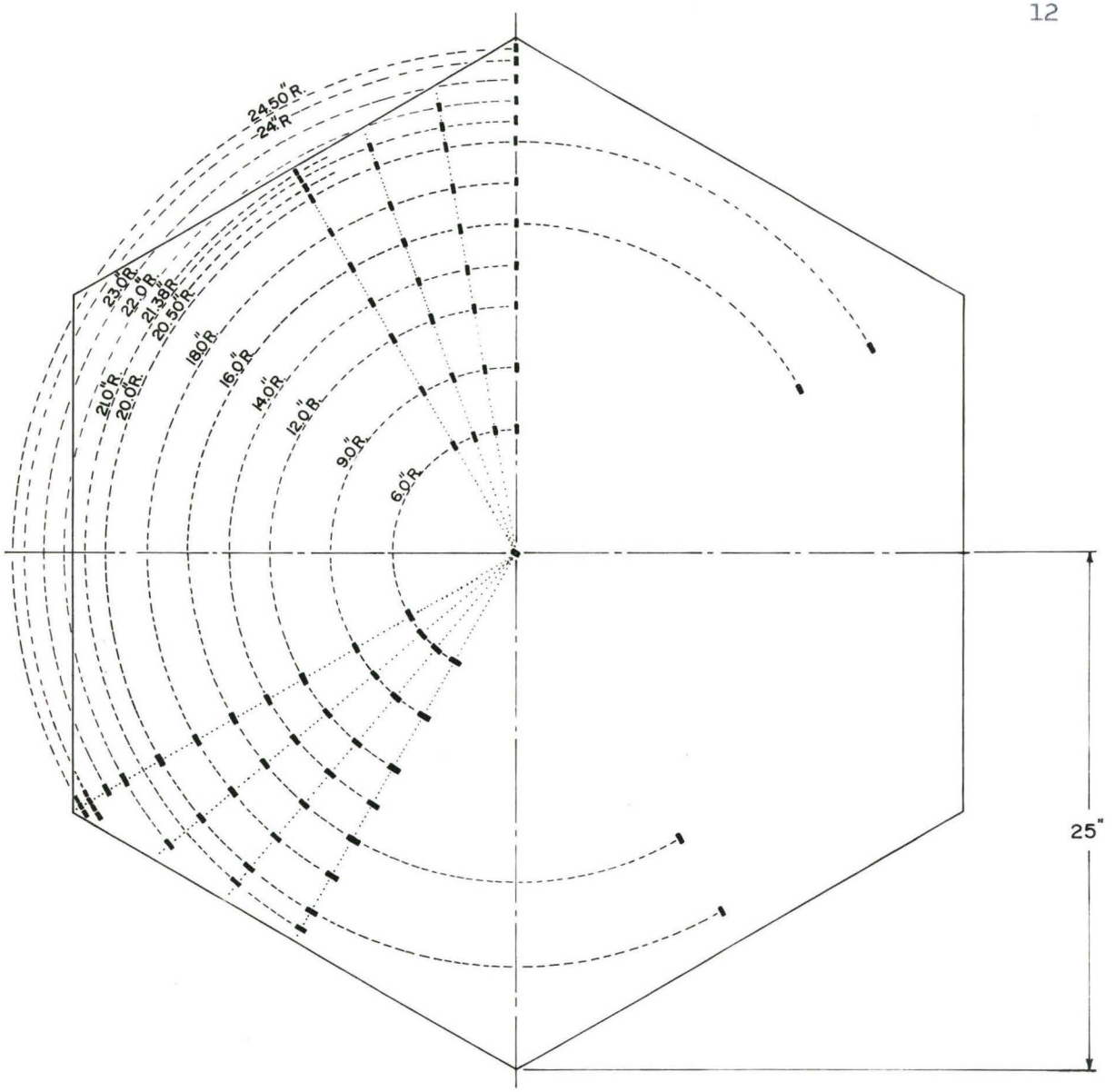

NOTES

1. All Dimensions Shown Are Horizontal.
2. Radial Distances Refer to Middle Surface. Corrections Were Applied to Locate Strain Gauges.
3. Strain Gauge Type - TATNALL C 12 121 for Aluminum, Gauge Factor 2.09

LOCATION OF STRAIN GAUGE STATIONS ON SHELL

Figure 4

SHELL ASSEMBLY AFTER STRAIN GAUGING AND BEFORE PRESSURE HEAD ATTACHEMENT

FIGURE 5

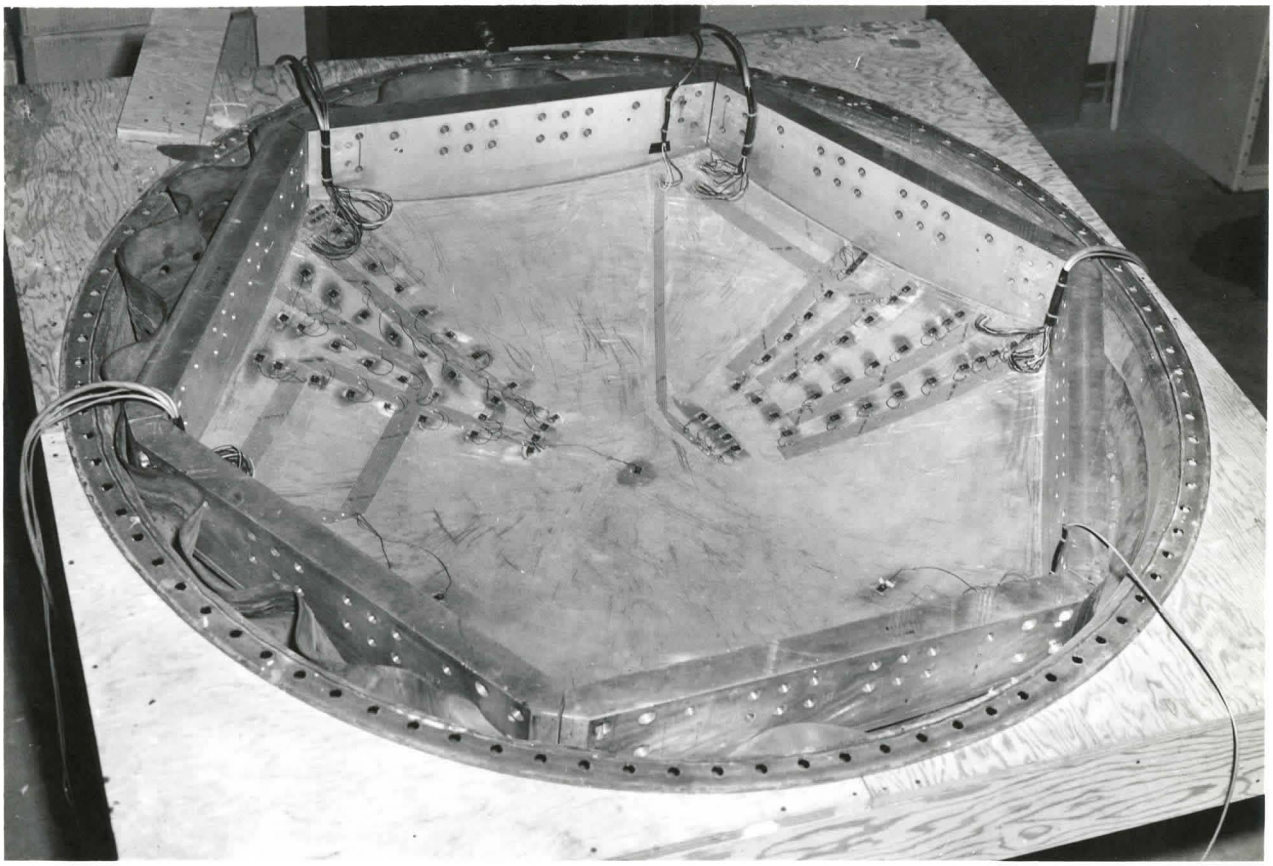

LOWER SURFACE OF SHELL SHOWING

RADIAL AND CIRCUMFERENTIAL STRAIN GAUGES

FIGURE 6

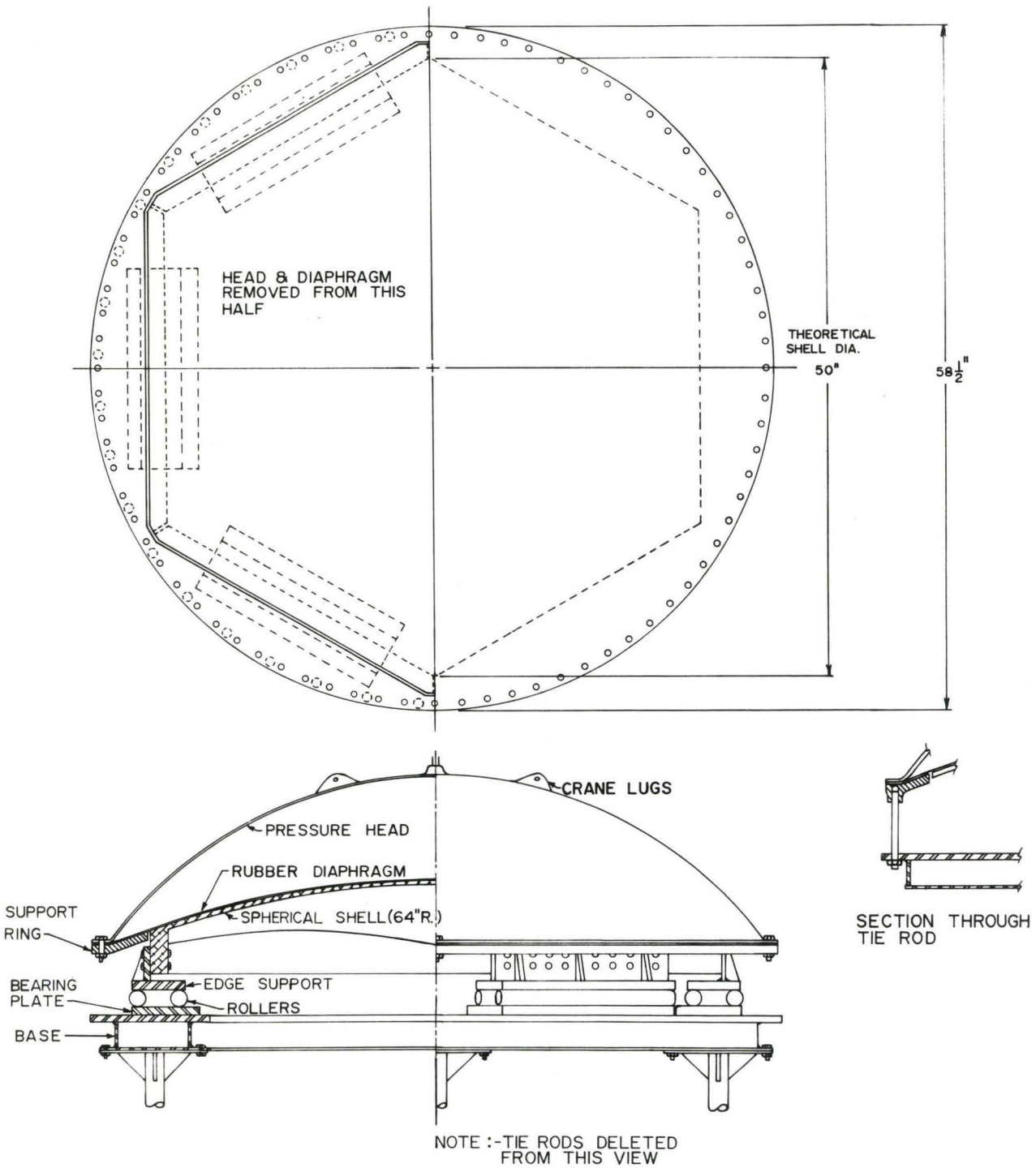

SHELL TEST ASSEMBLY

Figure 7

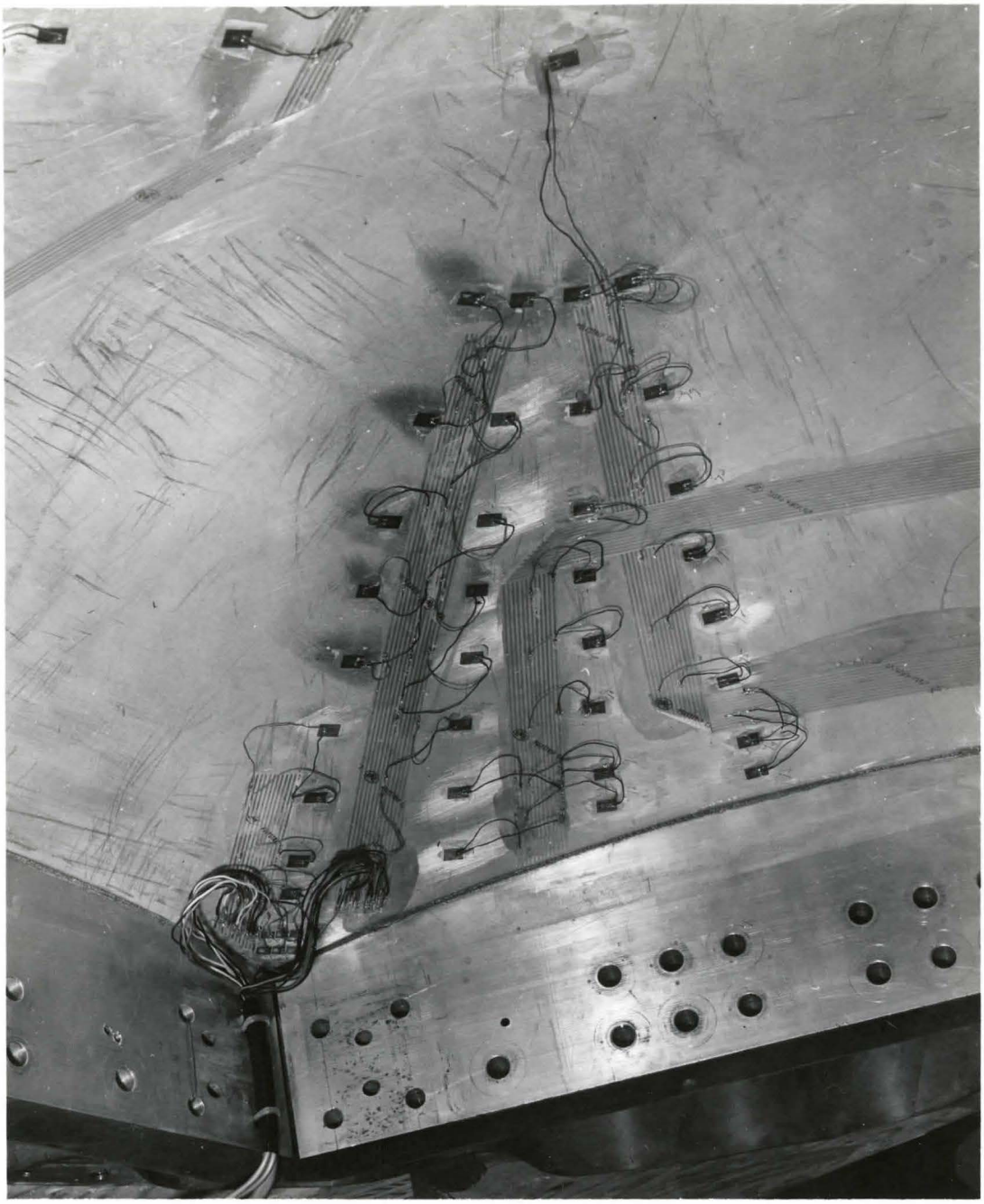

DETAIL OF SLIT CORNER SHOWING

CIRCUMFERENTIAL STRAIN GAUGES

FIGURE 8

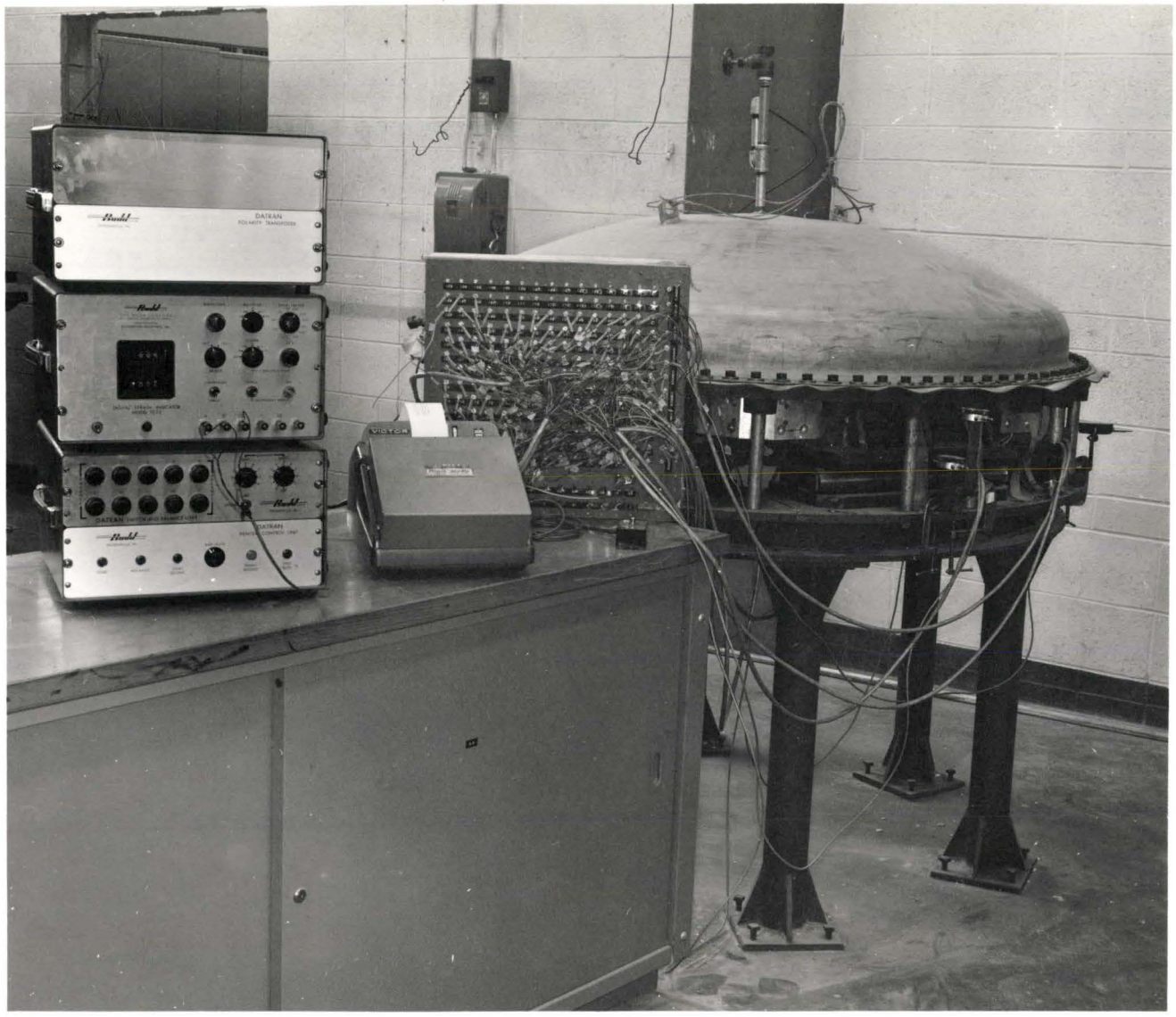

SHELL ASSEMBLY WITH DIGITAL STRAIN INDICATOR, PRINT-OUT RECORDER, AND SWITCHING UNIT

FIGURE 9

CHAPTER III

ANALYSIS OF EXPERIMENTAL RESULTS

III - 1 Resolution of the State of Strain

The measured strains were resolved into direct and flexural strains. In all strain expressions, the strain was assumed to be positive, or tensile. In the derivation of the flexural stress resultants, or stress couples, the strain in the top surface was assumed to be larger than the strain in the bottom surface. The strain was assumed to be a linear function of the thickness of the shell. Figure 10a and Figure 10b depict the resolution of the state of strain of the infinitesimal free body into its direct and flexural components.

III - 2 Direct Stress Resultants for Thin Shallow Shells

Figures 11a, b show the free body diagram with its impressed direct stress resultants, stress couples and applied load. It should be noted that the expressions for the direct stress resultants agree with those of other authors, while the expressions for the flexural stress couples differ from those of other authors. The reason for the latter discrepancy lies in the fact that direct kinematical methods are not used by other writers for stress couples and curvatures. The resolved direct strains $\epsilon_{rr}^{(d)}, \epsilon_{\theta\theta}^{(d)}$ at each station and at each pressure were used to evaluate the direct stress resultants shown in Figures (12 to 19), Figure 28, and Figure 29. Figure 11c shows

the lines where the strains were measured. These figures indicate the distribution of direct stress resultants for varying pressures along the horizontal distance r measured from the shell apex. The expressions used to calculate the stress resultants are easily derived from the tensorial stress-strain relations as follows:

The Hookean Stress-Strain Relation is given in its direct tensorial form

$$\bar{\bar{\sigma}} = 2\hat{\mu}\bar{\bar{\epsilon}} + \hat{\lambda}(\bar{\bar{\epsilon}}:\bar{\bar{I}})\bar{\bar{I}} = 2\hat{\mu}\bar{\bar{\epsilon}} + \hat{\lambda}\epsilon_1\bar{\bar{I}}$$

where

$$\hat{\mu} = \frac{E}{2(1+\nu)}$$

$$\hat{\lambda} = \frac{2\hat{\mu}\nu}{1-2\nu}$$

designate CAUCHY-LAMÉ elastic constants, the strain tensor of the middle surface

$$\bar{\bar{\epsilon}} = \epsilon^{(d)}_{ij}\bar{e}_i\bar{e}_j = \begin{bmatrix} \epsilon^{(d)}_{rr}\bar{e}_r\bar{e}_r + \epsilon^{(d)}_{r\theta}\bar{e}_r\bar{e}_\theta + 0\,\bar{e}_r\bar{e}_n \\ + \epsilon^{(d)}_{\theta r}\bar{e}_\theta\bar{e}_r + \epsilon^{(d)}_{\theta\theta}\bar{e}_\theta\bar{e}_\theta + 0\,\bar{e}_\theta\bar{e}_n \\ + 0\,\bar{e}_n\bar{e}_r + 0\,\bar{e}_n\bar{e}_h + \epsilon^{(d)}_{nn}\bar{e}_n\bar{e}_n \end{bmatrix}$$

Imposing

$$\sigma_{nn} = \bar{e}_n\bar{e}_h : \bar{\bar{\sigma}} = 0$$

from the plane stress condition in the stress-strain relation yields

$$\epsilon_{nn} = \bar{e}_n\bar{e}_n : \bar{\bar{\epsilon}}$$

$$= \frac{-\nu}{1-2\nu}\left[\epsilon^{(d)}_{rr} + \epsilon^{(d)}_{\theta\theta}\right]$$

By definition

$$F_{rr}(\sigma) = \int_{-h/2}^{+h/2} \bar{e}_r\bar{e}_r : \bar{\bar{\sigma}}\, d\alpha_n = \int_{-h/2}^{h/2} \sigma_{rr}\, d\alpha_n$$

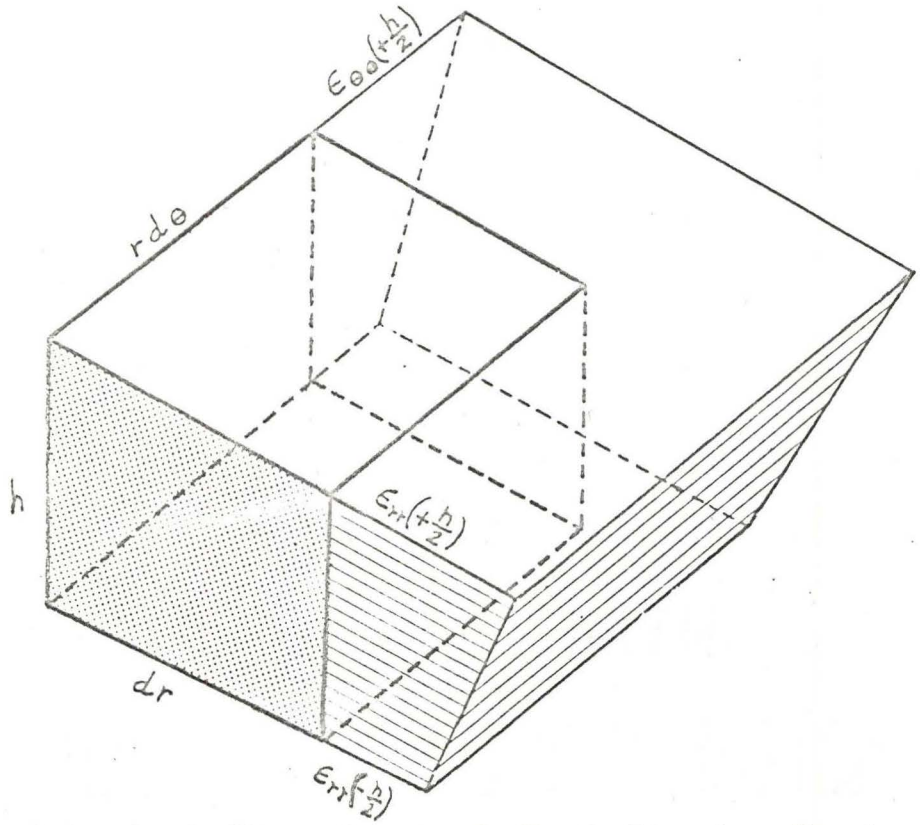

(a) Infinitesimal Free Body of Shell Showing Strain on Element

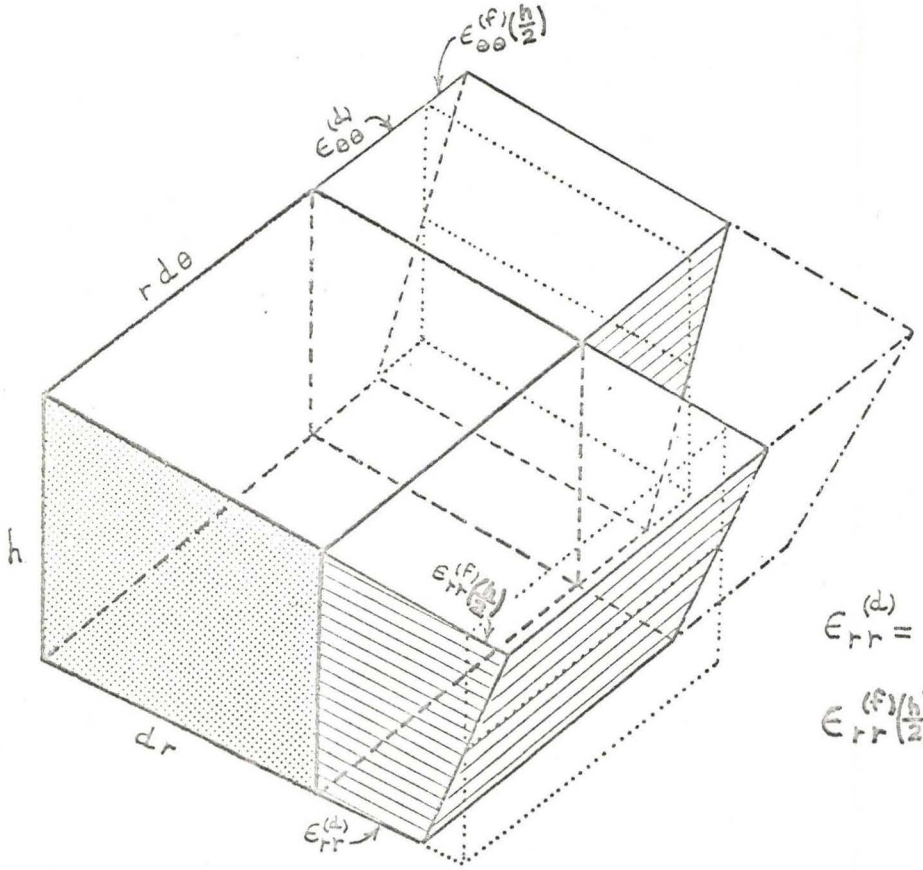

$$\epsilon_{rr}^{(d)} = \frac{\epsilon_{rr}(+\frac{h}{2}) + \epsilon_{rr}(-\frac{h}{2})}{2}$$

$$\epsilon_{rr}^{(f)}(\tfrac{h}{2}) = \epsilon_{rr}(+\tfrac{h}{2}) - \epsilon_{rr}^{(d)}$$

(b) Infinitesimal Free Body of Shell Showing Resolution into Direct and Flexural Strains

FIGURE 10(a,b)

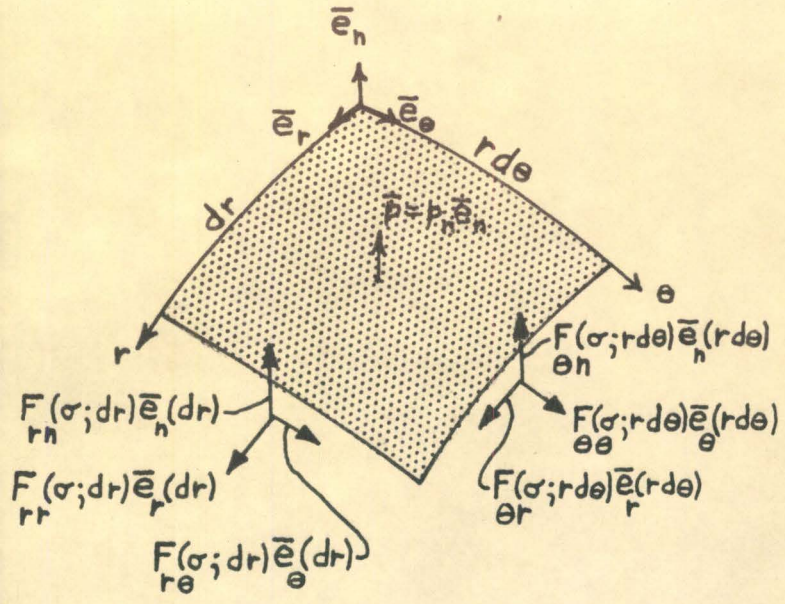

(a) DIFFERENTIAL SHELL ELEMENT SHOWING DIRECT STRESS RESULTANTS AND APPLIED LOAD

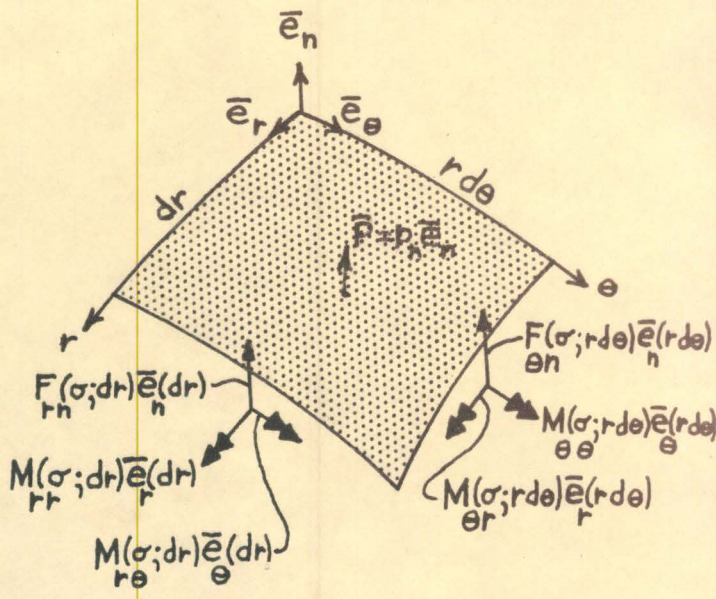

(b) DIFFERENTIAL SHELL ELEMENT SHOWING FLEXURAL STRESS RESULTANTS AND APPLIED LOAD

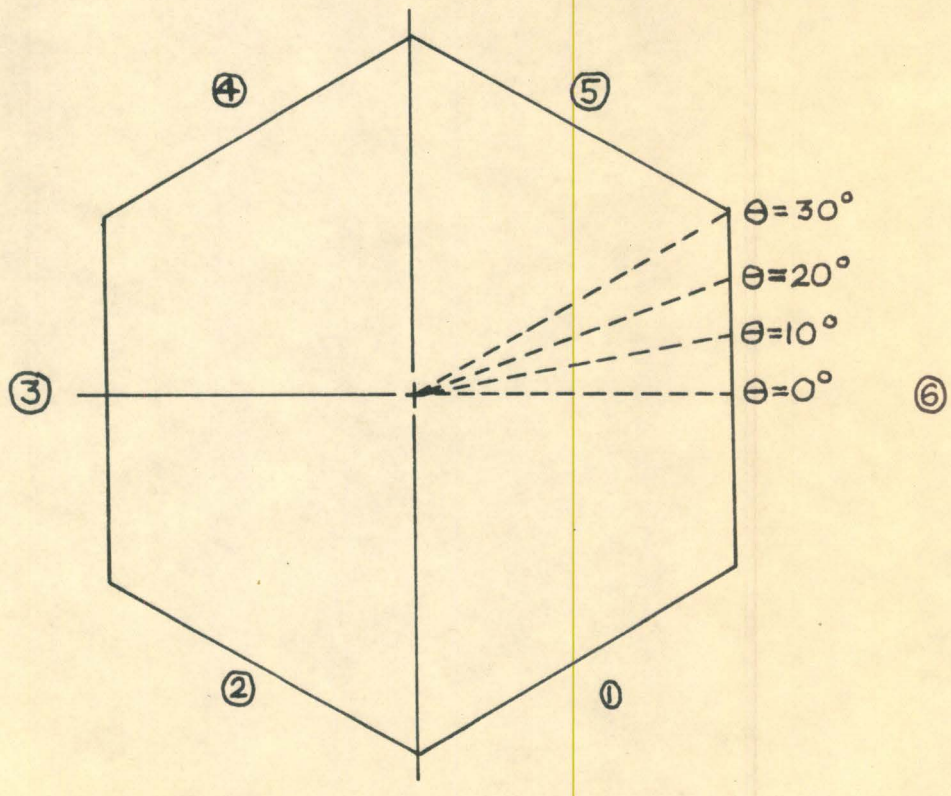

(c) PLAN OF SHELL SHOWING NUMBERING OF EDGES AND LOCATION OF STRAIN LINES

FIGURE 11

Substitution of the stress-strain relation delivers

$$F_{rr}(\sigma) = \int_{-h/2}^{+h/2} \bar{e}_r \bar{e}_r : \left[2\mu \bar{\bar{\epsilon}} + \lambda (\bar{\bar{\epsilon}} : \bar{\bar{I}}) \bar{\bar{I}} \right] d\alpha_n$$

$$= \int_{-h/2}^{+h/2} 2\mu \left\{ \epsilon_{rr}^{(d)} + \frac{\nu}{1-2\nu} \left[\epsilon_{rr}^{(d)} + \epsilon_{\theta\theta}^{(d)} - \frac{\nu}{1-\nu} \left(\epsilon_{rr}^{(d)} + \epsilon_{\theta\theta}^{(d)} \right) \right] \right\} d\alpha_n$$

$$= 2\mu \int_{-h/2}^{+h/2} \left[\epsilon_{rr}^{(d)} + \frac{\nu}{1-\nu} \left(\epsilon_{rr}^{(d)} + \epsilon_{\theta\theta}^{(d)} \right) \right] d\alpha_n$$

$$= \frac{E}{1-\nu^2} \left(\epsilon_{rr}^{(d)} + \nu \epsilon_{\theta\theta}^{(d)} \right) \int_{-h/2}^{+h/2} d\alpha_n$$

Finally

$$F_{rr}(\sigma) = \frac{Eh}{1-\nu^2} \left(\epsilon_{rr}^{(d)} + \nu \epsilon_{\theta\theta}^{(d)} \right)$$

since $\epsilon_{rr}^{(d)}$, $\epsilon_{\theta\theta}^{(d)}$ are postulated to be constant with respect to the thickness of the shell as shown in the graphical resolution of strain. Similarly

$$F_{\theta\theta}(\sigma) = \int_{-h/2}^{+h/2} \bar{e}_\theta \bar{e}_\theta : \bar{\bar{\sigma}} \, d\alpha_n = \frac{Eh}{1-\nu^2} \left(\epsilon_{\theta\theta}^{(d)} + \nu \epsilon_{rr}^{(d)} \right)$$

The direct strains $\epsilon_{rr}^{(d)}$, $\epsilon_{\theta\theta}^{(d)}$ were inserted in the above equations to yield the stress resultants at most of the strain recording stations shown in Figure 4. A value of $\frac{Eh}{1-\nu^2} = 4.21 \times 10^6$ was used corresponding to the properties of aluminum alloy 65S - T4 of E = 10 x 10^6 and Poisson's Ratio ν = 1/3.

III - 3 Flexural Stress Resultants or Stress Couples

Referring to Figure 10, the kinematic expression for flexural stress resultant, or stress couple, can be derived. Postulating $\epsilon_{rr}(+\frac{h}{2}) > \epsilon_{rr}(-\frac{h}{2})$ which is equivalent to imposing a positive increment $d\epsilon_{rr}$ with respect to $d\alpha_n$ for the co-ordinate system shown, the kinematic changes in curvature are easily established from the kinematics of deformation

$$\delta\bar{\kappa}_\theta = \delta\kappa_\theta \bar{e}_\theta = \frac{2}{h}\epsilon^{(f)}_{rr}(\tfrac{h}{2})\bar{e}_\theta$$

$$\delta\bar{\kappa}_r = \delta\kappa_r \bar{e}_r = -\frac{2}{h}\epsilon^{(f)}_{\theta\theta}(\tfrac{h}{2})\bar{e}_r$$

The kinematic curvature variations and stress couples are postulated to be positive dependent variables which undergo positive rates of change over positive increments of the independent variables. The variation of curvature

$$\delta\bar{\kappa}_\theta = \delta\kappa_\theta \bar{e}_\theta$$

is accompanied by a positive stress couple $M_{r\theta}(\sigma)\bar{e}_\theta$. If the infinitesimal shell element is a free body, then the curvature variation

$$\delta\bar{\kappa}_r = \delta\kappa_r \bar{e}_r$$

would cause a lateral POISSON's effect

$$\delta\bar{\kappa}_\theta = \nu\,\delta\kappa_r \bar{e}_\theta$$

in the curvature of the surface. However, the continuity in the shell requires the development of a constraining curvature

$$-\delta\bar{\kappa}_\theta = -\nu\,\delta\kappa_r \bar{e}_\theta$$

which is accompanied by a constraining stress couple

$$M_{r\theta}(\sigma) = -D\nu\,\delta\kappa_r$$

Consequently the flexural stress resultant or stress couple $M_{r\theta}(\sigma)$ will be given by the expression

$$M_{r\theta}(\sigma)\bar{e}_\theta = D\left[\delta\kappa_\theta - \nu\,\delta\kappa_r\right]\bar{e}_\theta$$

where $D = \frac{E h^3}{12(1-\nu^2)}$ denotes the flexural rigidity of the

shell.

Similarly

$$M_{\theta r}(\sigma)\bar{e}_r = D[\delta K_r - \nu \delta K_\theta]\bar{e}_r$$

The scalar components of these Kinematic Stress Couple-Curvature Relations are

$$M_{r\theta}(\sigma) = D[\delta K_\theta - \nu \delta K_r]$$

and

$$M_{\theta r}(\sigma) = D[\delta K_r - \nu \delta K_\theta]$$

Substitution for δK_r, δK_θ in the relations above gives the resultant stress couple in terms of the strains $\epsilon_{rr}^{(f)}(\frac{h}{2}), \epsilon_{\theta\theta}^{(f)}(\frac{h}{2})$

$$M_{r\theta}(\sigma) = \frac{E h^2}{6(1-\nu^2)}\left[\epsilon_{rr}^{(f)}(\tfrac{h}{2}) + \nu \epsilon_{\theta\theta}^{(f)}(\tfrac{h}{2})\right]$$

and

$$M_{\theta r}(\sigma) = \frac{-E h^2}{6(1-\nu^2)}\left[\epsilon_{\theta\theta}^{(f)}(\tfrac{h}{2}) + \nu \epsilon_{rr}^{(f)}(\tfrac{h}{2})\right]$$

Inserting the appropriate flexural strains from the test results in the above relations yield the stress couple distributions shown in Figures (20 - 27), Figure 30 and Figure 31. A value of $\frac{E h^2}{6(1-\nu^2)} = 0.263 \times 10^6$ was used in the calculations.

A formal derivation of the previous stress couple-strain relations can be achieved by utilizing the results of General Theory of Shallow Shells in Appendix A.

For shallow shells, a Kinematic Moment Tensor $\overline{\overline{M}}(\sigma)$ can be constructed such that

$$\overline{\overline{M}}(\sigma) = \bar{e}_i \, \bar{M}_i(\sigma)$$

As

$$\overline{\overline{\sigma}} = \overline{e}_i \, \overline{\sigma}_i$$

then the stress couple for shallow shells

$$\overline{M}_i(\sigma)\, ds_i = \int_{-h/2}^{+h/2} \overline{r} \times \overline{\sigma}_i \, dA_i \qquad \left(dA_i = d\alpha_n ds_i\right)$$

which per unit length

$$\overline{M}_i(\sigma) = \int_{-h/2}^{+h/2} \overline{r} \times \overline{\sigma}_i \frac{dA_i}{ds_i} = \int_{-h/2}^{+h/2} \alpha_n (\overline{e}_n \times \overline{\sigma}_i)\, d\alpha_n$$

since for infinitesimal free-bodies $\overline{r} \doteq \alpha_n \overline{e}_n$. Moreover,

$$\overline{M}_i(\sigma) = \overline{e}_i \cdot \overline{\overline{M}}(\sigma) = \overline{e}_i \cdot \left[\int_{-h/2}^{+h/2} -\alpha_n (\overline{\overline{\sigma}} \times \overline{e}_n)\, d\alpha_n \right]$$

where the stress can be expressed in terms of strain by HOOKE Law

$$\overline{\overline{\sigma}} = 2\hat{\mu}\overline{\overline{\epsilon}} + \hat{\lambda}\epsilon_I \overline{\overline{I}}$$

Substituting the strain tensor due to flexure for shallow shells from Appendix A yields the moment tensor

$$\overline{\overline{M}}(\sigma) = \frac{h^3}{12}\left[\mu\left(\delta K_r^{(t)} - \delta K_\theta^{(t)}\right)\overline{e}_r\overline{e}_r + \frac{E}{1-\nu^2}\left(\delta K_\theta^{(n)} - \nu\,\delta K_r^{(n)}\right)\overline{e}_r\overline{e}_\theta \right.$$
$$\left. + \frac{E}{1-\nu^2}\left(\delta K_r^{(n)} - \delta K_\theta^{(n)}\right)\overline{e}_\theta\overline{e}_r + \mu\left(\delta K_\theta^{(t)} - \delta K_r^{(t)}\right)\overline{e}_\theta\overline{e}_\theta \right]$$

The components of this kinematic moment tensor are

$$M_{r\theta}(\sigma) = \overline{e}_r\overline{e}_\theta : \overline{\overline{M}}(\sigma) = \frac{E h^3}{12(1-\nu^2)}\left(\delta K_\theta^{(n)} - \nu\,\delta K_r^{(n)}\right)$$

and

$$M_{\theta r}(\sigma) = \overline{e}_\theta\overline{e}_r : \overline{\overline{M}}(\sigma) = \frac{E h^3}{12(1-\nu^2)}\left(\delta K_r^{(n)} - \nu\,\delta K_\theta^{(n)}\right)$$

The flexural strains $\epsilon_{rr}^{(f)}, \epsilon_{\theta\theta}^{(f)}$ can be related to the variations in curvature by the relations (7.6) in Appendix A.

$$\epsilon_{rr}^{(f)} = +\alpha_n \delta K_\theta^{(n)} = \bar{e}_r \cdot (\delta K_\theta^{(n)} \bar{e}_\theta \times \alpha_n \bar{e}_n)$$

$$\epsilon_{\theta\theta}^{(f)} = -\alpha_n \delta K_r^{(n)} = \bar{e}_\theta \cdot (\delta K_r^{(n)} \bar{e}_r \times \alpha_n \bar{e}_n)$$

The variation of curvature can be extracted from these relations by setting $\alpha_n = \frac{h}{2}$

$$\delta K_r^{(n)} = -\frac{2}{h} \epsilon_{\theta\theta}^{(f)}\left(\frac{h}{2}\right)$$

$$\delta K_\theta^{(n)} = +\frac{2}{h} \epsilon_{rr}^{(f)}\left(\frac{h}{2}\right)$$

The final results for the stress couples are

$$M_{r\theta}(\sigma) = \frac{Eh^2}{6(1-\nu^2)}\left[\epsilon_{rr}^{(f)}\left(\frac{h}{2}\right) + \nu\, \epsilon_{\theta\theta}^{(f)}\left(\frac{h}{2}\right)\right]$$

$$M_{\theta r}(\sigma) = \frac{-Eh^2}{6(1-\nu^2)}\left[\epsilon_{\theta\theta}^{(f)}\left(\frac{h}{2}\right) + \nu\, \epsilon_{rr}^{(f)}\left(\frac{h}{2}\right)\right]$$

III - 4 Stress Distribution

The extent of transverse flexure in the thin shell can be clearly seen if the total stresses are tabulated. The comparative state of direct and flexural stresses in the exterior of the shell surface illustrate the strain deviations from the desirable extensional state of strain and its concomitant state of direct stress.

The results of the direct stress resultants and stress couples are utilized in these calculations. The comparative results are presented only for a pressure of $p_n = -30$ p.s.i.. The relations

describing the total stresses are detailed below:

$$\sigma_{rr}^{(d)} = F_{rr}(\sigma)/h$$

$$\sigma_{rr}^{(f)}(\pm\tfrac{h}{2}) = \frac{6}{h^2} M_{r\theta}(\sigma)$$

and

$$\sigma_{rr}^{(+)}(\pm h/2) = \sigma_{rr}^{(d)} + \sigma_{rr}^{(f)}(\pm h/2)$$

$$\sigma_{rr}^{(+)}(-h/2) = \sigma_{rr}^{(d)} - \sigma_{rr}^{(f)}(\pm h/2)$$

similarly

$$\sigma_{\theta\theta}^{(d)} = F_{\theta\theta}(\sigma)/h$$

$$\sigma_{\theta\theta}^{(f)}(\pm\tfrac{h}{2}) = -\frac{6}{h^2} M_{\theta r}(\sigma)$$

and

$$\sigma_{\theta\theta}^{(+)}(+h/2) = \sigma_{\theta\theta}^{(d)} + \sigma_{\theta\theta}^{(f)}(+h/2)$$

$$\sigma_{\theta\theta}^{(+)}(-h/2) = \sigma_{\theta\theta}^{(d)} - \sigma_{\theta\theta}^{(f)}(+h/2)$$

Substitution of the appropriate stress resultants yield the total stresses shown in the table below. Also, the maximum tensile and compressive stresses in the shell are indicated for a normal load $p_n = -30$ p.s.i.

	TOTAL STRESS (p.s.i.), LINE $\theta = 0^\circ$, $p_n = -30$ p.s.i.								
Radial Dist. r (in.)	0	6	9	12	14	16	18	20	21
$\sigma_{rr}^{(f)}(+h/2)$	- 239	+ 740	+ 43	- 873	-2260	-3210	-2930	+ 230	+3700
$\sigma_{rr}^{(d)}$	-2870	-2520	-2440	-2300	-2150	-1930	-1620	-1320	-1040
$\sigma_{rr}^{(+)}(+h/2)$	-3109	-1780	-2397	-3173	-4410	-5140	-4540	-1090	+2660
$\sigma_{rr}^{(+)}(-h/2)$	-2631	-3260	-2483	-1427	+ 110	+1280	+1300	-1550	-4740

	TOTAL STRESS (p.s.i.), LINE $\theta = 0^\circ$, $p_n = -30$ p.s.i.								
Radial Dist. r (in.)	0	6	9	12	14	16	18	20	21
$\sigma_{\theta\theta}^{(f)}(+h/2)$	- 239	+ 311	+ 252	+ 93	- 427	- 760	- 505	+ 517	+1640
$\sigma_{\theta\theta}^{(d)}$	-2870	-2530	-2890	-3020	-3110	-2460	-1050	+1240	+2400
$\sigma_{\theta\theta}^{(+)}(+h/2)$	-3109	-2219	-2638	-2927	-3537	-3220	-1555	+1757	+4040
$\sigma_{\theta\theta}^{(+)}(-h/2)$	-2631	-2841	-3142	-3113	-2683	-1700	+ 545	+ 723	+ 760

The calculated maximum stresses considering all lines $\theta = 0^{\circ}$ to 30° are given below:

STRESS p.s.i.	TENSILE	COMPRESSIVE
$\sigma_{rr}^{(+)}(+h/2)$	+2660	-6550
$\sigma_{rr}^{(+)}(-h/2)$	+1300	-3660
$\sigma_{\theta\theta}^{(+)}(+h/2)$	+4040	-3950
$\sigma_{\theta\theta}^{(+)}(-h/2)$	+ 14,220	-3185

These tabulated values of stresses illustrate the extent of transverse flexure that occurs when the boundary conditions are unsymmetric. It is to be noted that near the edge members the flexural and direct stresses are of the same order of magnitude; in fact in the radial direction the flexural stress is approximately three times as large as the direct stress. In the radial direction on the upper surface ($\alpha_n = +h/2$) compressive stress predominates except at the stations closest to the edge member. However, in the lower surface $(\alpha_n = -h/2)$ there are regions of fluctuating tensile and compressive stress with the latter predominating near the edge. This condition, in itself, indicates the extent of flexure at the boundary. In the θ direction, the conditions on the upper and lower surfaces are similar, as far as the compressive stress extends throughout the shell except for in the proximity of the boundary members. The maximum tensile stress of 14,220 p.s.i. exists near the slit corner along the line $\theta = 30^{\circ}$. This magnitude, being much larger than the other maximum stresses throughout the shell, indicates the high degree of stress

concentration that occurs at the re-entrant corner.

III - 5 The Degree of Rotational Periodicity of the Deformation of the Shell Structure

It was necessary to check the degree of symmetry that existed in the actual structure. This was attempted in several ways.

From the location of strain gauges in Figure 4, it can be seen that four gauges, two radial and two circumferential, were located on opposite sides of the shell in order to provide strain control. Assuming accurate locations of these gauges, the degree of symmetry is indicated by a comparison of the readings. The results are shown below for two of the gauges located at a radial distance r = 16".

	STRAIN MICRO-INCHES/INCH		
GAUGES	10 p.s.i.	20 p.s.i.	30 p.s.i.
Upper Surface	- 56	- 264	- 404
Radial Gauge	- 64	- 264	- 408
Lower Surface	+ 32	+ 116	+ 178
Radial Gauge	+ 28	+ 112	+ 184
Upper Surface	- 72	- 136	- 220
Circumferential Gauge	- 68	- 144	- 208
Lower Surface	+ 16	+ 32	+ 36
Circumferential Gauge	+ 12	+ 20	+ 44

The tabulated strains indicate that the symmetry in the radial direction

is more pronounced than in the circumferential direction.

As a further check, the horizontal boundary movements of the edge beams were recorded for all the test pressures, and are shown below for the same pressures used in the previous table. These readings were recorded with the dial gauges located in the middle of each edge beam. See Figure 11c for the numbering of the shell edges.

	HORIZONTAL DISPLACEMENT (in.)		
Number of side	10 p.s.i.	20 p.s.i.	30 p.s.i.
1	.0230	.0480	.0735
2	.0220	.0465	.0710
3	.0215	.0465	.0720
4	.0250	.0490	.0740
5	.0230	.0480	.0730
6	.0210	.0450	.0690

From the measurements shown in the table, the boundary movement is seen to be nonuniform, at least to a certain degree. The strain gauges were located in sectors 1 and 5 where the boundary movement showed good agreement, thus indicating that more reliable values of strain would be obtained.

III - 6 Boundary Rotation

The heavy edge members of the shell were mounted on rollers in order that they would be free to move horizontally and yet inhibit boundary rotation. This type of a boundary restraint admits a relatively

simple analytical boundary condition in the theoretical solution. However, in the actual behaviour of the shell structure, a certain amount of rotation is likely to occur. A series of tests were carried out to determine the extent of such rotations. The measurements obtained by two dial gauges placed vertically above one another at a distance of 3.75" against the edge members of the shell permitted an evaluation of the rotation of the boundary members. It was established that the edge members did not rotate uniformly along their lengths. The various edge beams exhibited rotations of varying magnitudes and even showed rotations which were nonuniform along any given side. The average rotations measured by the above method are presented in the table below.

	BOUNDARY ROTATION (RADIANS)		
BOUNDARY LOCATION	10 p.s.i	20 p.s.i.	30 p.s.i.
1	+.00043	+.00085	+.00110
2	+.00040	+.00053	+.00120
3	+.00091	+.00110	+.00140
4	+.00027	+.00040	+.00065
5	+.00042	+.00085	+.00054
6	+.00004	+.00013	+.00013

The strain gauge stations were located in sectors 1 and 5 and these edges rotated uniformly up to about 20 p.s.i. The nonuniform character of these rotations are easily seen from this table.

III - 7 Vertical Displacement Measurements

The vertical displacements of the lower shell surface procured from the dial gauge measurements are presented below for the positions specified in section II - 5. These experimental vertical displacements can be compared with the corresponding theoretical values shown in section IV - 6.

	VERTICAL DISPLACEMENT ALONG LINE $\theta = 30^{\circ}$ (in.)		
DIAL GAUGE LOCATIONS r (in.)	10 p.s.i.	20 p.s.i.	30 p.s.i.
0	.0155	.0295	.04280
6	.0150	.0270	.04030
9	.0153	.0286	.04225
12	.0167	.0315	.0465
14	.0164	.0305	.0465

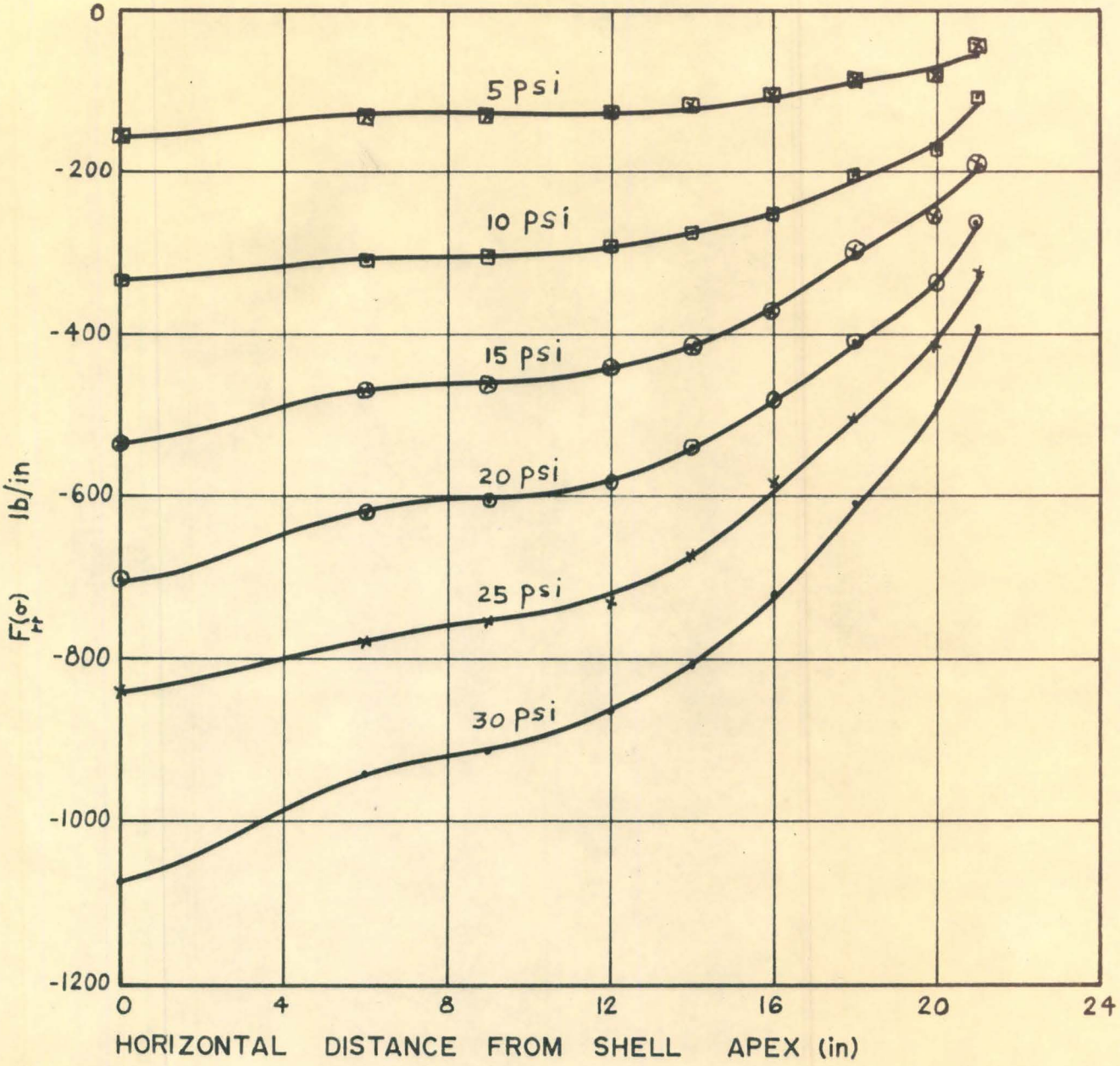

DISTRIBUTION OF DIRECT STRESS RESULTANT $F_{rr}^{(\sigma)}$ ALONG LINE $\theta = 0^\circ$

FIGURE 12

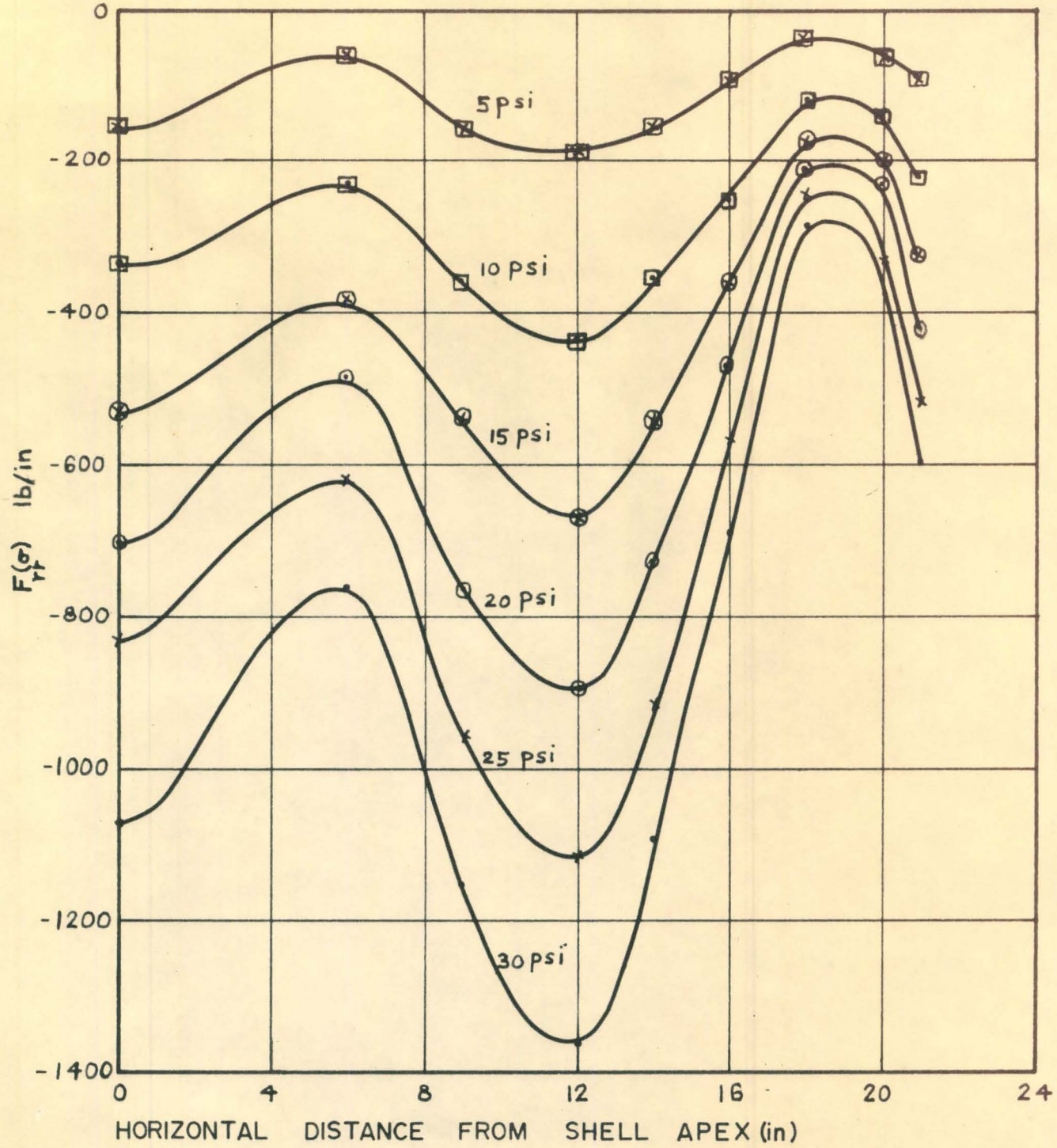

DISTRIBUTION OF DIRECT STRESS RESULTANT $F_{rr}^{(\sigma)}$ ALONG LINE $\theta = 10°$

FIGURE 13

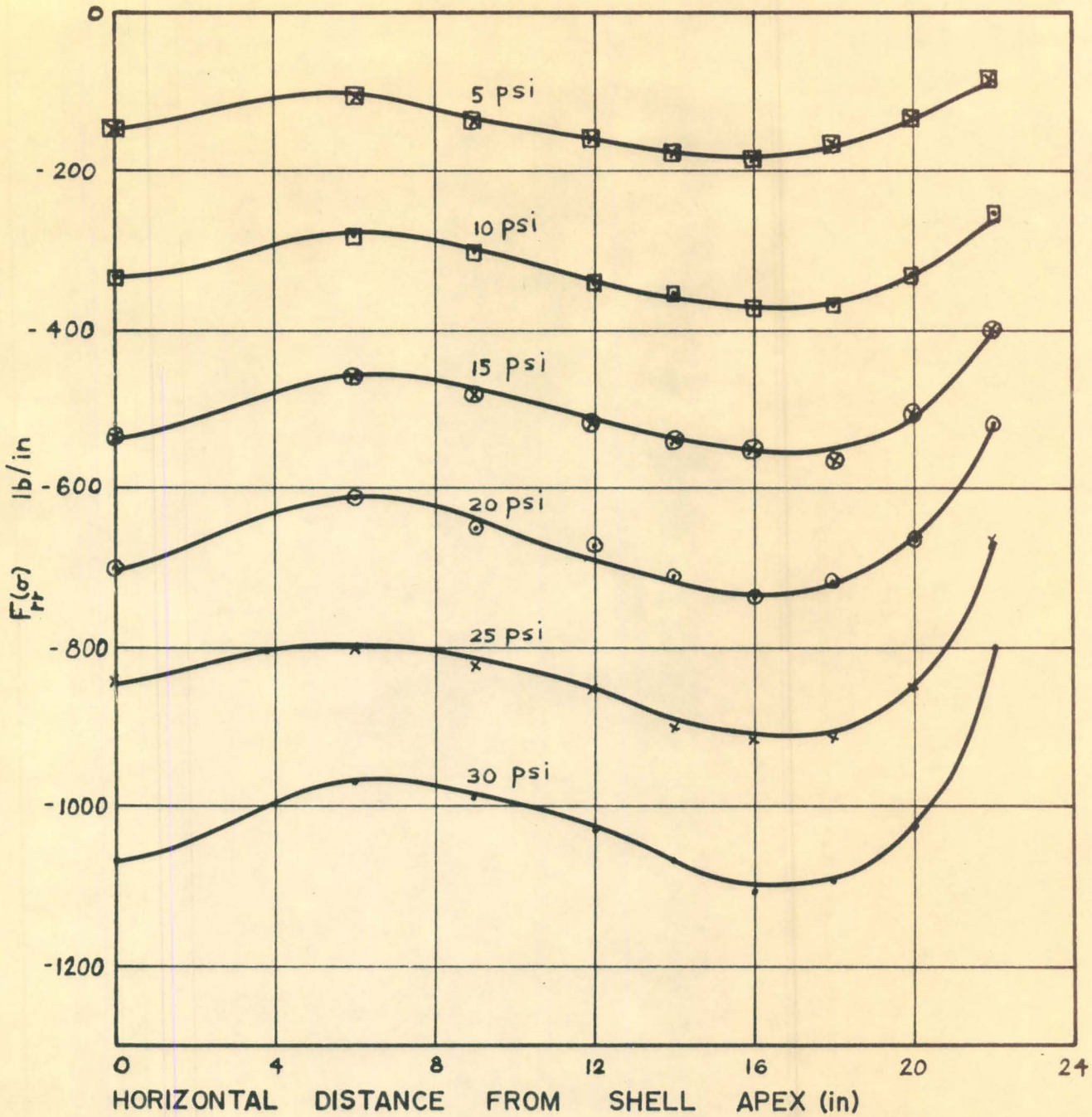

DISTRIBUTION OF DIRECT STRESS RESULTANT $F_{rr}^{(\sigma)}$ ALONG LINE $\theta = 20^{\circ}$

FIGURE 14

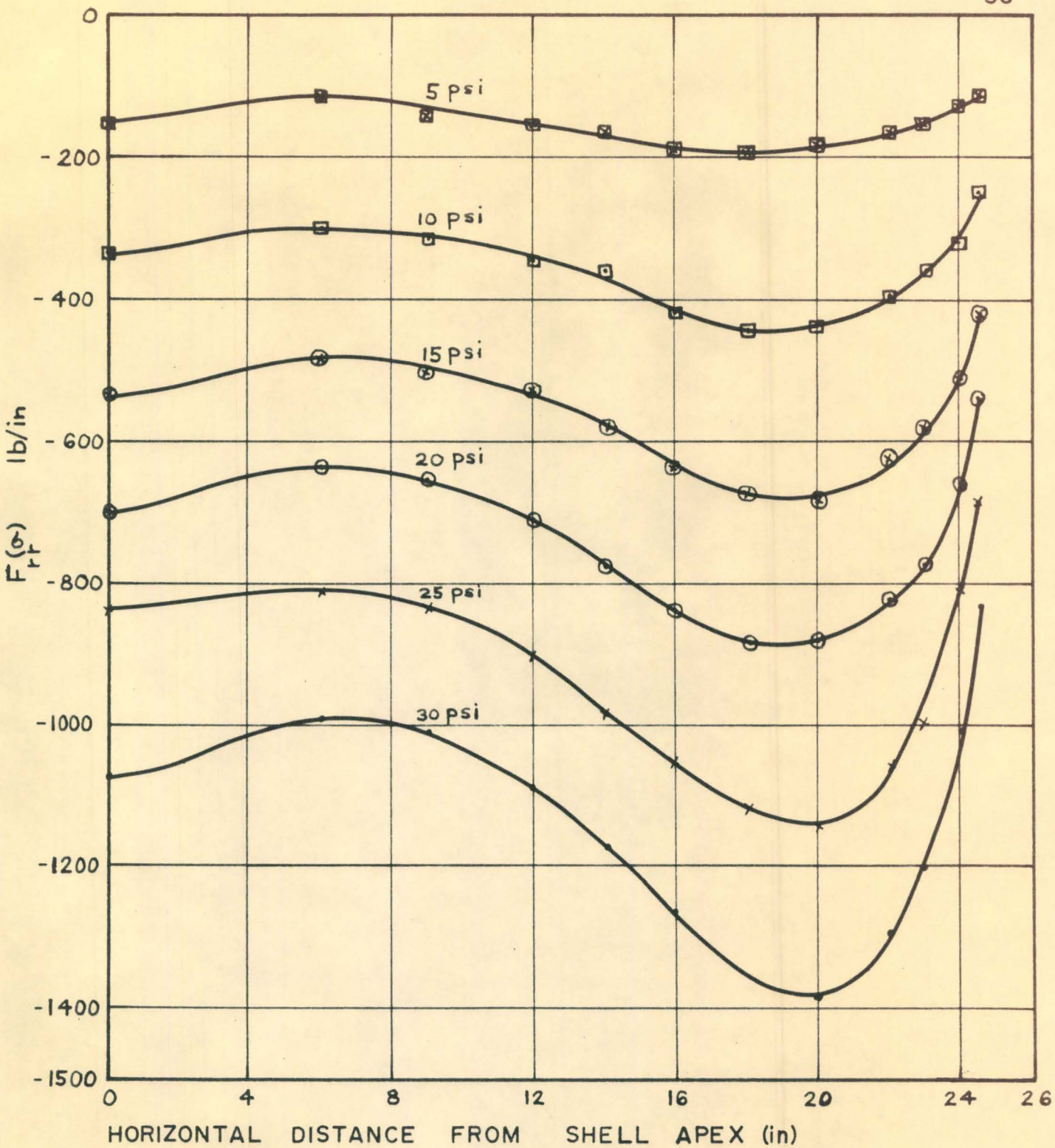

DISTRIBUTION OF DIRECT STRESS RESULTANT $F_{rr}(\sigma)$ ALONG LINE $\theta = 30^{\circ}$

FIGURE 15

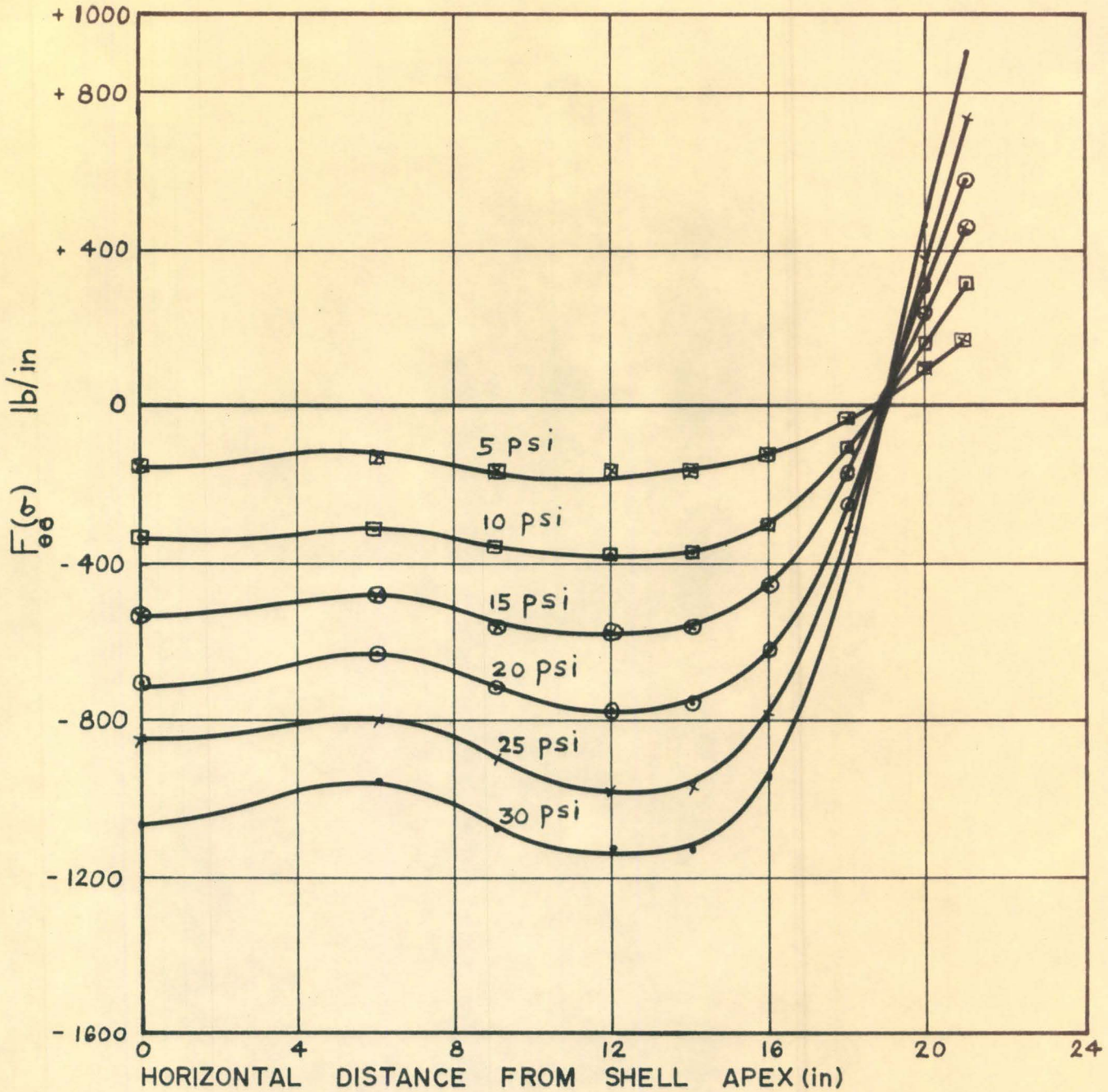

DISTRIBUTION OF DIRECT STRESS RESULTANT $F_{\theta\theta}(\sigma)$ ALONG LINE $\theta = 0°$

FIGURE 16

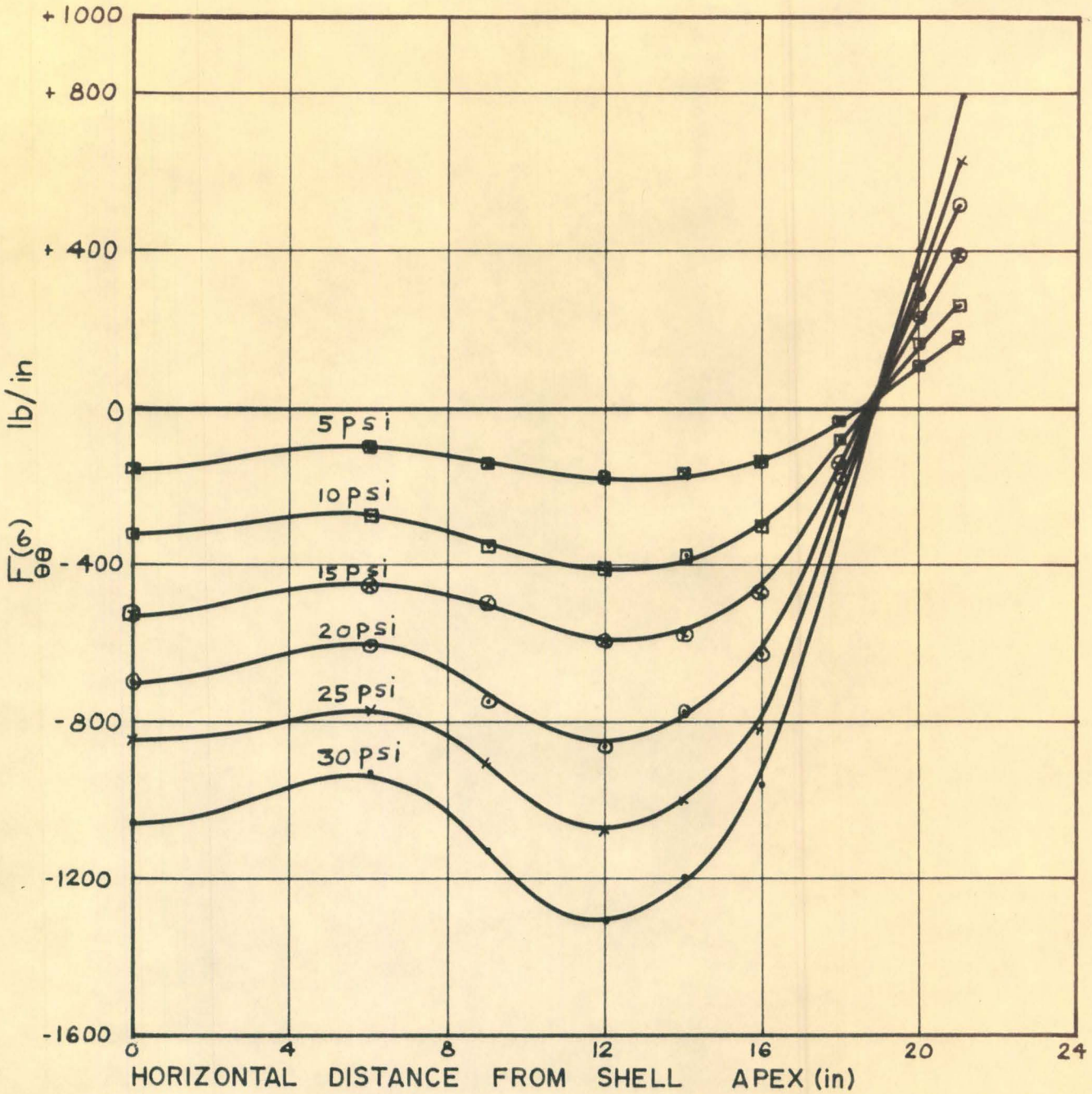

DISTRIBUTION OF DIRECT STRESS RESULTANT $F_{\theta\theta}(\sigma)$ ALONG LINE $\theta = 10^{\circ}$

FIGURE 17

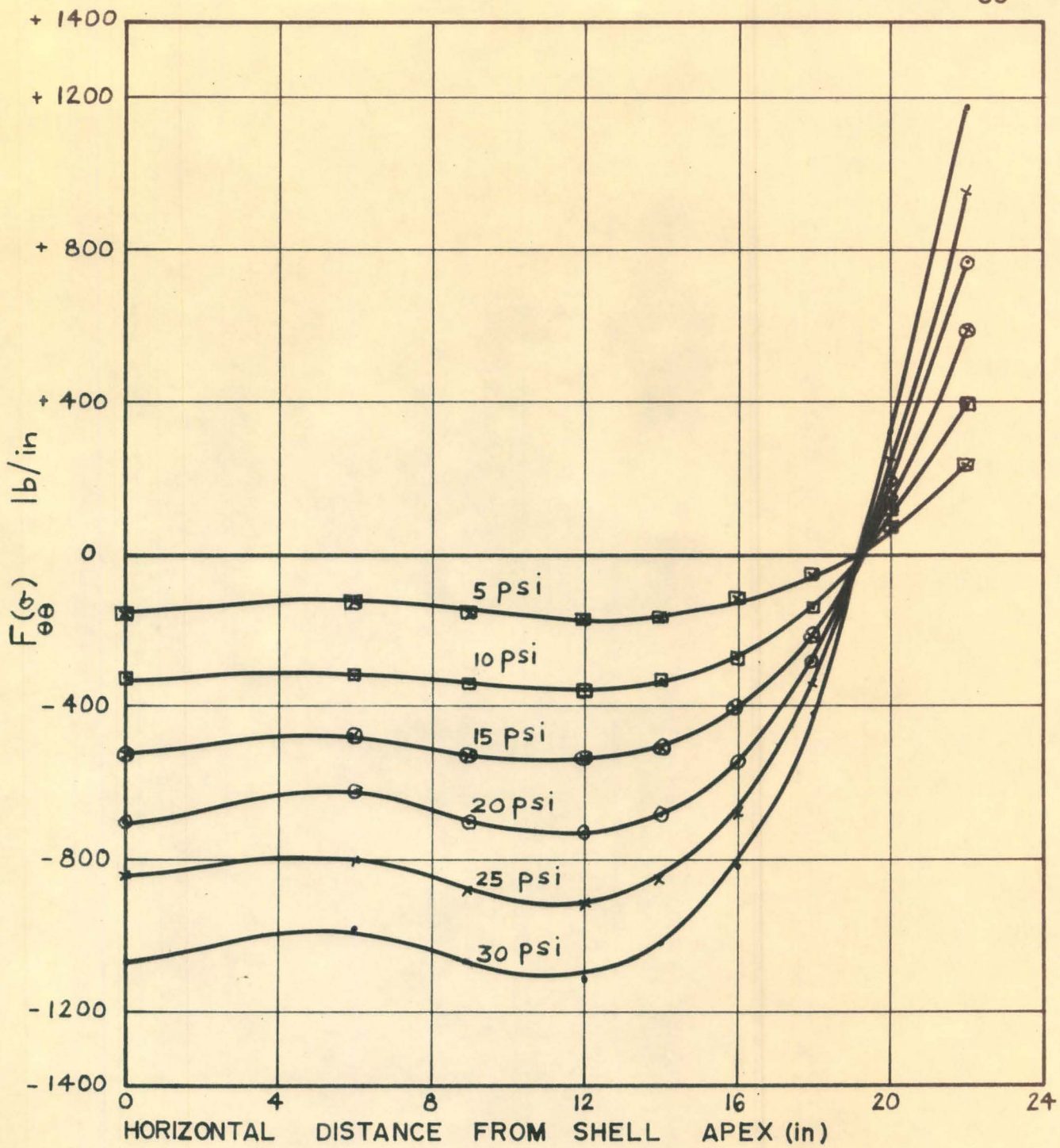

DISTRIBUTION OF DIRECT STRESS RESULTANT

$F_{\theta\theta}(\sigma)$ ALONG LINE $\theta=20^{\circ}$

FIGURE 18

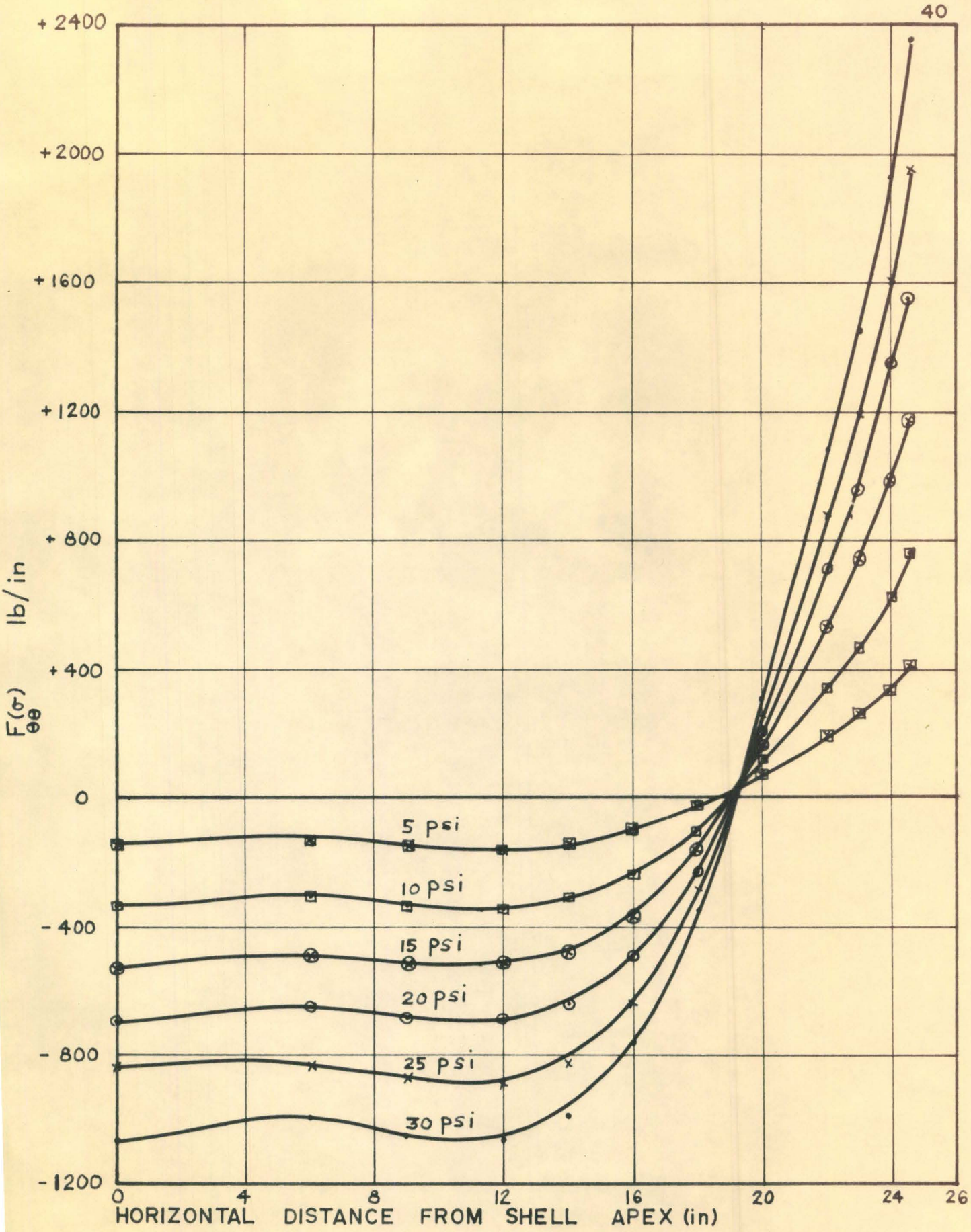

DISTRIBUTION OF DIRECT STRESS RESULTANT $F_{\theta\theta}^{(\sigma)}$ ALONG LINE $\theta = 30^\circ$

FIGURE 19

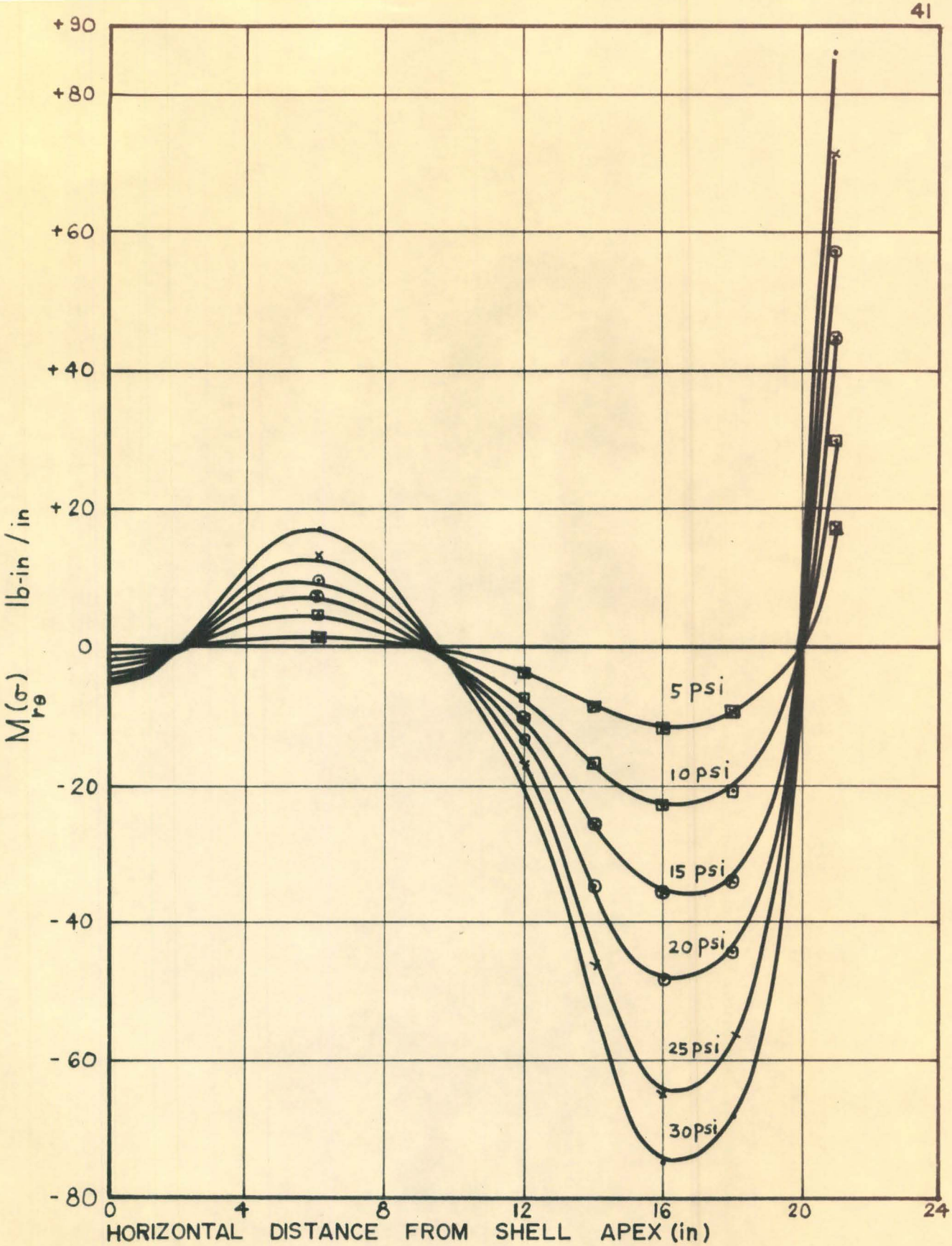

DISTRIBUTION OF STRESS COUPLE

$M_{r\theta}(\sigma)$ ALONG LINE $\theta = 0^{\circ}$

FIGURE 20

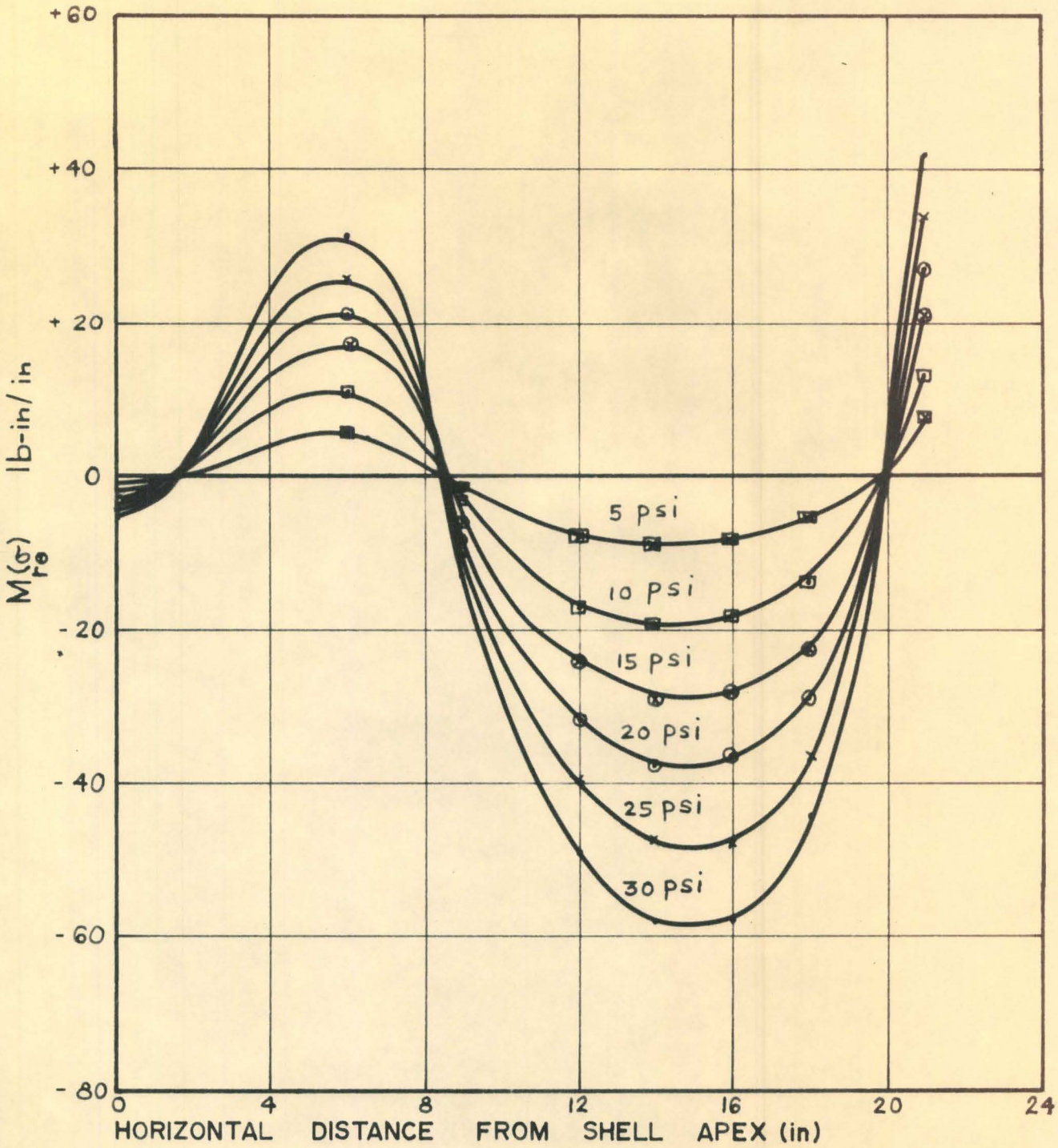

DISTRIBUTION OF STRESS COUPLE
$M_{r\theta}(\sigma)$ ALONG LINE $\theta = 10^{\circ}$

FIGURE 21

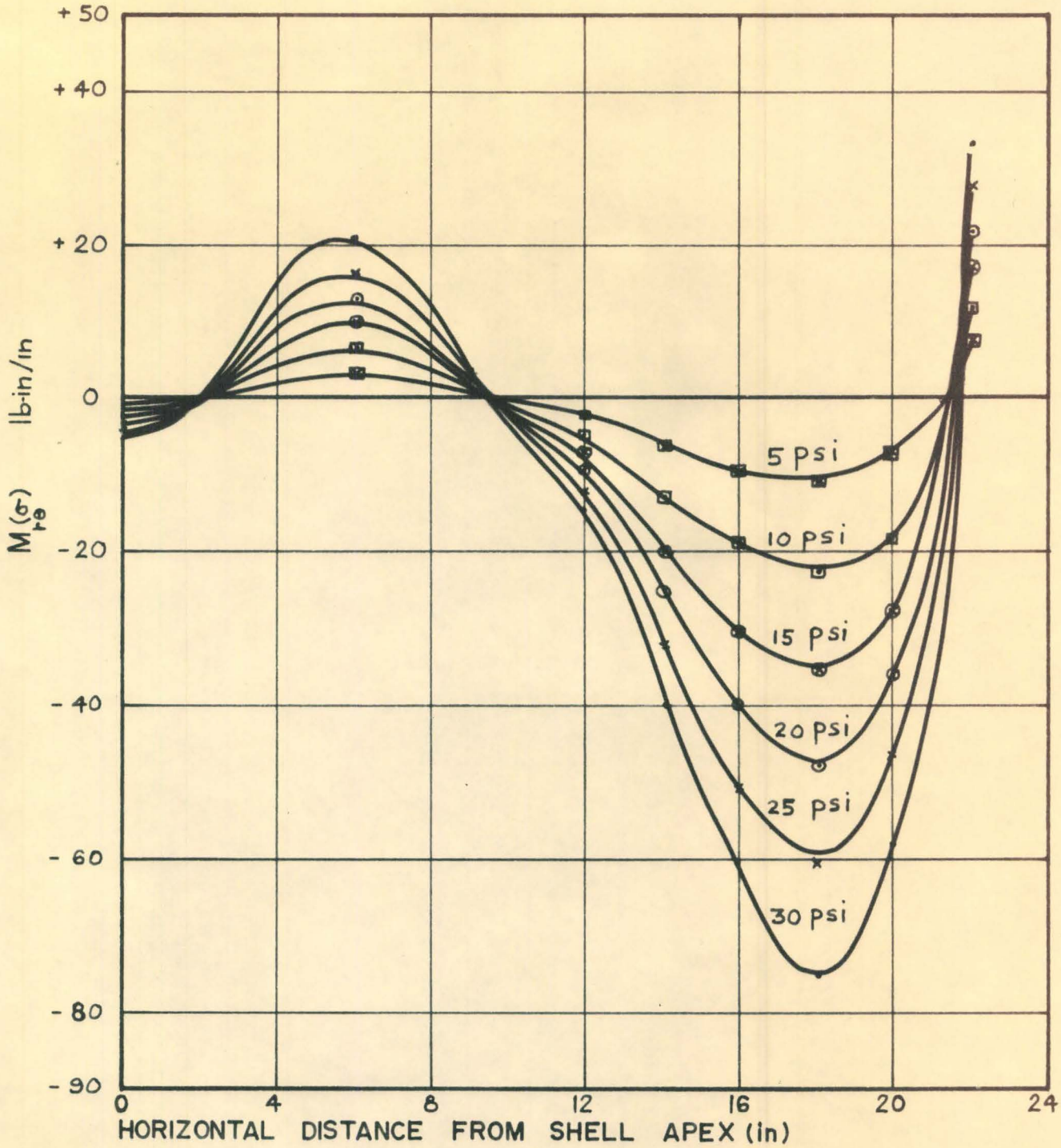

DISTRIBUTION OF STRESS COUPLE

$M_{r\theta}(\sigma)$ ALONG LINE $\theta = 20^{\circ}$

FIGURE 22

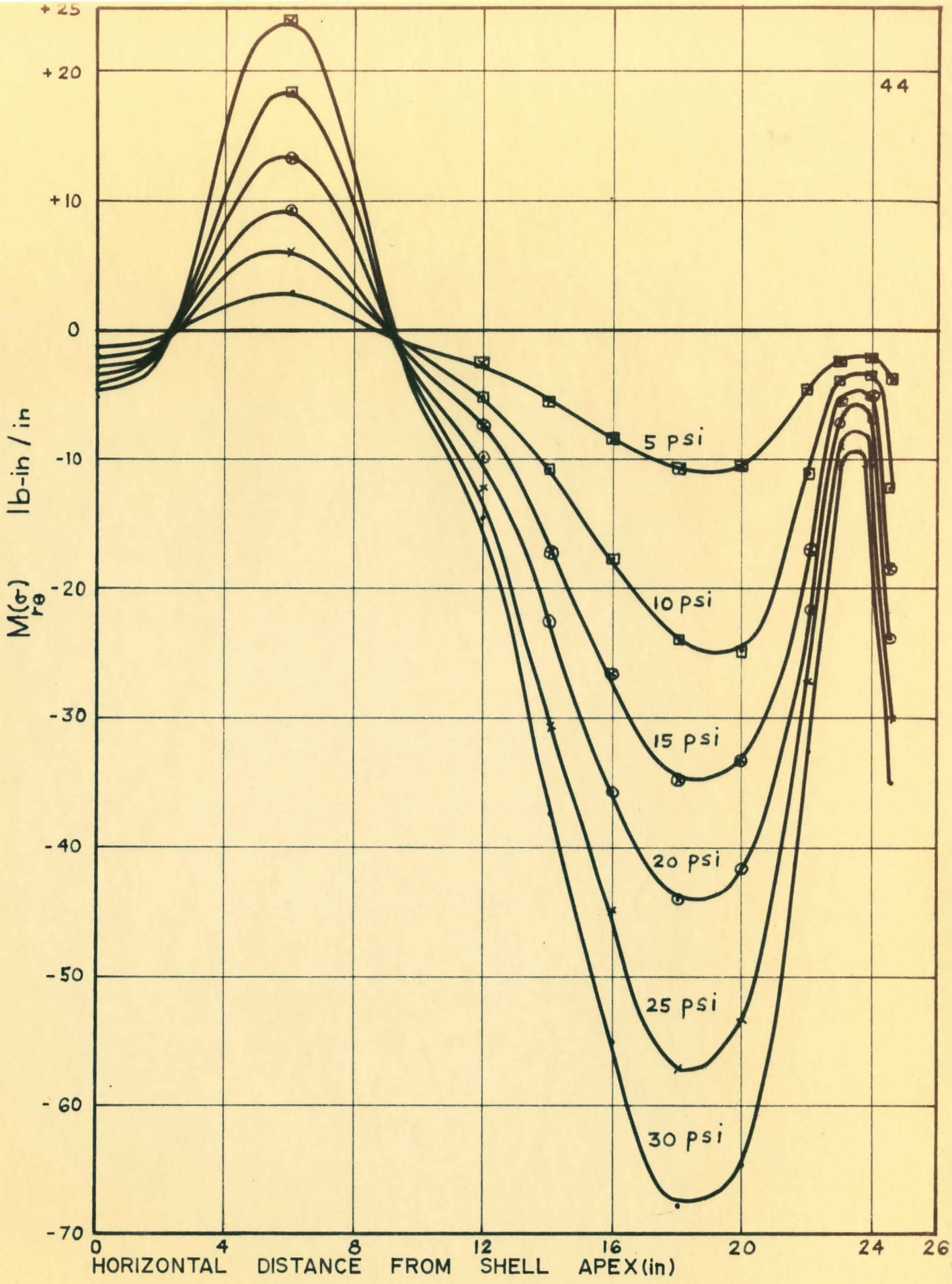

DISTRIBUTION OF STRESS COUPLE
$M_{r\theta}^{(\sigma)}$ ALONG LINE $\theta = 30°$

FIGURE 23

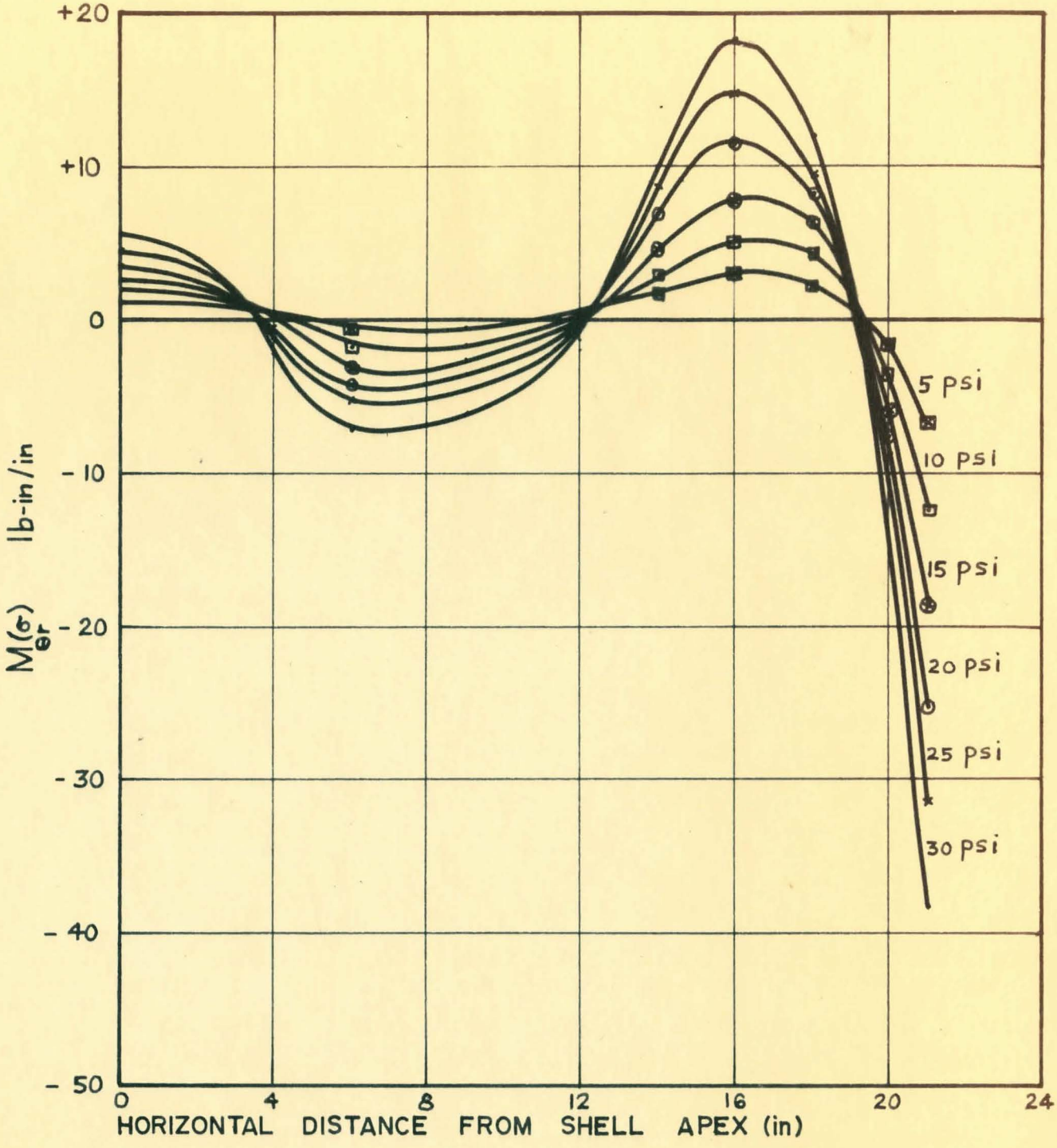

DISTRIBUTION OF STRESS COUPLE $M_{\theta r}(\sigma)$ ALONG LINE $\theta = 0^\circ$

FIGURE 24

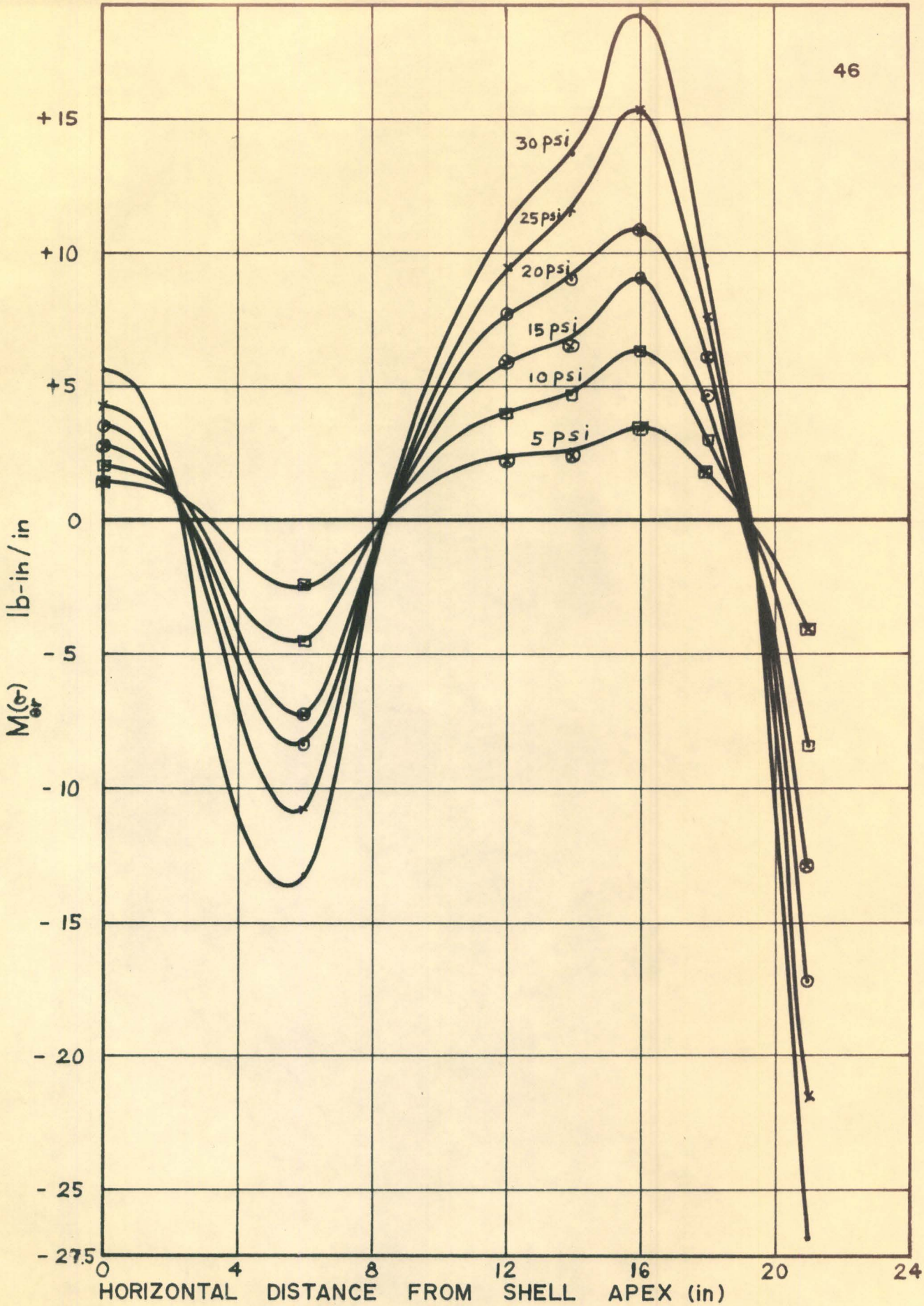

DISTRIBUTION OF STRESS COUPLE $M_{\theta r}^{(\sigma)}$ ALONG LINE $\theta = 10^{\circ}$

FIGURE 25

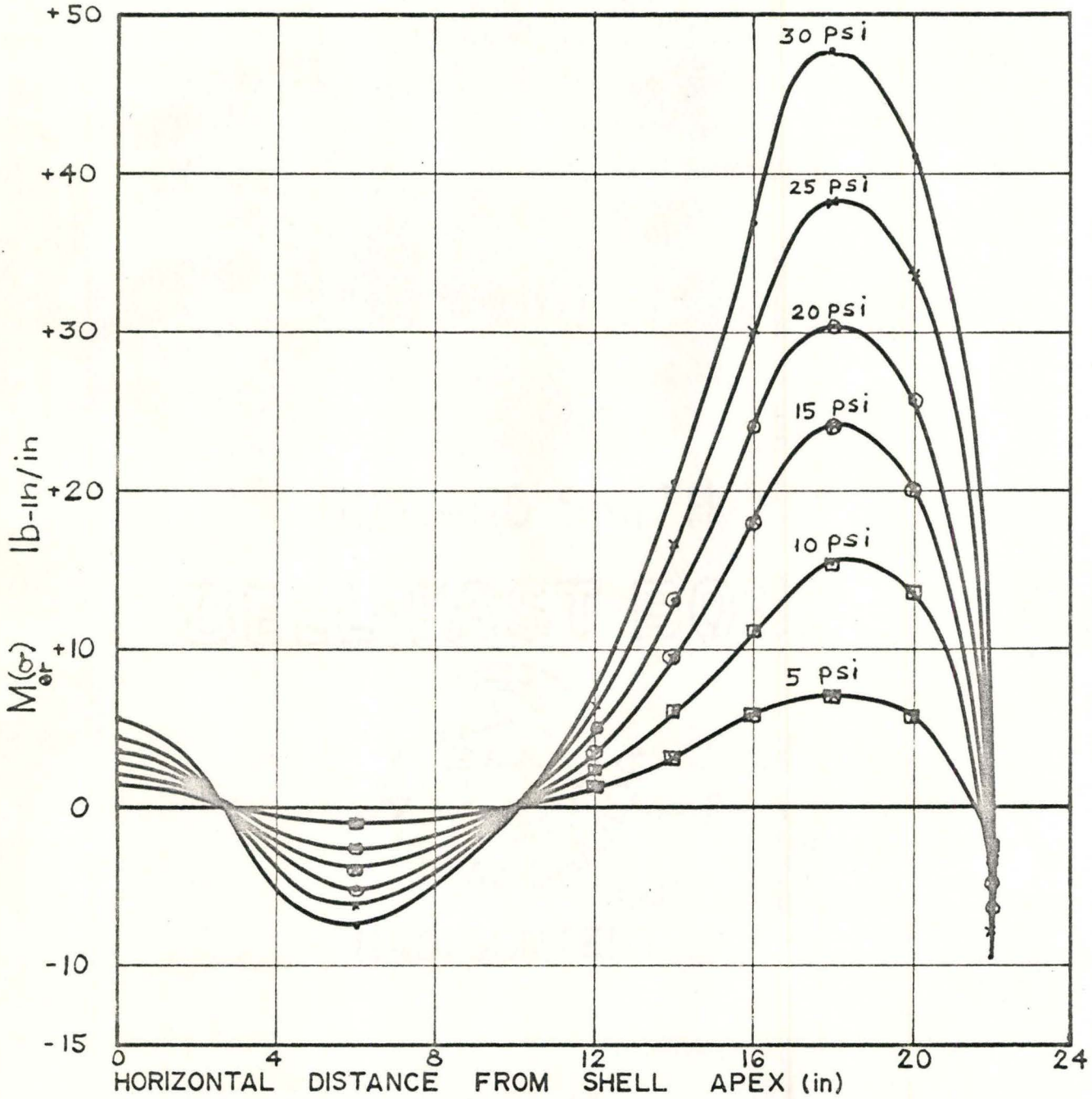

DISTRIBUTION OF STRESS COUPLE
$M_{\theta r}(\sigma)$ ALONG LINE $\theta = 20^{\circ}$

FIGURE 26

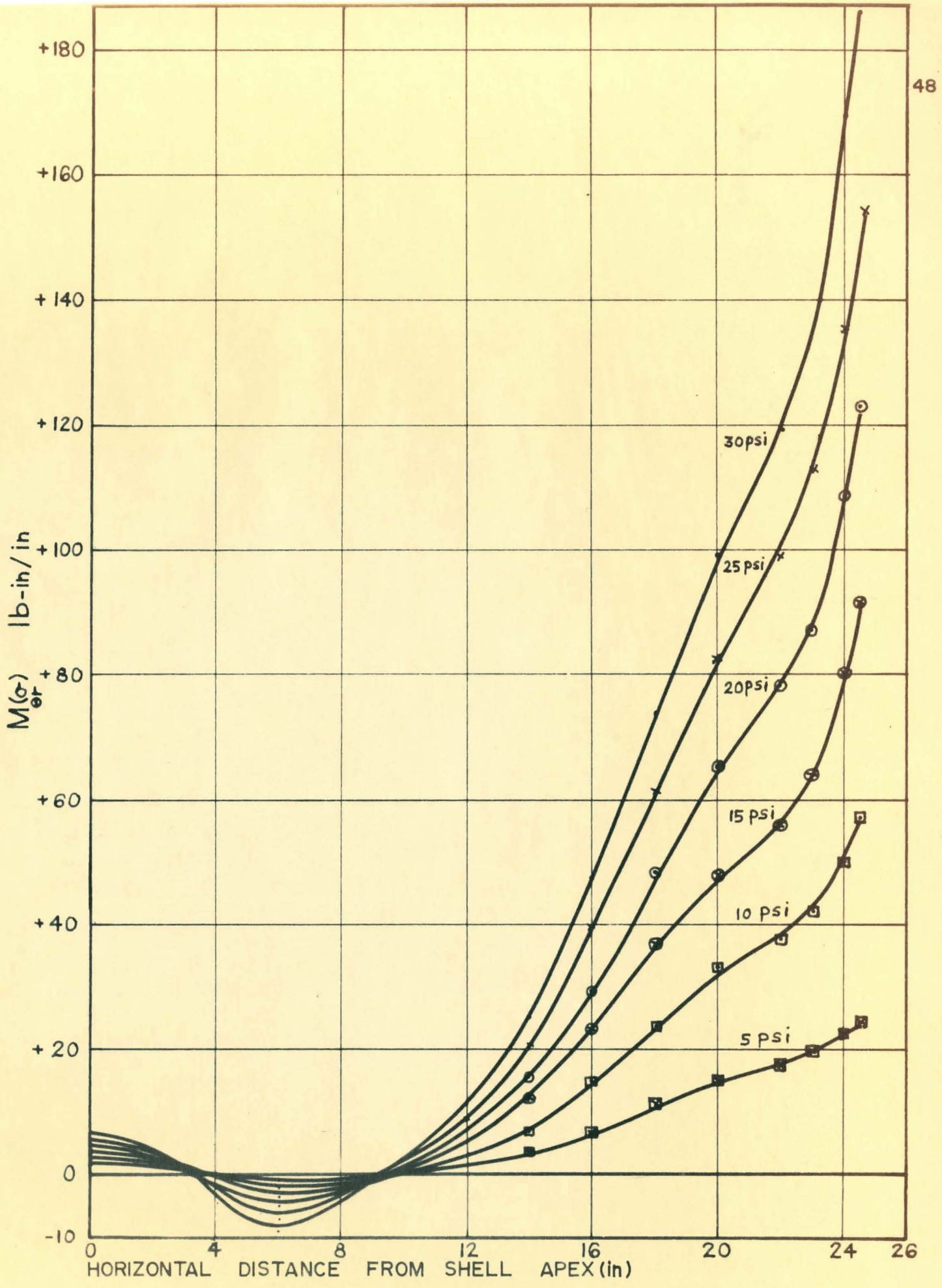

Figure 27

DISTRIBUTION OF STRESS COUPLE $M_{\theta r}(\sigma)$ ALONG LINE $\theta = 30°$

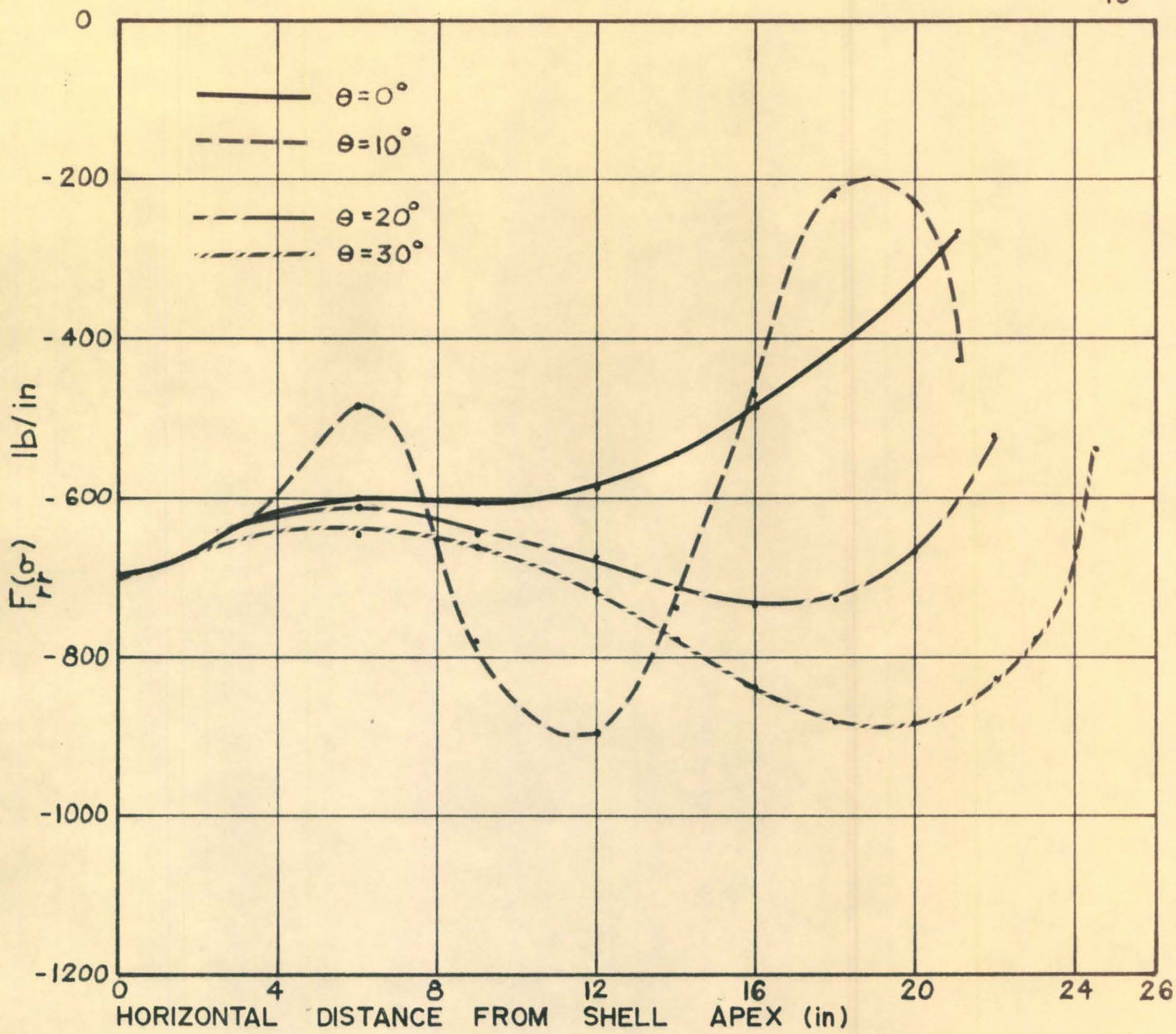

DISTRIBUTION OF DIRECT STRESS RESULTANT $F_{rr}^{(\sigma)}$ FOR P_n=-20 psi

FIGURE 28

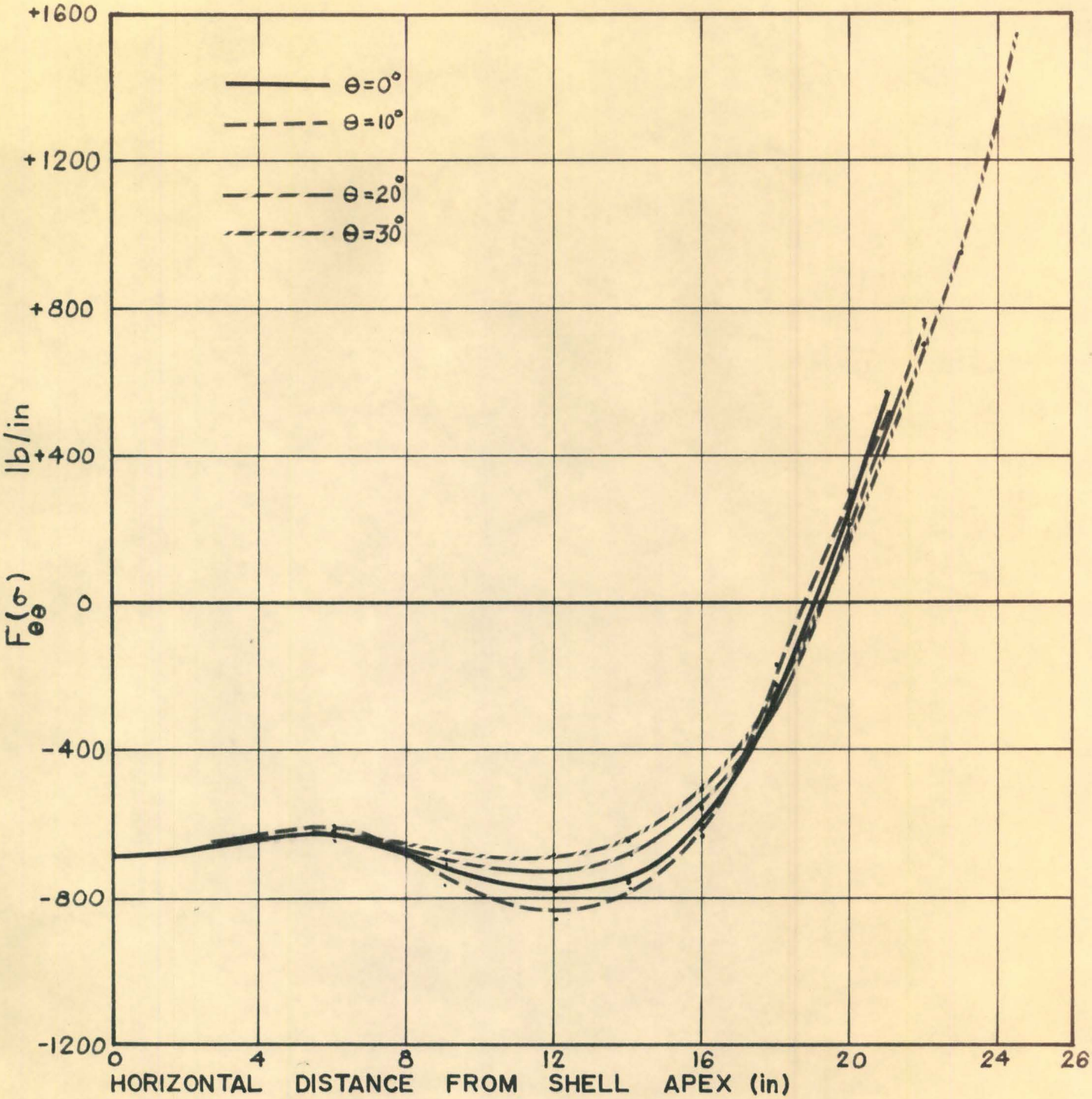

DISTRIBUTION OF DIRECT STRESS RESULTANT $F_{\theta\theta}(\sigma)$ FOR P_n =-20 psi

FIGURE 29

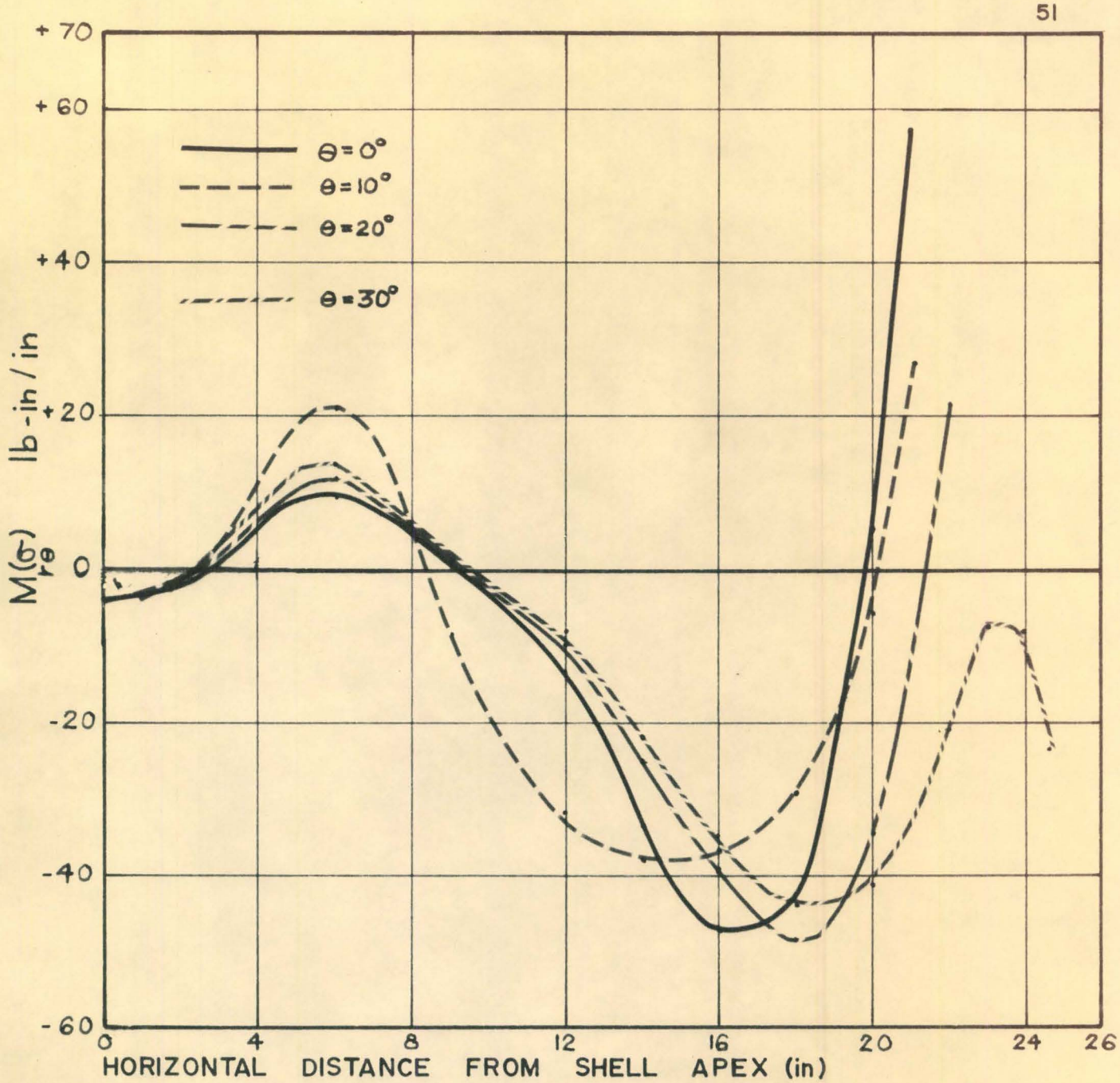

DISTRIBUTION OF STRESS COUPLE FOR P_h =-20psi
$M(\sigma)_{r\theta}$

FIGURE 30

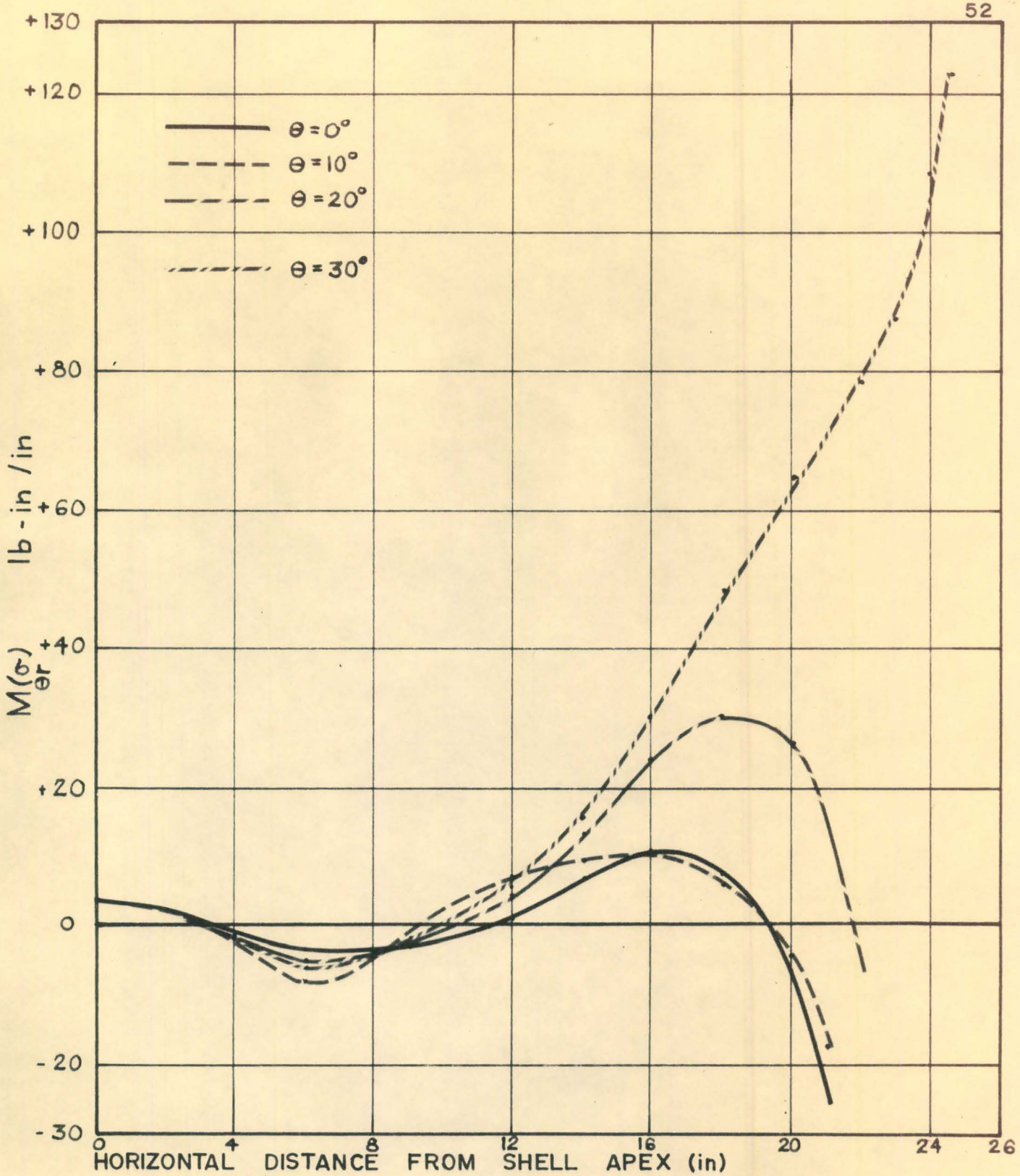

DISTRIBUTION OF STRESS COUPLE $M_{(\sigma)\theta r}$ FOR P_n=-20psi

FIGURE 31

CHAPTER IV

THEORETICAL SOLUTION

IV - 1 Introduction

This chapter is concerned with an approximate solution applicable to the analysis of thin, shallow, calotte shells of spherical middle surface, based on the method given by ORAVAS in 1957. Many stress analyses have been carried out for spherical calotte shells which disregard the transverse flexural stiffness of the shell. In this investigation the general solution for shallow shells is attempted in which the shell's flexural stiffness is not ignored. It is postulated that the shear deformation of the shell is small compared with the flexural and dilatational deformations of the shell. In this case the type of a spherical calotte shell investigated encloses a hexagonal base.

IV - 2(a) Formulation and Solution of Fundamental Differential Equations for Thin Shallow Elastic Shells

The fundamental differential equations for isothermal deformation of shallow elastic shells expressed in terms of generalized coordinates and for normal pressure p_n, (derived in Appendix A in conformance with VLASOV's theory) are:

$$\nabla^4 \Phi - Eh \nabla_K^2 u_n = 0 \tag{1}$$

$$\nabla^4 u_n + \frac{1}{D} \nabla_K^2 \Phi = \frac{p_n}{D} \tag{2}$$

with

$$\nabla^2 \equiv \frac{1}{A_1 A_2}\left\{\frac{\partial}{\partial \alpha_1}\left[\frac{A_2}{A_1}\frac{\partial}{\partial \alpha_1}\right] + \frac{\partial}{\partial \alpha_2}\left[\frac{A_1}{A_2}\frac{\partial}{\partial \alpha_2}\right]\right\} \equiv \frac{d}{d\bar{r}_o}\cdot\frac{d}{d\bar{r}_o}$$

$$\nabla_K^2 \equiv \frac{1}{A_1 A_2}\left\{\frac{\partial}{\partial \alpha_1}\left[-K_1^{(n)}\frac{A_2}{A_1}\frac{\partial}{\partial \alpha_1}\right] + \frac{\partial}{\partial \alpha_2}\left[K_2^{(n)}\frac{A_1}{A_2}\frac{\partial}{\partial \alpha_2}\right]\right\}$$

$$\nabla^4 \equiv \nabla^2\nabla^2 \equiv \left(\frac{d}{d\bar{r}_o}\cdot\frac{d}{d\bar{r}_o}\right)\left(\frac{d}{d\bar{r}_o}\cdot\frac{d}{d\bar{r}_o}\right)$$

where A_1, A_2 denote fundamental magnitudes of the first order for the shell's middle surface and $K_1^{(n)}$ $K_2^{(n)}$ designate normal curvatures of the co-ordinate lines α_1 = constant, α_2 = constant (Figure 32). The method of solution will be summarized in the following exposition.

The two coupled differential equations of the form

$$\left(\nabla^4 + m_i^2 \nabla_K^2\right) f_i = F_i \qquad (i = 1,2)$$

can be solved by introducing a pseudo-complex dependent variable

$$V = f_1 + i\,\omega\, f_2$$

a method introduced by Herbert WEBB in 1925 in a problem of torsional buckling of columns and used in thin shell analysis by Friedrich TÖLKE in 1938. Multiplying equation (1) by $i\omega$ and adding to equation (2), while imposing the condition

$$\omega = \frac{\sqrt{12(1-\nu^2)}}{E\,h^2}$$

yields the complex differential equation

$$\left[\nabla^4 - i\,E h \omega \nabla_K^2\right] V = p_n / D \qquad (3)$$

where

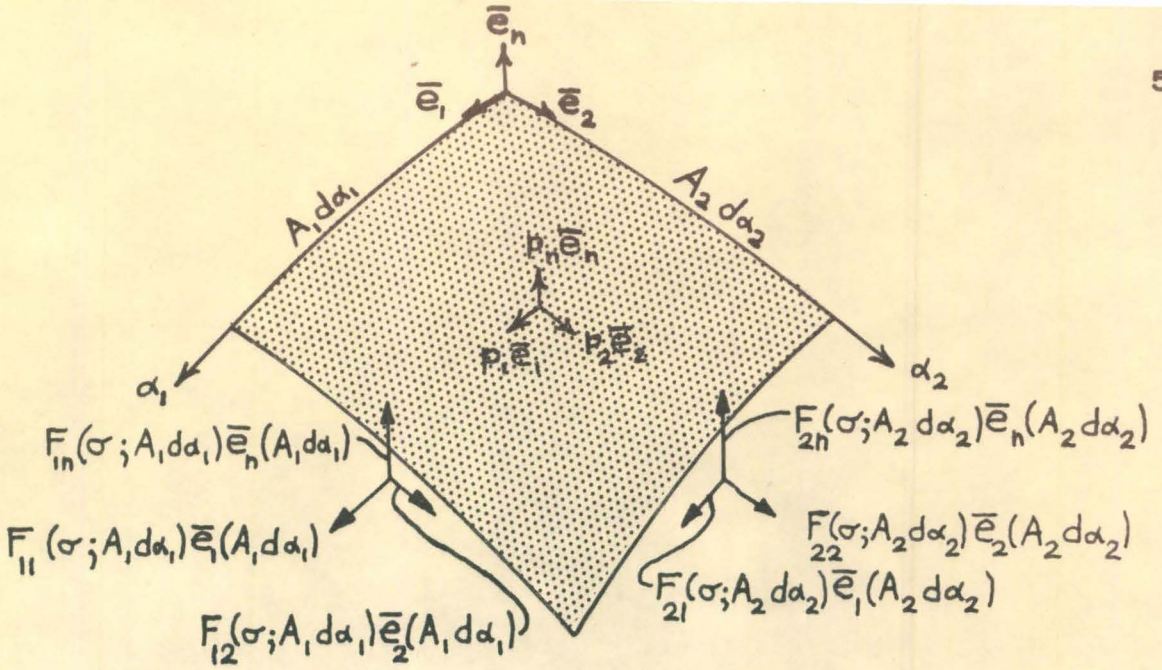

(a) DIFFERENTIAL SHELL ELEMENT SHOWING STRESS RESULTANTS AND SURFACE LOADS

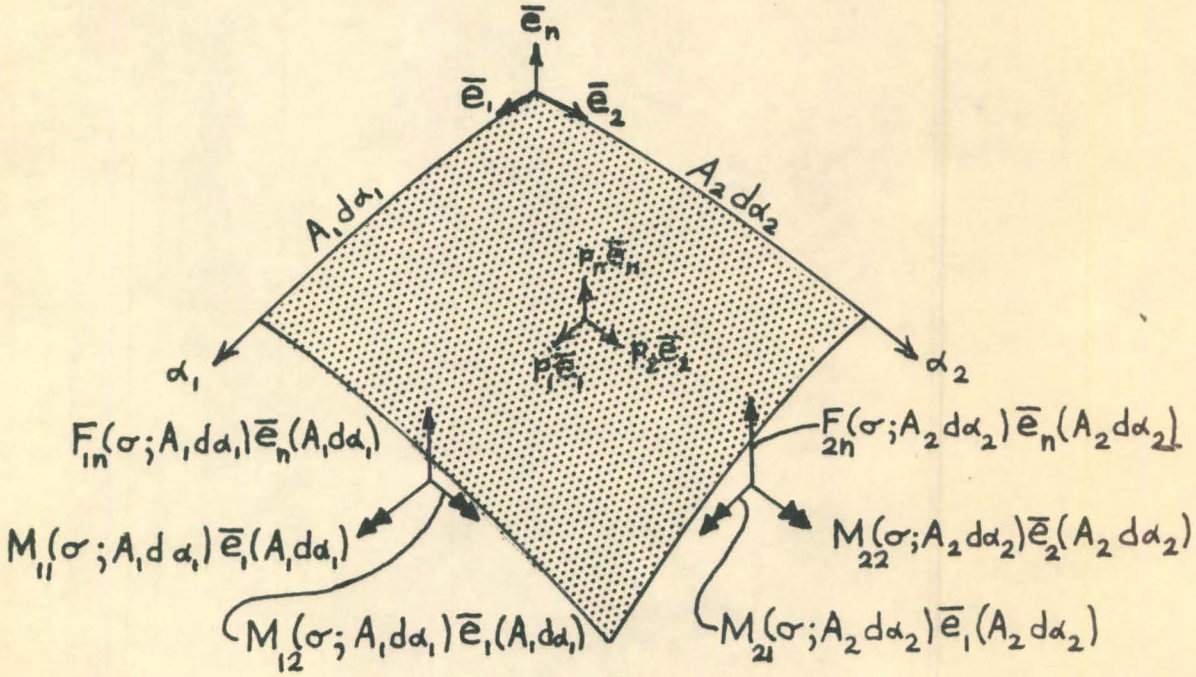

(b) DIFFERENTIAL SHELL ELEMENT SHOWING STRESS COUPLES AND SURFACE LOADS

FIGURE 32

$$V = u_n + i\,\omega\,\Phi$$

The original functions Φ and u_n can be expressed in terms of the complex function V as follows

$$u_n = \tfrac{1}{2}(V + V^*)$$
$$\Phi = \frac{-i}{2\omega}(V - V^*) \qquad (4)$$

where the complex conjugate of V is

$$V^* = u_n - i\,\omega\,\Phi$$

For shallow spherical shells the fundamental magnitudes of the first order become

$$A_1^2 = 1, \qquad A_2^2 = r^2$$

the parametric co-ordinates are

$$\alpha_1 = r \;, \quad \alpha_2 = \Theta$$

and the normal curvatures of the middle surface

$$K_r^{(n)} = -\frac{1}{R}$$
$$K_\Theta^{(n)} = +\frac{1}{R}$$

where R denotes the radius of curvature. This simplifies the differential operators and allows the sectional resultant stress quantities to be expressed by

$$F_{rr}(\sigma) = \frac{1}{r^2}\frac{\partial^2 \Phi}{\partial \Theta^2} + \frac{1}{r}\frac{\partial \Phi}{\partial r} \qquad (5a)$$

$$F_{\Theta\Theta}(\sigma) = \frac{\partial^2 \Phi}{\partial r^2} \qquad (5b)$$

$$F_{r\Theta}(\sigma) = F_{\Theta r}(\sigma) = -\frac{\partial}{\partial r}\left[\frac{1}{r}\frac{\partial \Phi}{\partial \Theta}\right] \qquad (5c)$$

$$M_{r\theta}(\sigma) = -D\left[\frac{\partial^2 u_n}{\partial r^2} + \nu\left(\frac{1}{r^2}\frac{\partial^2 u_n}{\partial \theta^2} + \frac{1}{r}\frac{\partial u_n}{\partial r}\right)\right] \tag{5d}$$

$$M_{\theta r}(\sigma) = D\left[\frac{1}{r^2}\frac{\partial^2 u_n}{\partial \theta^2} + \frac{1}{r}\frac{\partial u_n}{\partial r} + \nu\left(\frac{\partial^2 u_n}{\partial r^2}\right)\right] \tag{5e}$$

$$M_{rr}(\sigma) = -M_{\theta\theta}(\sigma) = D(1-\nu)\left\{\frac{\partial}{\partial r}\left[\frac{1}{r}\frac{\partial u_n}{\partial \theta}\right]\right\} \tag{5f}$$

$$F_{\theta n}(\sigma) = -D\left\{\frac{1}{r}\frac{\partial}{\partial \theta}(\nabla^2 u_n)\right\} \tag{5g}$$

$$F_{rn}(\sigma) = -D\left\{\frac{\partial}{\partial r}(\nabla^2 u_n)\right\} \tag{5h}$$

Equation (3) simplifies to

$$\nabla^2\left[\nabla^2 - i\left(\frac{\sqrt{12(1-\nu^2)}}{Rh}\right)\right]V = \nabla^2\left[\nabla^2 - i\lambda^2\right]V = p_n/D \tag{6}$$

where

$$\lambda^2 = \sqrt{12(1-\nu^2)}/Rh$$

The solution of **(6)** can be expressed by superposition of three particular solutions

$$V = V_o + V_1 + V_2$$

where V_o is a solution corresponding to the normal pressure p_n, and V_o, V_1, V_2 are given by the equations

$$\nabla^2\left[\nabla^2 - i\lambda^2\right]V = \nabla^2\left[\nabla^2 - i\lambda^2\right](V_o + V_1 + V_2) = \nabla^2\left[\nabla^2 - i\lambda^2\right]V_o$$

$$+\left[\nabla^2 - i\lambda^2\right]\nabla^2 V_1 + \nabla^2\left[\nabla^2 V_2 - i\lambda^2 V_2\right] = p_n/D$$

which can be satisfied by imposing the particular conditions

$$\nabla^2[\nabla^2 - i\lambda^2]V_o = \frac{p_n}{D} \tag{7a}$$

$$[\nabla^2 - i\lambda^2]\nabla^2 V_1 = \nabla^2 V_1 = 0 \tag{7b}$$

$$\nabla^2 V_2 - i\lambda^2 V_2 = 0 \tag{7c}$$

Solutions for the type of equations (7b), (7c) can be assumed in Daniel BERNOULLI's Semi-Direct form.

$$V_1 = \sum_{n=0}^{\infty} V_n^1(r)\begin{Bmatrix}\cos(n\theta)\\ \sin(n\theta)\end{Bmatrix}$$

$$V_2 = \sum_{n=0}^{\infty} V_n^2(r)\begin{Bmatrix}\cos(n\theta)\\ \sin(n\theta)\end{Bmatrix}$$

which reduces the partial differential equations into ordinary differential equations. For rotationally periodic deformation problems the cosine series constitutes the appropriate solutions. Substitution of V_1 in equation (7b) yields for n = 0 a solution

$$V_n^1(r) = A_o + B_o \ln(\lambda r)$$

and for $n = m \geq 1$ a solution

$$V_m^1(r) = C_m r^m + D_m r^{-m}$$

The complete solution for V_1 related to the cosine term is

$$V_1 = A_o + B_o \ln(\lambda r) + \sum_{n=1}^{\infty}\left[C_n r^n + D_n r^{-n}\right]\cos(n\theta) \tag{8}$$

Inserting the assumed solution V_2 into (7c) furnishes the ordinary differential equation in v_n^2 as

$$r^2 \frac{d^2 V_n^2}{dr^2} + r \frac{dV_n^2}{dr} - \left[i(\lambda r)^2 + n^2 \right] V_n^2 = 0$$

The solution of this modified Bessels equation is

$$V_n^2 = F_n I_n(i^{1/2} \lambda r) + G_n K_n(i^{1/2} \lambda r)$$

where F_n, G_n are integration constants, and I_n, K_n represent Modified Bessel Functions (see McLACHLAN in 1955). This solution, in turn, can be expressed in terms of Kelvin Functions of the n-th order

$$V_n^2 = F_n \left[ber_n(\lambda r) + i\, bei_n(\lambda r) \right] + G_n \left[Ker_n(\lambda r) + i\, Kei_n(\lambda r) \right] \qquad (9)$$

if it is observed that the Modified BESSEL Functions of the First Kind

$$I_n(i^{1/2} \lambda r) = \left[ber_n(\lambda r) + i\, bei_n(\lambda r) \right] e^{-\frac{1}{2} n \pi i}$$

and the Modified BESSEL Functions of the Second Kind

$$K_n(i^{1/2} \lambda r) = \left[ker_n(\lambda r) + kei_n(\lambda r) \right] i^n$$

The complete solution for V_2 is

$$V_2 = \sum_{n=0}^{\infty} V_n^2 \cos(n\theta) = F_o \left[ber(\lambda r) + i\, bei(\lambda r) \right] + G_o \left[Ker(\lambda r) + i Kei(\lambda r) \right]$$

$$+ \sum_{n=1}^{\infty} \left\{ F_n \left[ber_n(\lambda r) + i\, bei_n(\lambda r) \right] + G_n \left[Ker_n(\lambda r) + i Kei_n(\lambda r) \right] \right\} \cos(n\theta) \qquad (10)$$

All arbitrary constants in the solution of V are taken to be complex. The particular solution can easily be determined for symmetric normal

pressure $\bar{p} = p_n \bar{e}_n$ by assuming V_o to be a complex quadratic polynomial

$$V_o = V_o(r) = (a_o + a_1 r + a_2 r^2) + i\omega(b_o + b_1 r + b_2 r^2)$$

Then

$$\nabla^2[\nabla^2 - i\lambda^2]V_o(r) = \nabla^4 V_o(r) - i\lambda^2 \nabla^2 V_o(r) = p_n/D$$

and substituting for $V_o(r)$ yields

$$-i\lambda^2\left[4a_2 + \frac{a_1}{r}\right] + \lambda^2\omega\left[4b_2 + \frac{b_1}{r}\right] = p_n/D = p_n \frac{12(1-\nu^2)}{Eh^3}$$

which is satisfied if

$$4a_2 + \frac{a_1}{r} = 0 \qquad \therefore a_1 = a_2 = 0$$

$$4b_2 + \frac{b_1}{r} = \frac{p_n}{D\lambda^2\omega} \qquad \therefore b_1 = 0\,,\ b_2 = \frac{p_n}{4D\lambda^2\omega} = \frac{p_n R}{4}$$

The solution is

$$V_o = V_o(r) = a_o + i\omega \frac{p_n R r^2}{4} = \frac{p_n R^2}{Eh} + i\omega \frac{p_n R r^2}{4}$$

$$= u_o + i\omega \Phi$$

where for convenience the constant normal displacement for the momentless theory is used, i.e.

$$a_o = u_o = \frac{p_n R^2}{Eh}$$

IV - 2(b) General Solution

Insertion of the complex integration constants and particular

solution into the general solution for V yields

$$V = V_0 + V_1 + V_2$$

$$= \left\{ \frac{p_n R^2}{Eh} + A_0' \, ber(\lambda r) + A_0^2 \, bei(\lambda r) + B_0' \, Ker(\lambda r) + B_0^2 \, Kei(\lambda r) \right.$$

$$+ F_0' \ln(\lambda r) + E_0' + \sum_{n=1}^{\infty} \left[A_n' \, ber_n(\lambda r) + A_n^2 \, bei_n(\lambda r) + B_n' \, Ker_n(\lambda r) \right.$$

$$\left. \left. + B_n^2 \, Kei(\lambda r) + C_n' r^n + D_n' r^{-n} \right] \cos(n\theta) \right\} + i \left\{ \omega \frac{p_n R r^2}{Eh} + A_0' \, bei(\lambda r) \right.$$

$$- A_0^2 \, ber(\lambda r) + B_0' \, Kei(\lambda r) - B_0^2 \, Ker(\lambda r) + F_0^2 \ln(\lambda r) + E_0^2$$

$$\left. + \sum_{n=1}^{\infty} \left[A_n' \, bei_n(\lambda r) - A_n^2 \, ber_n(\lambda r) + B_n' \, Kei_n(\lambda r) - B_n^2 \, Ker_n(\lambda r) + C_n^2 r^n + D_n^2 r^{-n} \right] \cos(n\theta) \right\}$$

The final solution in terms of the basic parameters u_n, Φ can be obtained by imposing the conditions (4).

$$u_n = \frac{p_n R^2}{Eh} + A_0' \, ber(\lambda r) + A_0^2 \, bei(\lambda r) + B_0' \, Ker(\lambda r) + B_0^2 \, Kei(\lambda r)$$

$$+ F_0' \ln(\lambda r) + E_0' + \sum_{n=1}^{\infty} \left[A_n' \, ber_n(\lambda r) + A_n^2 \, bei_n(\lambda r) + B_n' \, Ker_n(\lambda r) \right.$$

$$\left. + B_n^2 \, Kei_n(\lambda r) + C_n' r^n + D_n' r^{-n} \right] \cos(n\theta) \qquad (11a)$$

$$\Phi = \frac{p_n R r^2}{4} + \frac{1}{\omega} \left\{ A_0' \, bei(\lambda r) - A_0^2 \, ber(\lambda r) + B_0' \, Kei(\lambda r) - B_0^2 \, Ker(\lambda r) \right.$$

$$+ F_0^2 \ln(\lambda r) + E_0^2 + \sum_{n=1}^{\infty} \left[A_n' \, bei_n(\lambda r) - A_n^2 \, ber_n(\lambda r) + B_n' \, Kei_n(\lambda r) \right.$$

$$\left. \left. - B_n^2 \, Ker_n(\lambda r) + C_n^2 r^n + D_n^2 r^{-n} \right] \cos(n\theta) \right\} \qquad (11b)$$

IV - 3 Boundary Condition Relevant to a Closed Spherical Calotte Shell Over a Hexagonal Base

It is assumed that an uncoupling of boundary effects is possible for this thin shell since the shell possesses no inner boundary. Because of the singular nature of $\ker_n(x)$, $\mathrm{kei}_n(x)$, and r^{-n} at the origin, they are irrelevant for the shell problem under investigation and can be eliminated from the solution by setting $B_n^1 = B_n^2 = D_n^1 = D_n^2 = 0$. This shallow spherical shell, which is subjected to rotationally symmetric loading, encloses a base of a regular hexagonal configuration, and its state of stress and strain acquires a similar hexagonal periodicity about the axis of rotation of the shell. Accordingly, the stress and displacement function of such a spherical calotte shell of hexagonal base exhibit similar characteristics of 6-fold periodicity. Therefore

$$U_n = \frac{P_n R^2}{Eh} + A_0^2\,\mathrm{bei}(\lambda r) + A_0'\,\mathrm{ber}(\lambda r) + E_0' + \sum_{n=1}^{\infty}\left[A_{6n}^2\,\mathrm{bei}_{6n}(\lambda r) + A_{6n}'\,\mathrm{ber}_{6n}(\lambda r) + C_{6n}'\,r^{6n}\right]\cos(6n\theta) \tag{12a}$$

$$\Phi = \frac{P_n R r^2}{4} + \frac{1}{\omega}\left\{A_0'\,\mathrm{bei}(\lambda r) - A_0^2\,\mathrm{ber}(\lambda r) + \sum_{n=1}^{\infty}\left[A_{6n}'\,\mathrm{bei}_{6n}(\lambda r) - A_{6n}^2\,\mathrm{ber}_{6n}(\lambda r) + C_{6n}^2\,r^{6n}\right]\cos(6n\theta)\right\} \tag{12b}$$

IV - 4 Satisfaction of Boundary Conditions by TÖLKE's Collocation Method

An exact solution of the edge restraint for spherical shells over

polygonal base is for practical purposes quite impossible since the boundary of the shell does not coincide with the co-ordinate system, and therefore it is necessary to use the method of point collocation to achieve at least point by point satisfaction of the prescribed boundary conditions. This collocation method for surface structures was originated by Friedrich TÖLKE in 1934 in an approximate solution of the transverse flexure of a continuous plate directly supported over equidistant columns. The following boundary conditions seemed best suited to describe a reasonable edge behaviour for the calotte shell under investigation:

at $r = \tilde{r}$

$$F_{nn}(\sigma) = 0 \tag{13}$$

$$\delta\left(\frac{\partial u_n}{\partial n}\right) = 0 \tag{14}$$

$$u_n = 0 \tag{15}$$

$$\epsilon_{ss} = 0 \tag{16}$$

where

$\tilde{r}$ designates the cylindrical radius to the collocation point on the boundary

and ϵ_{ss} denotes the strain tangential to the boundary member of the shell.

IV - 4(a) Boundary Condition $F_{nn}(\sigma) = 0$

By definition the stress resultant per unit length of boundary is

$$F_{nn}(\sigma) = \int_{-h/2}^{+h/2} \sigma_{nn}\, d\alpha_n = \int_{-h/2}^{h/2} \bar{n}\bar{n} : \bar{\bar{\sigma}}\, d\alpha_n$$

$$= (\bar{n}.\bar{e}_i)(\bar{n}.\bar{e}_j) \int_{-h/2}^{+h/2} \sigma_{ij}\, d\alpha_n \qquad (i,j = r,\theta,n)$$

$$= (\bar{n}.\bar{e}_i)(\bar{n}.\bar{e}_j)\, F_{ij}(\sigma)$$

$$= (\bar{n}.\bar{e}_r)(n.e_r)\, F_{rr}(\sigma) + 2(\bar{n}.\bar{e}_r)(\bar{n}.\bar{e}_\theta)\, F_{r\theta}(\sigma) + (\bar{n}.\bar{e}_\theta)(\bar{n}.\bar{e}_\theta)\, F_{\theta\theta}(\sigma)$$

Using (see Figure 33a)

$$\bar{n}.\bar{e}_\theta = \cos \xi_{n\theta} = \cos\left(\frac{\pi}{2} - \xi\right) = \sin \xi$$

$$\bar{n}.\bar{e}_r = \cos \xi_{nr} = \cos \xi$$

For the particular boundary under consideration (Figure 33b)

$$\xi = -\theta$$

Consequently

$$F_{nn}(\sigma) = F_{rr}(\sigma)\cos^2\theta - 2F_{r\theta}(\sigma)\sin\theta\cos\theta + F_{\theta\theta}(\sigma)\sin^2\theta$$

Inserting the fundamental stress function (5) yields

$$F_{nn}(\sigma) = \left[\frac{1}{r^2}\frac{\partial^2\Phi}{\partial\theta^2} + \frac{1}{r}\frac{\partial\Phi}{\partial r}\right]\cos^2\theta + \left[\frac{\partial^2\Phi}{\partial r^2}\right]\sin^2\theta + \frac{\partial}{\partial r}\left(\frac{1}{r}\frac{\partial\Phi}{\partial\theta}\right)\sin 2\theta = 0 \qquad (13a)$$

IV - 4(b) Variation of Boundary Slope $\delta\left(\frac{\partial u_n}{\partial n}\right) = 0$

The kinematic rotation of the co-ordinate lines with $\bar{u} \doteq u_n \bar{e}_n$

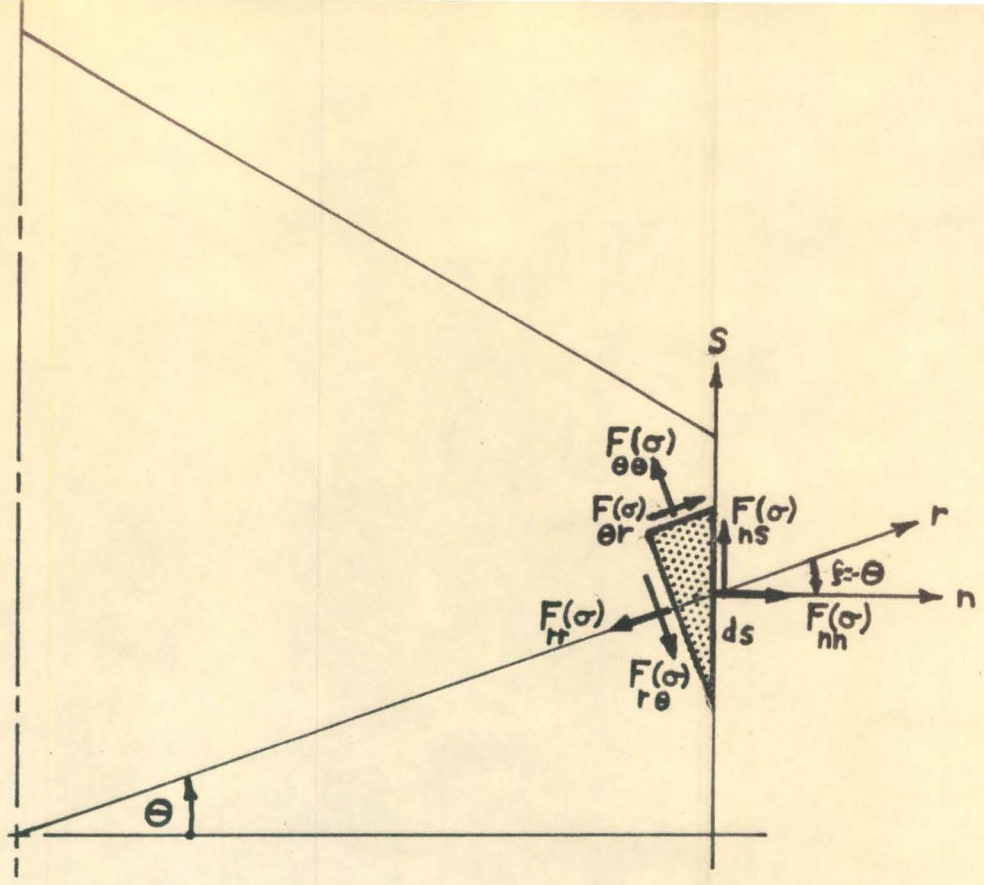

(b) STRESS RESULTANTS ACTING AT BOUNDARY OF SHELL OVER HEXAGONAL BASE

NOTE: The Directional Qualities of Vectors in Fig. 33 are Graphically Depicted.

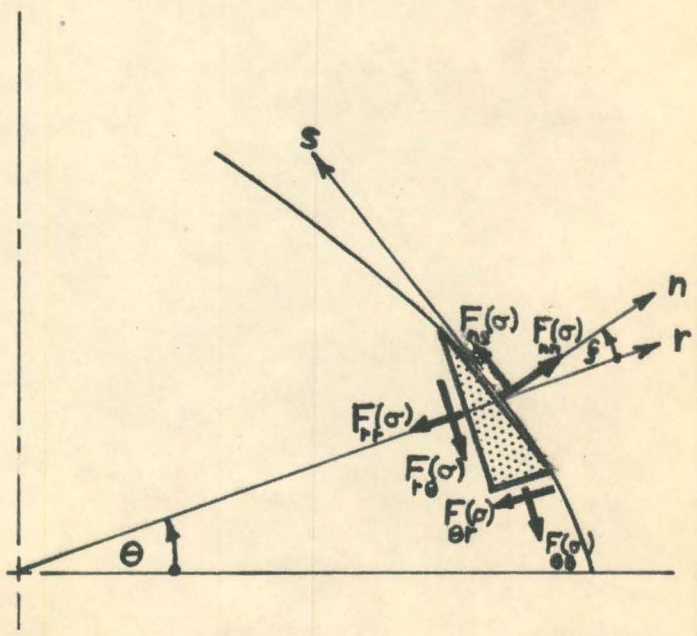

(a) STRESS RESULTANTS ACTING AT BOUNDARY OF SHELL

FIGURE 33

is

$$\delta\bar{\Phi}_\theta = \bar{e}_r \times \frac{\partial \bar{u}}{\partial r} = \bar{e}_r \times \frac{\partial u_n}{\partial r} + \bar{e}_r \times u_n \frac{\partial \bar{e}_n}{\partial r}$$

$$= (\bar{e}_r \times e_n) \frac{\partial u_n}{\partial r} + (\bar{e}_r \times \bar{e}_r) u_n$$

$$= -\frac{\partial u_n}{\partial r} \bar{e}_\theta$$

and

$$\delta\bar{\Phi}_r = \bar{e}_\theta \times \frac{1}{r} \frac{\partial \bar{u}}{\partial \theta} = \bar{e}_\theta \times \frac{1}{r} \frac{\partial u_n}{\partial \theta} \bar{e}_n + \bar{e}_\theta \times \frac{u_n}{r} \frac{\partial \bar{e}_n}{\partial \theta}$$

$$= (\bar{e}_\theta \times \bar{e}_n) \frac{\partial u_n}{\partial \theta}$$

$$= \frac{1}{r} \frac{\partial u_n}{\partial \theta} \bar{e}_r$$

Consequently, the variation of boundary rotation <u>about</u> s is

$$\delta\Phi_s = \delta\left(\frac{\partial u_n}{\partial n}\right) = \frac{\partial u_n}{\partial n} = \bar{e}_s \cdot (\delta\bar{\Phi}_r + \delta\bar{\Phi}_\theta)$$

$$= -\frac{\partial u_n}{\partial r} (\bar{e}_s \cdot \bar{e}_\theta) + \frac{1}{r} \frac{\partial u_n}{\partial \theta} (\bar{e}_s \cdot \bar{e}_r)$$

for

$$\bar{e}_s = \cos\xi\, \bar{e}_\theta - \sin\xi\, \bar{e}_r$$

$$\therefore \quad \delta\left(\frac{\partial u_n}{\partial n}\right) = -\frac{\partial u_n}{\partial r} \cos\xi - \frac{1}{r} \frac{\partial u_n}{\partial \theta} \sin\xi$$

For the shell under investigation $\xi = -\theta$

$$\therefore\ \delta\left(\frac{\partial u_n}{\partial n}\right) = -\frac{\partial u_n}{\partial r}\cos\theta + \frac{1}{r}\frac{\partial u_n}{\partial \theta}\sin\theta \qquad (14a)$$

IV - 4(c) Strain Tangential to Boundary $\epsilon_{ss} = 0$

Since the edge members of the boundary of the shell have quite substantial cross sections in comparison with the shell, it was assumed that very little strain would develop in the $\bar{e}_s$ direction at the boundary member, where the shell and edge beam were metal-bonded together.

The middle surface strain tensor is

$$\bar{\bar{\epsilon}}(\bar{r}_o) = \left[\epsilon_{rr}\bar{e}_r\bar{e}_r + \epsilon_{r\theta}\bar{e}_r\bar{e}_\theta + \epsilon_{\theta r}\bar{e}_\theta\bar{e}_r + \epsilon_{\theta\theta}\bar{e}_\theta\bar{e}_\theta\right]$$

where (see Appendix A)

$$\epsilon_{rr} = \frac{1}{Eh}\left(F_{rr}(\sigma) - \nu F_{\theta\theta}(\sigma)\right)$$

$$\epsilon_{\theta\theta} = \frac{1}{Eh}\left(F_{\theta\theta}(\sigma) - \nu F_{rr}(\sigma)\right)$$

$$\epsilon_{r\theta} = \frac{(1+\nu)}{Eh}F_{r\theta}(\sigma)$$

then

$$\epsilon_{ss} = \bar{e}_s\bar{e}_s : \bar{\bar{\epsilon}} = \bar{e}_s \cdot \left[\epsilon_{rr}\bar{e}_r(\bar{e}_r\cdot\bar{e}_s) + \epsilon_{r\theta}e_r(\bar{e}_\theta\cdot\bar{e}_s) + \epsilon_{\theta r}\bar{e}_\theta(\bar{e}_r\cdot\bar{e}_s) + \epsilon_{\theta\theta}\bar{e}_\theta(\bar{e}_\theta\cdot\bar{e}_s)\right]$$

$$= \epsilon_{rr}(\bar{e}_r\cdot\bar{e}_s)^2 + 2\epsilon_{r\theta}(\bar{e}_r\cdot\bar{e}_s)(\bar{e}_\theta\cdot\bar{e}_s) + \epsilon_{\theta\theta}(\bar{e}_\theta\cdot\bar{e}_s)^2$$

where $\epsilon_{r\theta} \doteq \epsilon_{\theta r}$ for shallow shells.

Substituting for $\bar{\epsilon}_s$ yields

$$\epsilon_{ss} = \epsilon_{rr} \sin^2\xi + \epsilon_{\theta\theta} \cos^2\xi - 2\epsilon_{r\theta} \sin\xi \cos\xi$$

Again, for the shell under investigation $\xi = -\theta$, thus

$$\epsilon_{ss} = \epsilon_{rr} \sin^2\theta + \epsilon_{r\theta} \sin 2\theta + \epsilon_{\theta\theta} \cos^2\theta$$

Expressing strains in terms of stress resultants and utilizing VLASOV's Force Function Φ (5) yields

$$Eh\,\epsilon_{ss} = \left[\frac{1}{r}\frac{\partial\Phi}{\partial r} + \frac{1}{r^2}\frac{\partial^2\Phi}{\partial\theta^2} - \nu\frac{\partial^2\Phi}{\partial r^2}\right]\sin^2\theta + \left[\frac{\partial^2\Phi}{\partial r^2} - \nu\left(\frac{1}{r}\frac{\partial\Phi}{\partial r} + \frac{1}{r^2}\frac{\partial^2\Phi}{\partial\theta^2}\right)\right]\cos^2\theta$$

$$-\left[(1+\nu)\frac{\partial}{\partial r}\left(\frac{1}{r}\frac{\partial\Phi}{\partial r}\right)\right]\sin 2\theta = 0 \qquad (16a)$$

IV - 4(d) Collective Boundary Conditions

Substituting the fundamental solutions of u_n and Φ (12a, 12b) in the boundary conditions 13a, 14a, 15 and 16a delivers the linear equations

$$A_o^1\psi_1 + A_o^2\psi_2 + \sum_{n=1}^{\infty}\left[A_{6n}^1\psi_3 + A_{6n}^2\psi_4 + C_{6n}^2\psi_5\right] = \frac{-p_n R}{2} \qquad (13b)$$

$$A_o^1\psi_6 + A_o^2\psi_7 + \sum_{n=1}^{\infty}\left[A_{6n}^1\psi_8 + A_{6n}^2\psi_9 + C_{6n}^1\psi_{10}\right] = 0 \qquad (14b)$$

$$A_o^1\psi_{11} + A_o^2\psi_{12} + E_o^1 + \sum_{n=1}^{\infty}\left[A_{6n}^1\psi_{13} + A_{6n}^2\psi_{14} + C_{6n}^2 U_{15}\right] = \frac{-p_n R^2}{Eh} \qquad (15b)$$

$$A_o^1\psi_{16} + A_o^2\psi_{17} + \sum_{n=1}^{\infty}\left[A_{6n}^1\psi_{18} + A_{6n}^2\psi_{19} + C_{6n}^2\psi_{20}\right] = -(1-\nu)\frac{P_n R}{2} \qquad (16b)$$

The coefficients in the boundary conditions are given by

$$\psi_1 = \frac{1}{\omega}\left(\frac{\lambda}{\tilde{r}}\right)\mathrm{bei}'(\mu)\cos^2\tilde{\theta} + \frac{\lambda^2}{\omega}\mathrm{bei}''(\mu)\sin^2\tilde{\theta}$$

$$\psi_2 = -\frac{1}{\omega}\left(\frac{\lambda}{\tilde{r}}\right)\mathrm{ber}'(\mu)\cos^2\tilde{\theta} + \frac{\lambda^2}{\omega}\mathrm{ber}''(\mu)\sin^2\tilde{\theta}$$

$$\psi_3 = \left\{\left[\frac{1}{\omega}\left(\frac{\lambda}{\tilde{r}}\right)\mathrm{bei}_{6n}'(\mu) - \frac{1}{\omega}\left(\frac{6n}{\tilde{r}}\right)^2\mathrm{bei}_{6n}(\mu)\right]\cos^2\tilde{\theta} + \left[\frac{\lambda^2}{\omega}\mathrm{bei}_{6n}''(\mu)\right]\sin^2\tilde{\theta}\right\}\cos 6n\tilde{\theta}$$

$$+ \left\{\left[-\frac{6n}{\omega}\left(\frac{\lambda}{\tilde{r}}\right)\mathrm{bei}_{6n}'(\mu) + \frac{6n}{\omega}\frac{1}{\tilde{r}^2}\mathrm{bei}_{6n}(\mu)\right]\sin 2\tilde{\theta}\right\}\sin 6n\tilde{\theta}$$

$$\psi_4 = \left\{\left[-\frac{1}{\omega}\left(\frac{\lambda}{\tilde{r}}\right)\mathrm{ber}_{6n}'(\mu) + \frac{1}{\omega}\left(\frac{6n}{\tilde{r}}\right)^2\mathrm{ber}_{6n}(\mu)\right]\cos^2\tilde{\theta} - \left[\frac{\lambda^2}{\omega}\mathrm{ber}_{6n}''(\mu)\right]\sin^2\tilde{\theta}\right\}\cos 6n\tilde{\theta}$$

$$+ \left\{\left[\frac{6n}{\omega}\left(\frac{\lambda}{\tilde{r}}\right)\mathrm{ber}_{6n}'(\mu) - \frac{6n}{\omega}\frac{1}{\tilde{r}^2}\mathrm{ber}_{6n}(\mu)\right]\sin 2\tilde{\theta}\right\}\sin 6n\tilde{\theta}$$

$$\psi_5 = \tilde{r}^{6n-2}\frac{6n(6n-1)}{\omega}\left[\left(\sin^2\tilde{\theta} - \cos^2\tilde{\theta}\right)\cos 6n\tilde{\theta} - \sin 2\tilde{\theta}\sin 6n\tilde{\theta}\right]$$

$$\psi_6 = -\lambda\, \mathrm{ber}'(\mu)\cos\tilde{\theta}$$

$$\psi_7 = -\lambda\, \mathrm{bei}'(\mu)\cos\tilde{\theta}$$

$$\psi_8 = -\left[\lambda\, \mathrm{ber}'_{6n}(\mu)\cos\tilde{\theta}\right]\cos 6n\tilde{\theta} - \left[\frac{6n}{\tilde{r}}\,\mathrm{ber}_{6n}(\mu)\sin\tilde{\theta}\right]\sin 6n\tilde{\theta}$$

$$\psi_9 = -\left[\lambda\, \mathrm{bei}'_{6n}(\mu)\cos\tilde{\theta}\right]\cos 6n\tilde{\theta} - \left[\frac{6n}{\tilde{r}}\,\mathrm{bei}_{6n}(\mu)\sin\tilde{\theta}\right]\sin 6n\tilde{\theta}$$

$$\psi_{10} = -\left[6n\tilde{r}^{\,6n-1}\cos\tilde{\theta}\right]\cos 6n\tilde{\theta} - \left[6n\tilde{r}^{\,6n-1}\sin\tilde{\theta}\right]\sin 6n\tilde{\theta}$$

$$\psi_{11} = \mathrm{ber}(\mu)$$

$$\psi_{12} = \mathrm{bei}(\mu)$$

$$\psi_{13} = \mathrm{ber}_{6n}(\mu)\cos 6n\tilde{\theta}$$

$$\psi_{14} = \mathrm{bei}_{6n}(\mu)\cos 6n\tilde{\theta}$$

$$\psi_{15} = \tilde{r}^{\,6n}\cos 6n\tilde{\theta}$$

$$\psi_{16} = \left[\frac{1}{\omega}\left(\frac{\lambda}{\tilde{r}}\right)\mathrm{bei}'(\mu) - \nu\frac{\lambda^2}{\omega}\,\mathrm{bei}''(\mu)\right]\sin^2\tilde{\theta} + \left[\frac{\lambda^2}{\omega}\,\mathrm{bei}''(\mu) - \frac{\nu}{\omega}\left(\frac{\lambda}{\tilde{r}}\right)\mathrm{bei}'(\mu)\right]\cos^2\tilde{\theta}$$

$$\psi_{17} = \left[\nu\frac{\lambda^2}{\omega}\,\mathrm{ber}''(\mu) - \frac{1}{\omega}\left(\frac{\lambda}{\tilde{r}}\right)\mathrm{ber}'(\mu)\right]\sin^2\theta + \left[\frac{\nu}{\omega}\left(\frac{\lambda}{\tilde{r}}\right)\mathrm{ber}'(\mu) - \frac{\lambda^2}{\omega}\,\mathrm{ber}''(\mu)\right]\cos^2\tilde{\theta}$$

$$\psi_{18} = \left\{\left[\frac{1}{\omega}\left(\frac{\lambda}{\tilde{r}}\right)\mathrm{bei}'_{6n}(\mu) - \frac{1}{\omega}\left(\frac{6n}{\tilde{r}^2}\right)^2\mathrm{bei}_{6n}(\mu) - \nu\frac{\lambda^2}{\omega}\,\mathrm{bei}''_{6n}(\mu)\right]\sin^2\tilde{\theta}\right.$$
$$\left. + \left[\frac{\lambda^2}{\omega}\,\mathrm{bei}''_{6n}(\mu) - \frac{\nu}{\omega}\left(\frac{\lambda}{\tilde{r}}\right)\mathrm{bei}'_{6n}(\mu) + \frac{\nu}{\omega}\left(\frac{6n}{\tilde{r}}\right)^2\mathrm{bei}_{6n}(\mu)\right]\cos^2\tilde{\theta}\right\}\cos 6n\tilde{\theta}$$
$$+ \left\{(1+\nu)\frac{6n}{\omega}\left[\left(\frac{\lambda}{\tilde{r}}\right)\mathrm{bei}'_{6n}(\mu) - \frac{1}{\tilde{r}^2}\,\mathrm{bei}_{6n}(\mu)\right]\sin 2\tilde{\theta}\right\}\sin 6n\tilde{\theta}$$

$$\psi_{19} = \left\{\left[-\frac{1}{\omega}\left(\frac{\lambda}{\tilde{r}}\right) ber'_{6n}(\mu) + \frac{1}{\omega}\left(\frac{6n}{\tilde{r}}\right)^2 ber_{6n}(\mu) + \nu\frac{\lambda^2}{\omega} ber''_{6n}(\mu)\right] \sin^2\tilde{\theta}\right.$$
$$\left. + \left[-\frac{\lambda^2}{\omega} ber''(\mu) + \frac{\nu}{\omega}\left(\frac{\lambda}{\tilde{r}}\right) ber'_{6n}(\mu) - \frac{\nu}{\omega}\left(\frac{6n}{\tilde{r}}\right)^2 ber_{6n}(\mu)\right]\cos^2\tilde{\theta}\right\}\cos 6n\tilde{\theta}$$
$$- \left\{(1+\nu)\frac{6n}{\omega}\left[-\frac{1}{\tilde{r}^2} ber_{6n}(\mu) + \frac{\lambda}{\tilde{r}} ber'_{6n}(\mu)\right]\sin 2\tilde{\theta}\right\}\sin 6n\tilde{\theta}$$

$$\psi_{20} = \frac{1+\nu}{\omega} 6n(6n-1)\tilde{r}^{6n-2}\left[\left(\cos^2\tilde{\theta} - \sin^2\tilde{\theta}\right)\cos 6n\tilde{\theta} + \sin 2\tilde{\theta}\,\sin 6n\tilde{\theta}\right]$$

For shells of arbitrary boundary set $\tilde{\xi} = -\tilde{\theta}$ and $kn\tilde{\theta} = 6n\tilde{\theta}$.

Here ($\mu = \lambda\tilde{r}$) $\tilde{r}$, $\tilde{\theta}$ are the co-ordinates of collocation points and $ber'_{6n}(\mu)$, $ber''_{6n}(\mu)$ indicate first and second derivatives of KELVIN functions of 6n-th order with respect to μ. Second derivatives of KELVIN Functions can be expressed by

$$ber''_{6n}(\mu) = -\frac{1}{\mu} ber'_{6n}(\mu) + \left(\frac{6n}{\mu}\right)^2 ber_{6n}(\mu) - bei_{6n}(\mu)$$

$$bei''_{6n}(\mu) = -\frac{1}{\mu} bei'_{6n}(\mu) + \left(\frac{6n}{\mu}\right)^2 bei_{6n}(\mu) + ber_{6n}(\mu)$$

The sectional stress resultants (5) can be expressed in terms of the fundamental solutions 12a, 12b. Only the results for $F_{rr}(\sigma)$, $F_{\theta\theta}(\sigma)$, $M_{r\theta}(\sigma)$ and $M_{\theta r}(\sigma)$ are given here:

$$F_{rr}(\sigma) = \frac{P_n R}{2} + A^1_o\left[\frac{\lambda}{\omega}\frac{1}{r} bei'(\lambda r)\right] - A^2_o\left[\frac{\lambda}{\omega}\frac{1}{r} ber'(\lambda r)\right]$$
$$+ \sum_{n=1}^{\infty}\left\{A^1_{6n}\left[-\frac{1}{\omega}\left(\frac{6n}{r}\right)^2 bei_{6n}(\lambda r) + \frac{\lambda}{\omega}\frac{1}{r} bei'_{6n}(\lambda r)\right] + A^2_{6n}\left[\frac{1}{\omega}\left(\frac{6n}{r}\right)^2 ber_{6n}(\lambda r)\right.\right.$$

$$-\frac{\lambda}{\omega}\frac{1}{r}\,\mathrm{ber}_{6n}'(\lambda r)\Big] + C_{6n}^{2}\,\frac{6n(6n-1)}{\omega}\,r^{6n-2}\Big\}\cos 6n\theta \tag{17}$$

$$F_{\theta\theta}(\sigma) = \frac{P_n R}{2} + A_o^1\Big[\frac{\lambda^2}{\omega}\,\mathrm{bei}''(\lambda r)\Big] - A_o^2\Big[\frac{\lambda^2}{\omega}\,\mathrm{ber}''(\lambda r)\Big] + \sum_{n=1}^{\infty}\Big\{A_{6n}'\Big[\frac{\lambda^2}{\omega}\,\mathrm{bei}_{6n}(\lambda r)\Big]$$

$$- A_{6n}^{2}\Big[\frac{\lambda^2}{\omega}\,\mathrm{ber}_{6n}''(\lambda r)\Big] + C_{6n}^{2}\Big[\frac{6n(6n-1)}{\omega}\,r^{6n-2}\Big]\Big\}\cos 6n\theta \tag{18}$$

$$M_{r\theta}(\sigma) = D\Big\{-A_o'\Big[\lambda^2\,\mathrm{ber}''(\lambda r) + \nu\frac{\lambda}{r}\,\mathrm{ber}'(\lambda r)\Big] - A_o^2\Big[\lambda^2\,\mathrm{bei}''(\lambda r) + \nu\frac{\lambda}{r}\,\mathrm{bei}'(\lambda r)\Big]$$

$$+\sum_{n=1}^{\infty}\Big[A_{6n}'\Big(-\lambda^2\,\mathrm{ber}_{6n}''(\lambda r) + \nu\Big(\frac{6n}{r}\Big)^2\mathrm{ber}_{6n}(\lambda r) - \nu\frac{\lambda}{r}\,\mathrm{ber}_{6n}'(\lambda r)\Big)$$

$$+ A_{6n}^{2}\Big(-\lambda^2\,\mathrm{bei}_{6n}''(\lambda r) + \nu\Big(\frac{6n}{r}\Big)^2\mathrm{bei}_{6n}(\lambda r) - \nu\frac{\lambda}{r}\,\mathrm{bei}_{6n}'(\lambda r)\Big)$$

$$- C_{6n}'(1-\nu)6n(6n-1)r^{6n-2}\Big]\cos 6n\theta\Big\} \tag{19}$$

$$M_{\theta r}(\sigma) = D\Big\{A_o'\Big[\frac{\lambda}{r}\,\mathrm{ber}'(\lambda r) + \nu\lambda^2\,\mathrm{ber}''(\lambda r)\Big] + A_o^2\Big[\frac{\lambda}{r}\,\mathrm{bei}'(\lambda r) + \nu\lambda^2\,\mathrm{bei}''(\lambda r)\Big]$$

$$+\sum_{n=1}^{\infty}\Big[A_{6n}'\Big(-\Big(\frac{6n}{r}\Big)^2\mathrm{ber}_{6n}(\lambda r) + \frac{\lambda}{r}\,\mathrm{ber}_{6n}'(\lambda r) + \nu\lambda^2\,\mathrm{ber}_{6n}''(\lambda r)\Big)$$

$$+ A_{6n}^{2}\Big(-\Big(\frac{6n}{r}\Big)^2\mathrm{bei}_{6n}(\lambda r) + \frac{\lambda}{r}\,\mathrm{bei}_{6n}(\lambda r) + \nu\lambda^2\,\mathrm{bei}_{6n}''(\lambda r)\Big)$$

$$- C_{6n}^{2}(1-\nu)6n(6n-1)r^{6n-2}\Big]\cos 6n\theta\Big\} \tag{20}$$

IV - 5 Numerical Solution

In order to determine the number of terms to be used in any solution, the pattern of collocation points on the shell boundary must be established. It seems reasonable to assume that an increase in the number of boundary collocation points, with the corresponding satisfaction of all prescribed boundary conditions, increases the accuracy of the ultimate solution, yet this assertion is not strictly correct. Figure 34 illustrates the pattern of collocation points on the hexagonal boundary that was used in the approximate solution. It is to be noted that only half the boundary need be considered due to the symmetry about the radial line $\theta = 0^{\circ}$ of the cosine series solution in each sector.

From equations 13b to 16b, the number of terms in the solution series corresponding to three collocation points can be determined. It was decided to impose four boundary conditions for all the collocation points except the point located by $\theta = 30^{\circ}$, where only three conditions would be used. The strain ϵ_{ss}, being uncertain at the point $\theta = 30^{\circ}$ because of the boundary discontinuity (slit corner), certainly would not be negligible. TÖLKE's Boundary Collocation Method requires the use of the truncated series solution with n = 0, 1, 2 which contains eleven unknown coefficients, thus converting the boundary conditions 13b to 16b, into eleven simultaneous linear equations with eleven unknown constants. Since extensive numerical work was involved in the solution of this problem, it was expedient to resort to the use of the I.B.M. 7040 computer at the University.

The first difficulty was encountered in the evaluation of the KELVIN functions of higher orders. For instance, using three collocation

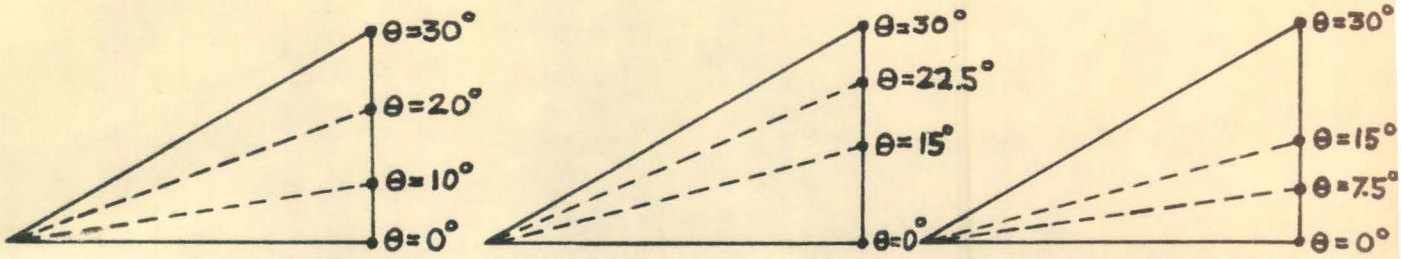

4 COLLOCATION POINTS

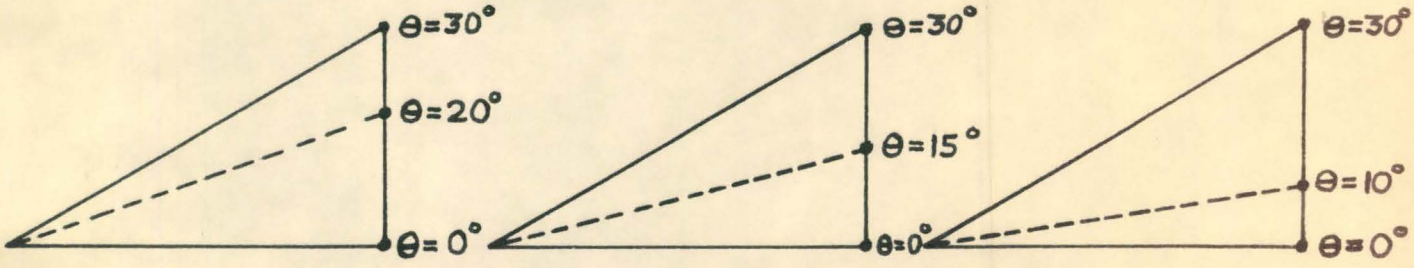

3 COLLOCATION POINTS

LOCATION OF BOUNDARY POINTS OF THE COLLOCATION METHOD

FIGURE 34

points, KELVIN functions up to order twelve were required. DWIGHT in 1957 gave the forward recurrence formulas for the calculation of KELVIN functions of any order, which can be readily set up on the computer and tabulated, but the accuracy of the values obtained was questionable especially for low arguments such as $\lambda r=1$. The range of λr in this shell was approximately $0 < \lambda r < 10$. It was found that by recurring to higher orders for the KELVIN functions $ber_n(x)$, $bei_n(x)$ with arguments $\lambda r < 1$, a linear combination of $ber_n\ x$, $ker_n\ x$ and $bei_n\ x$, $kei_n\ x$ resulted. The reason for this peculiar behaviour lies in the nature of the function $J_n(i^{3/2}z)$ where $z = x + iy$, which decreases exponentially for $n > z$. MICHELS in 1964 indicated that only for $n < z$ can good accuracy be obtained from forward recurrence techniques. As a result, reliable KELVIN functions of any given order could not be obtained from forward recurrence methods for the entire range of arguments. APPENDIX B describes MILLER's Method of Backward Recurrence by means of which this difficulty was overcome. It was found that the Backward Recurrence Method yielded consistent results for the entire scope of functional orders and arguments necessary for the number of collocation points used. The upper limit for the orders of KELVIN functions that could be calculated is determined by the capacity of the computer. Using single precision, KELVIN functions of order 25 could be accurately evaluated before floating point overflow occurred, i.e. before a number 10^{38} occurred in the calculations. Thus, the computer capacity established a practical limit on the number of collocation points that could be used in this method of solution, within which all functional values would still be reliable.

A program was initiated for the evaluation of the co-efficients

ψ_1 to ψ_{20}, the solution of the simultaneous linear boundary equations for the unknown coefficients of the truncated series solution, and, subsequently the evaluation of the stress resultants and stress couples given by Equations (17) to (20). Values of KELVIN functions for arguments could not be tabulated because of floating point overflow, thus the stress resultants and stress couples were calculated for a lower limit of $\lambda r = 1$.

The sectional quantities given by Equations (17) to (20), and the normal displacement function given by Equation 12a were calculated for the prescribed boundary conditions using the three and four collocation points shown in Figure 34. Initially, it was planned to try more collocation points, but due to floating point overflow in the computer for several of the coefficients pertaining to five collocation points, it was necessary to concentrate on various combinations of three and four points. All these calculations were based on a normal pressure $p_n = 20$ p.s.i.

IV - 6 Discussion of Results

The plan of the pattern of collocation points considered in the analysis of the calotte shell is shown in Figure 34. Comparative representations for the theoretical solution employing three collocation points and the experimental results are depicted in Figure 35 to Figure 38.

Figure 35 describes the distributions of experimental and theoretical stress resultant $F_{rr}^{(\sigma)}$ along the line $\theta = 20^\circ$. For a pattern of four collocation points a slightly better agreement is obtained near the boundary of the shell; this distribution has been inserted in Figure 35 for the sake of comparison.

Figure 36 illustrates the distribution of experimental and theoretical

stress resultant $F^{(\sigma)}_{\theta\theta}$ along the line $\theta = 20^{\circ}$. The similarities in the functional distributions of the theoretical and experimental results are observable.

Figure 37 represents the distribution of experimental and theoretical stress couple $M^{(\sigma)}_{r\theta}$ along the line $\theta = 0^{\circ}$. All these distributions are applicable for a normal load $p_n = 20$ p.s.i.

A greater discrepancy between the experimental and theoretical stress couples exists, and is due to the greater sensitivity of the theoretical solution to the truncation errors of the fundamental solution, as well as to the physical limitations of the experimental shell. The characteristics of the distributions of the theoretical and experimental curves are similar, yet their differences may be due to both the geometric imperfections in the experimental shell as well as to the finite character in the Boundary Collocation Procedure. In fact, throughout this analysis, it was found that the stress resultant system along the line $\theta = 30^{\circ}$ was considerably influenced by any change in the distribution of a given number of boundary points. A change in the location of collocation points seems to affect the circumferential stress resultant $F^{(\sigma)}_{\theta\theta}$ to a greater extent than the radial stress resultant $F^{(\sigma)}_{rr}$, as would be expected for this type of calotte shell. It can be observed that as the apex of the shell (axis of rotational symmetry) is approached the $n = 0$ terms, which are independent of the circumferential co-ordinate θ, begin to dominate the solution of the calotte shell problem, thus indicating the prevalence of rotationally symmetric behaviour of the shell in the proximity of the apex. This characteristic feature in the deformation

of the calotte shell is quite logical, for its periodically deviating boundary from the circular boundary is the direct cause of the disturbance from the rotationally symmetric behaviour of the spherical shell.

Greater variations in the stress resultants were obtained from redistributions of four collocation points than of three collocation points. For instance at the boundary, along the radial line $\theta = 0^{\circ}$, the redistribution of three collocation points induced a variation in the radial stress resultant from -60 lb/in to -80 lb/in., while a redistribution of four collocation points exhibited a corresponding variation from + 20 lb/in. to -85 lb/in. In general, this larger variation due to the redistribution of four, rather than three collocation points, is true for both stress resultants $F^{(\sigma)}_{rr}$ and $F^{(\sigma)}_{\theta\theta}$. Again, the largest variation in the stress resultants and stress couples for four collocation points occurs for the radial line $\theta = 30^{\circ}$.

In general, the location of collocation points has a more pronounced effect upon the stress couple distributions than on the stress resultant distributions, especially for the radial line $\theta = 30^{\circ}$. At the boundary of the radial line $\theta = 0^{\circ}$, the variation in the stress couple $M^{(\sigma)}_{r\theta}$ due to a redistribution of three collocation points is from + 91 lb in/in. to + 92 lb in/in., while due to a redistribution of four collocation points, the corresponding variation is considerably higher. A similar trend is noted in the stress couple $M^{(\sigma)}_{\theta r}$. This would seem to indicate that an increase in the number of collocation points does not necessarily increase the accuracy of any particular solution, since occasionally the location, rather than the number, of the collocation points can have a more critical influence upon the accuracy of the solution. The stress couples and stress

resultants corresponding to the solution employing three collocation points are shown in Figure 39 to Figure 42.

If the location of the collocation points are fixed, then the effect of an increase in the number of collocation points upon the solution can be considered. It was found that closer agreement to the experimental stress couple distributions was obtained by using three, rather than four, collocation points. Figure 27 shows the distribution of the experimental stress couple $M_{\theta r}(\sigma)$ along the radial line $\theta = 30^{\circ}$; this distribution was not closely matched by the theoretical solution shown in Figure 42. The stress couple $M_{\theta r}(\sigma)$ along this line for either three four collocation points remained negative at the boundary. This would seem to indicate that the stress concentration in the vicinity of the re-entrant slit corner affected the distribution of stress couple in a pronounced manner. Such was not the case for the stress couple $M_{r\theta}(\sigma)$ where the distribution along the radial line $\theta = 30^{\circ}$ had similar characteristics for experimental and theoretical solutions (see Figure 26 and Figure 41). The particular procedure of the collocation method seems to have a greater influence upon the solution in $\bar{e}_{\theta}$ direction, than on the solution in $\bar{e}_{r}$ direction. In view of the nature of the solution which replaces an infinite number of degrees of freedom system by a finite number of degrees of freedom system, this property of the solution is to be expected. In general, the effect of increasing the number of collocation points was not as pronounced on the solution of the direct stress resultants as on the solution of the stress couples.

Since the experimental results indicated a rotation of the edge member, it was decided to modify the previous calculations by including the rotational effect. In boundary condition (14) the right hand side was replaced by the angle of rotation in radians. The tendency of this rotation evidently reduces the magnitudes of the positive stress couples $M_{r\theta}^{(\sigma)}$ and $M_{\theta r}^{(\sigma)}$ at the boundary. The distributions for the modified stress couples $M_{r\theta}^{(\sigma)}$ and $M_{\theta r}^{(\sigma)}$ are shown in Figure 43 and Figure 44 and can be compared with the corresponding stress couple distributions for a non-rotating boundary shown in Figure 41 and Figure 42. The direct stress resultants $F_{rr}^{(\sigma)}$, $F_{\theta\theta}^{(\sigma)}$ were not affected to the same extent by a boundary rotation. The largest change in the radial stress resultant $F_{rr}^{(\sigma)}$ was 9% and in the circumferential stress resultant was 20%. Again it can be observed that the effect of a boundary rotation upon the circumferential quantities is more pronounced than upon the radial quantities. The sensitivity of TÖLKE's Point Collocation Method on the accuracy of the solution for the distributions of the physical quantities in the circumferential direction lies at the very root of the method, and its truncated series form of solution is in itself quite sensitive to the number of terms included in the series.

The normal displacement function u_n given by Equation (12a) was calculated for various normal load intensities p_n and compares favourably with the experimental measurements taken on the shell by means of dial gauges (see Chapter III – 6). Figure 45 illustrates the normal displacement distribution u_n obtained from the theoretical solution based on a pattern of three collocation points. Along the

radial line $\theta = 30^{\circ}$, the normal displacement in the vicinity of the boundary is larger than at the apex of the shell. This condition appears to be at variance with the physical tests and may again be due to the presence of the slit corner in the experimental shell structure.

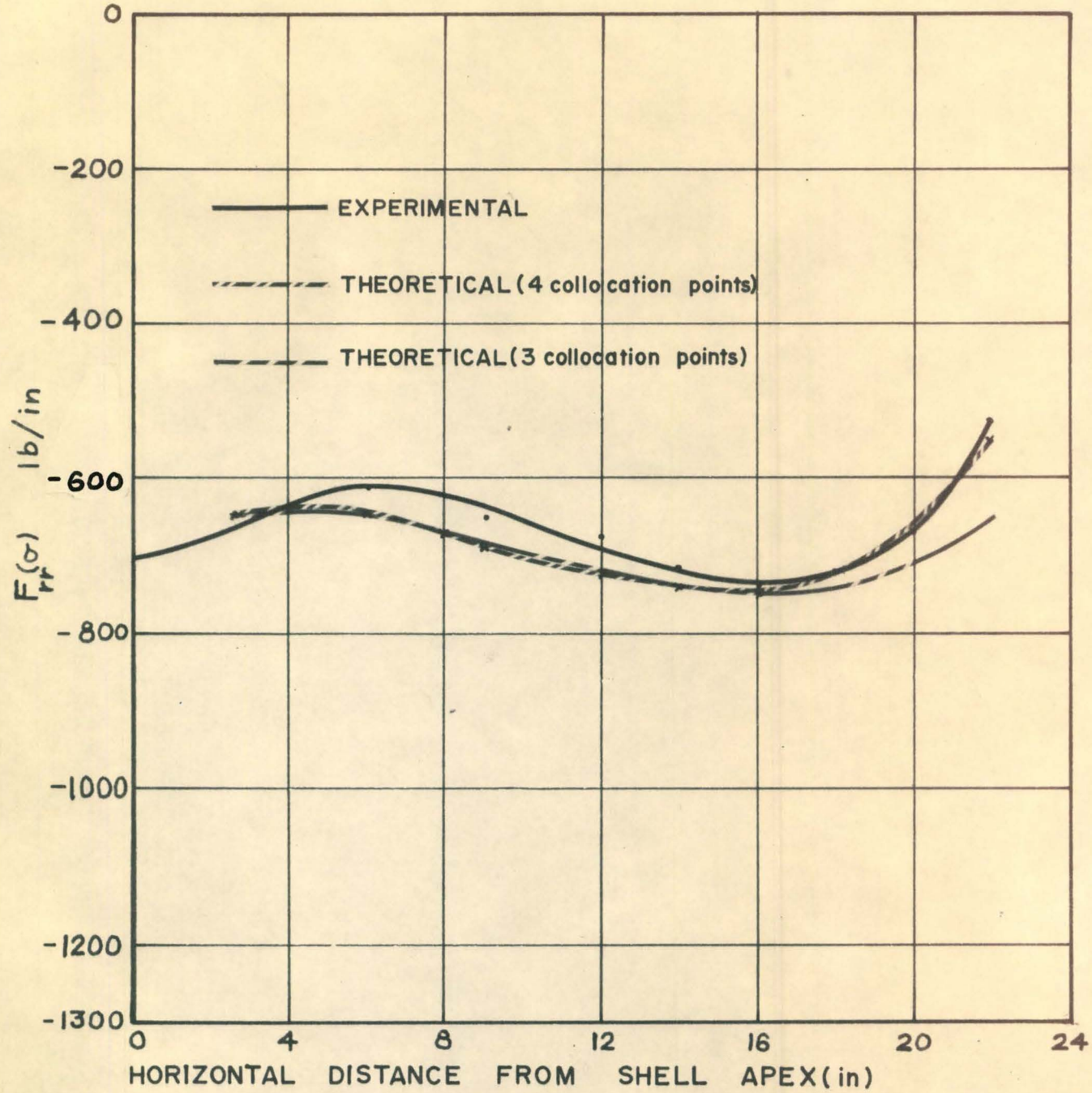

EXPERIMENTAL AND THEORETICAL DISTRIBUTION OF DIRECT STRESS RESULTANT $F_{rr}(\sigma)$ ALONG LINE $\theta = 20^{\circ}$

$P_n = -20$ psi

FIGURE 35

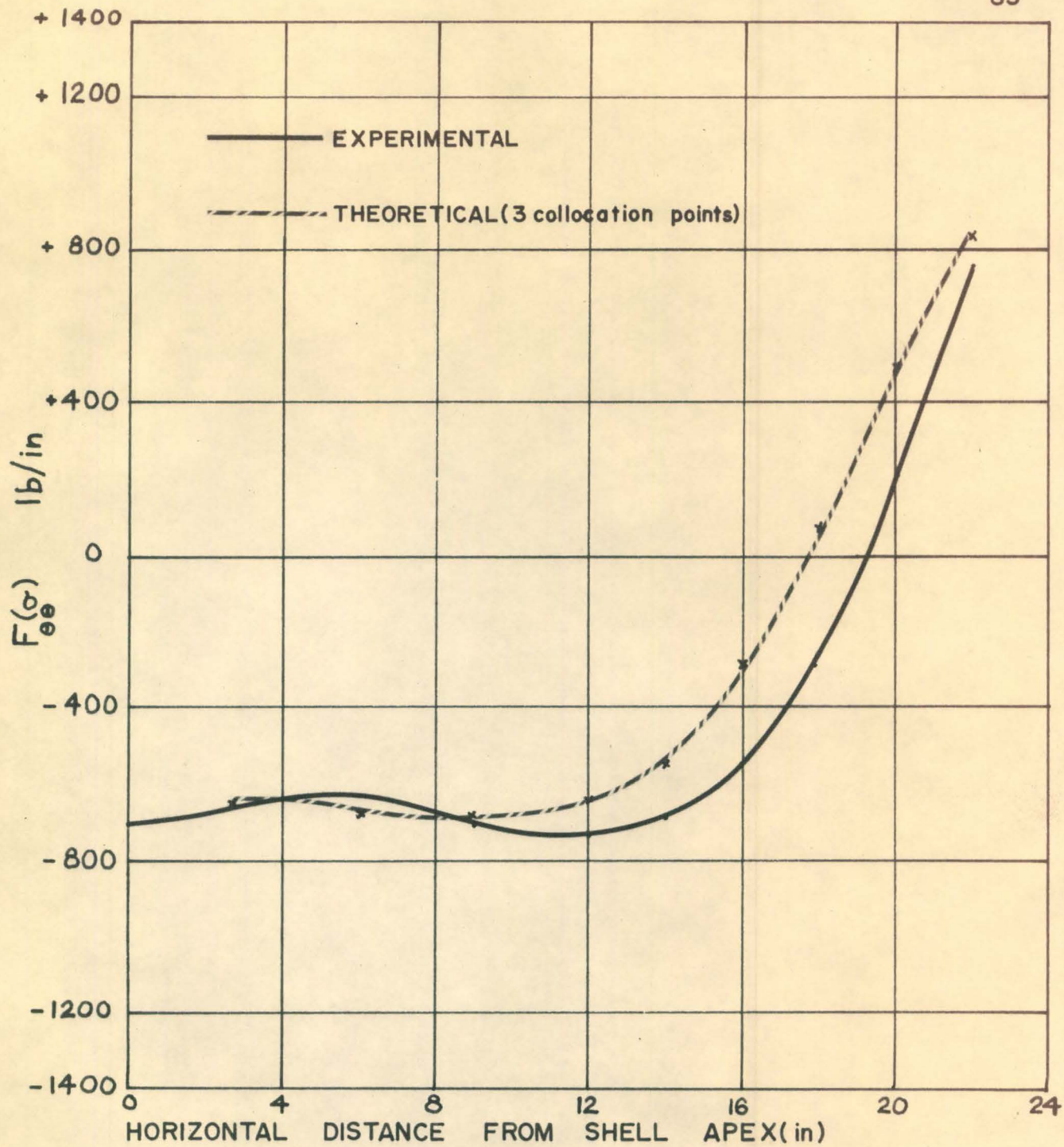

EXPERIMENTAL AND THEORETICAL DISTRIBUTION OF DIRECT STRESS RESULTANT $F_{\theta\theta}(\sigma)$ ALONG LINE $\theta = 20^\circ$
P_n =-20 psi

FIGURE 36

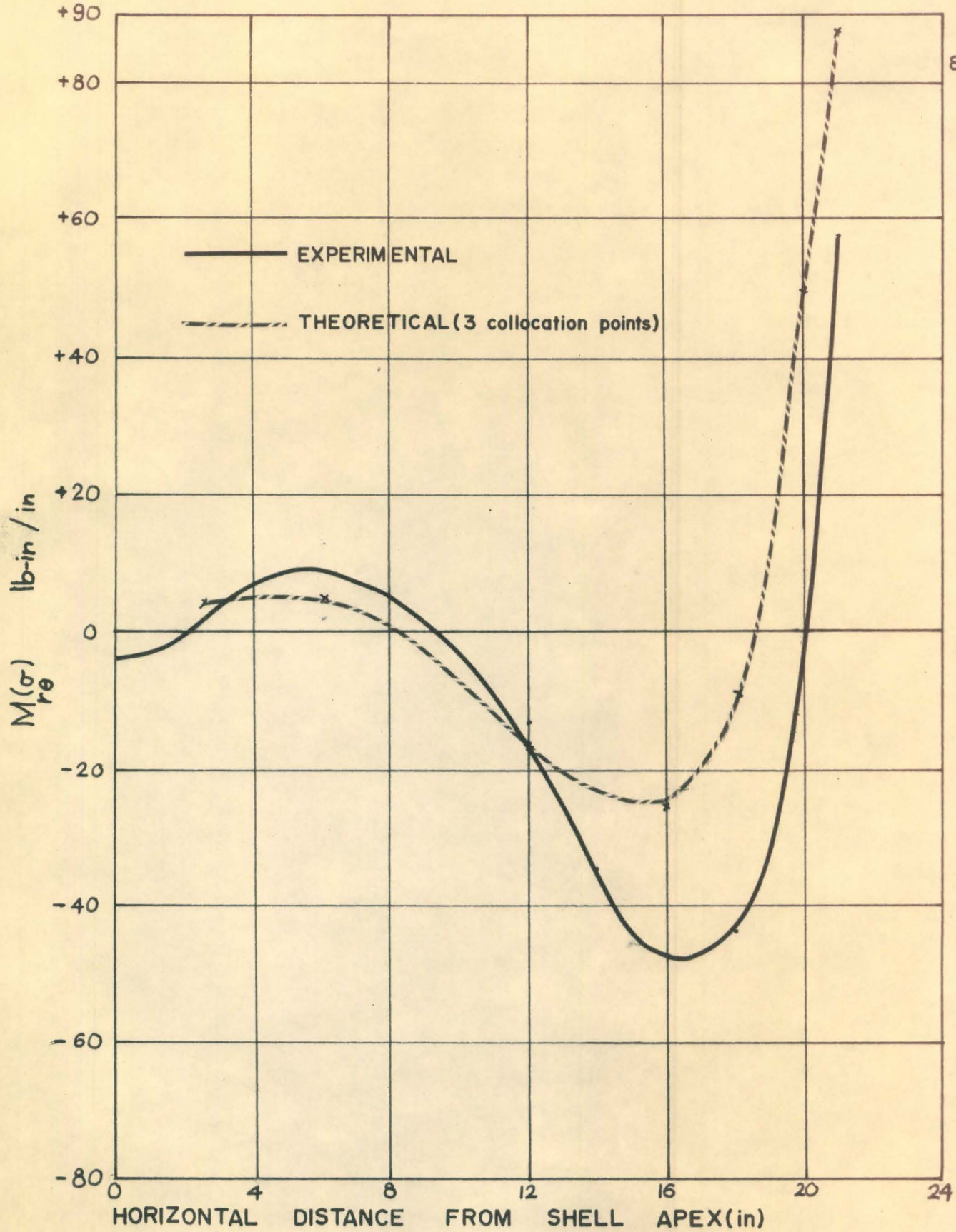

EXPERIMENTAL AND THEORETICAL DISTRIBUTION OF STRESS COUPLE $M_{r\theta}(\sigma)$ ALONG LINE $\theta = 0^{\circ}$, $P_n = -20$ psi

FIGURE 37

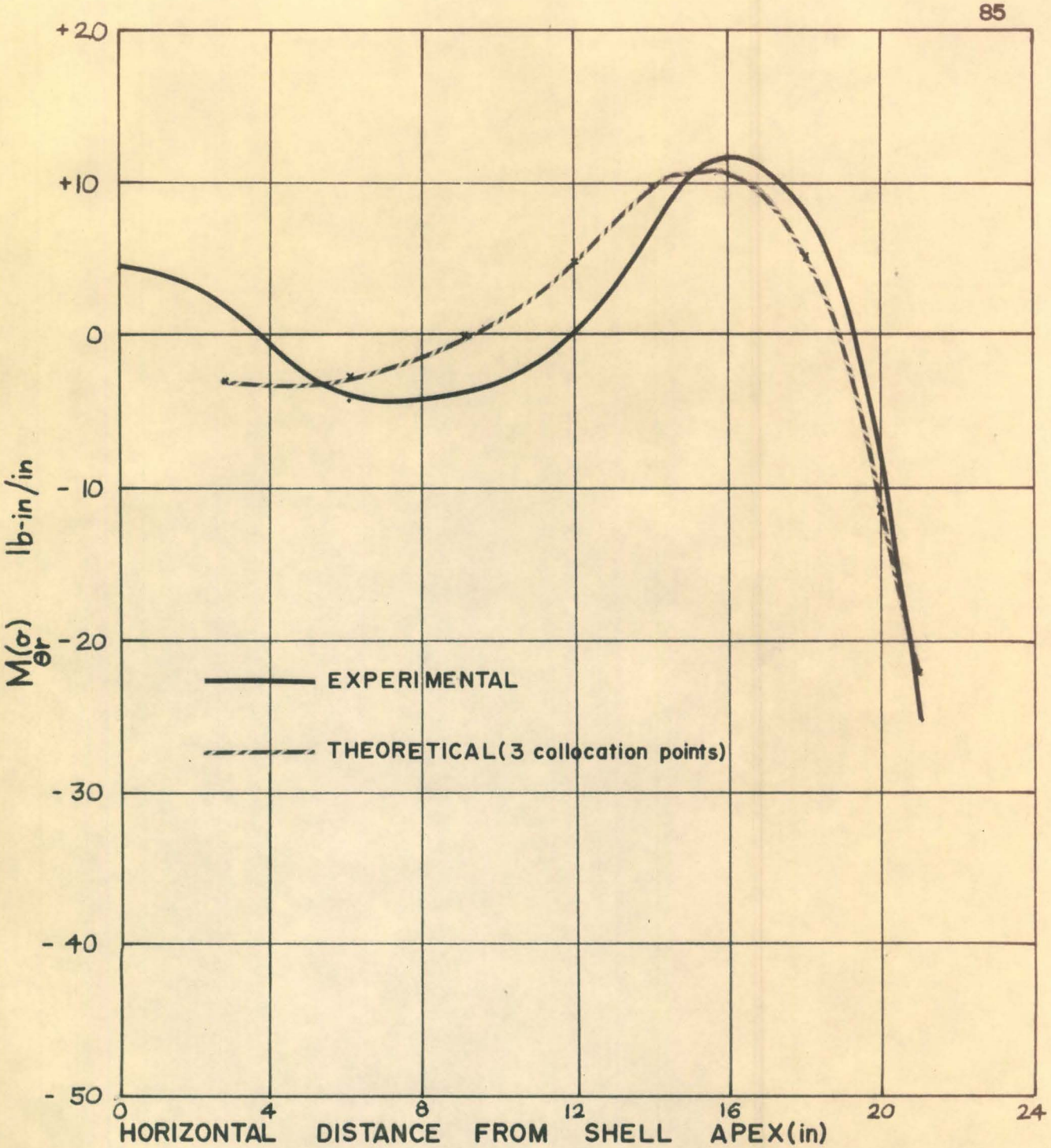

EXPERIMENTAL AND THEORETICAL DISTRIBUTION OF STRESS COUPLE $M_{\theta r}(\sigma)$ ALONG LINE $\theta = 0^{\circ}$, $P_h = -20$ psi

FIGURE 38

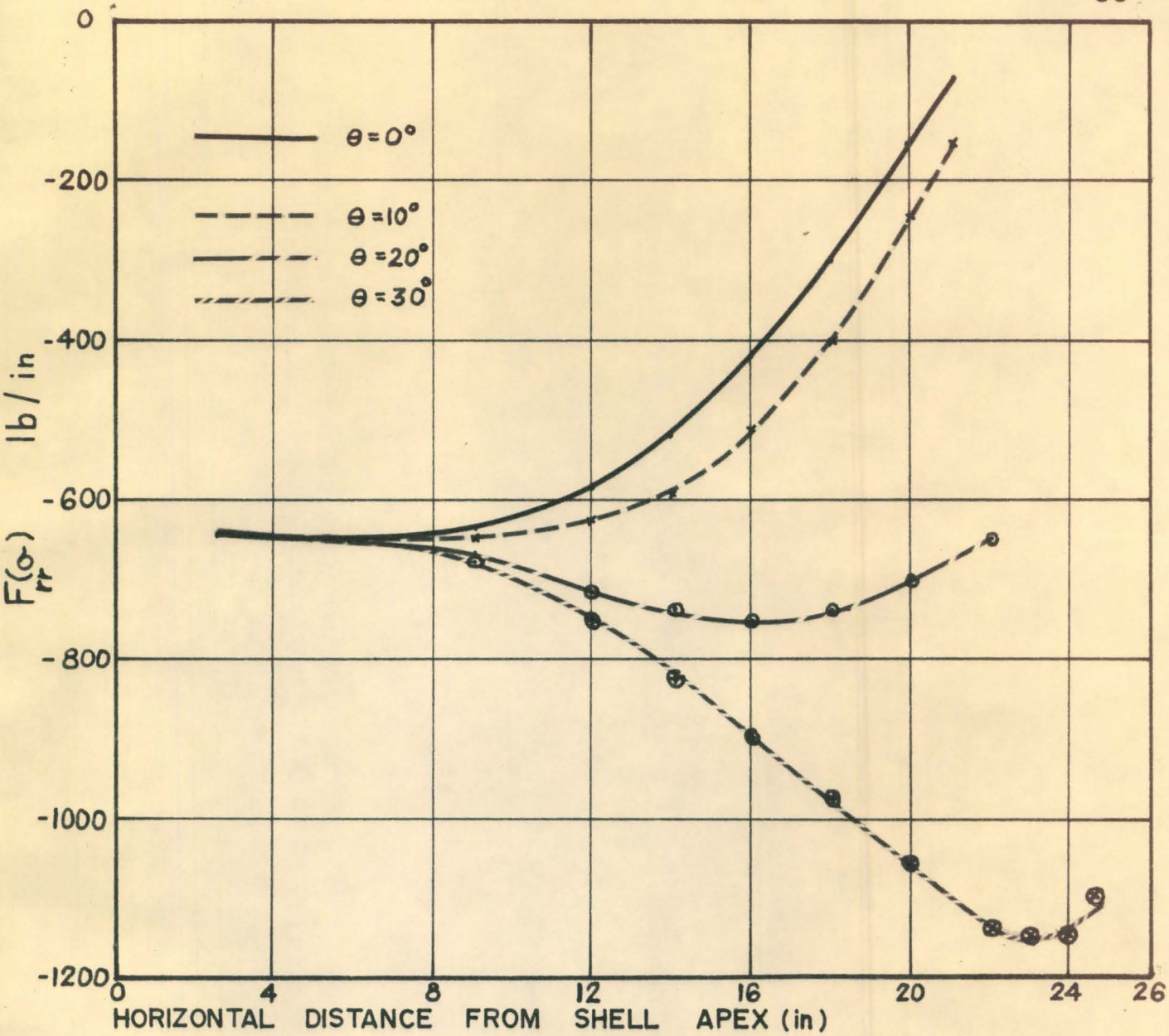

DISTRIBUTION OF DIRECT STRESS RESULTANT $F_{rr}(\sigma)$

FOR 3 COLLOCATION POINTS $0^\circ, 15^\circ, 30^\circ$

$P_n = -20$ psi

FIGURE 39

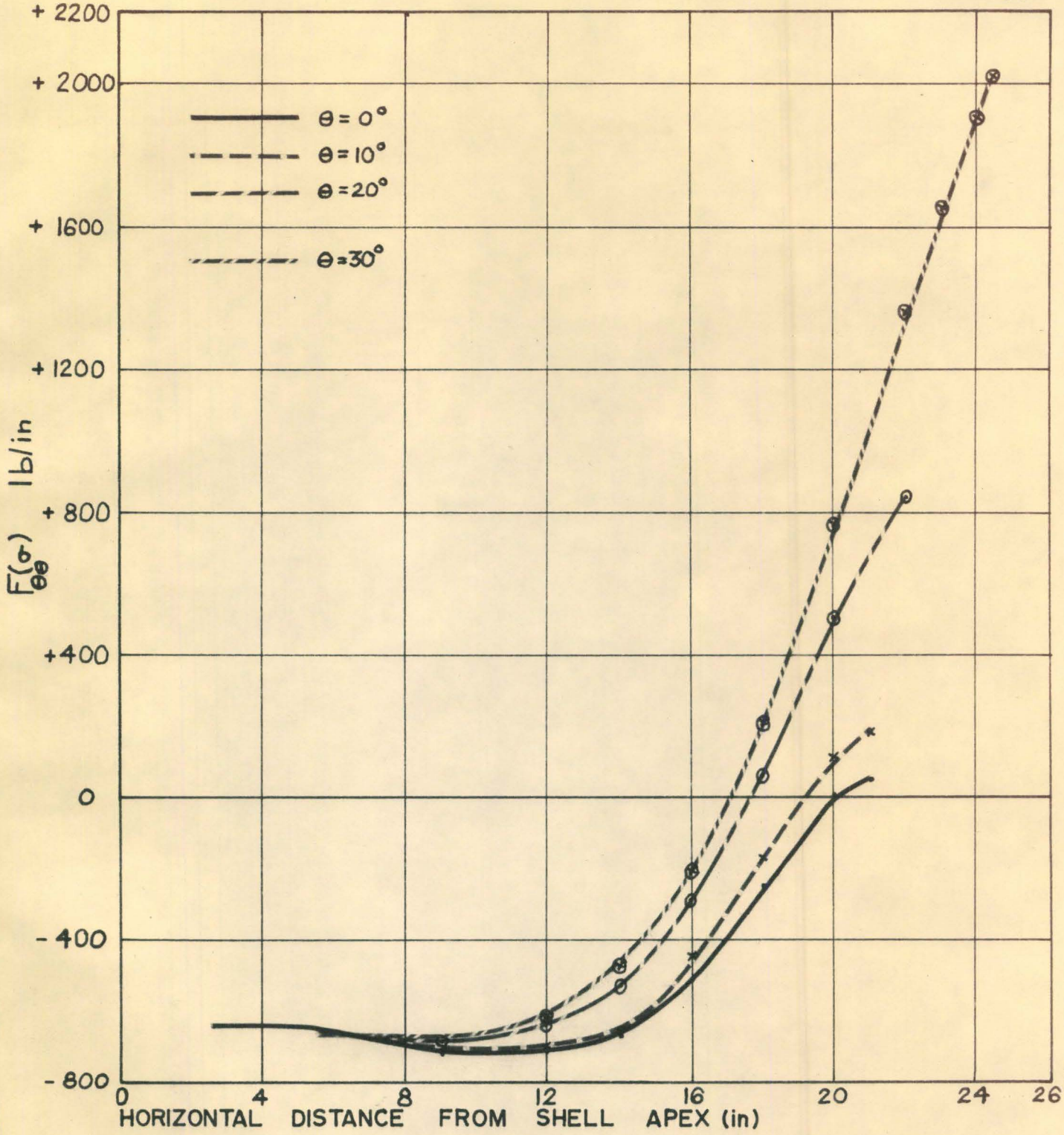

DISTRIBUTION OF DIRECT STRESS RESULTANT $F_{\theta\theta}^{(\sigma)}$
FOR 3 COLLOCATION POINTS 0°, 10°, 30°
P_h = -20 psi
FIGURE 40

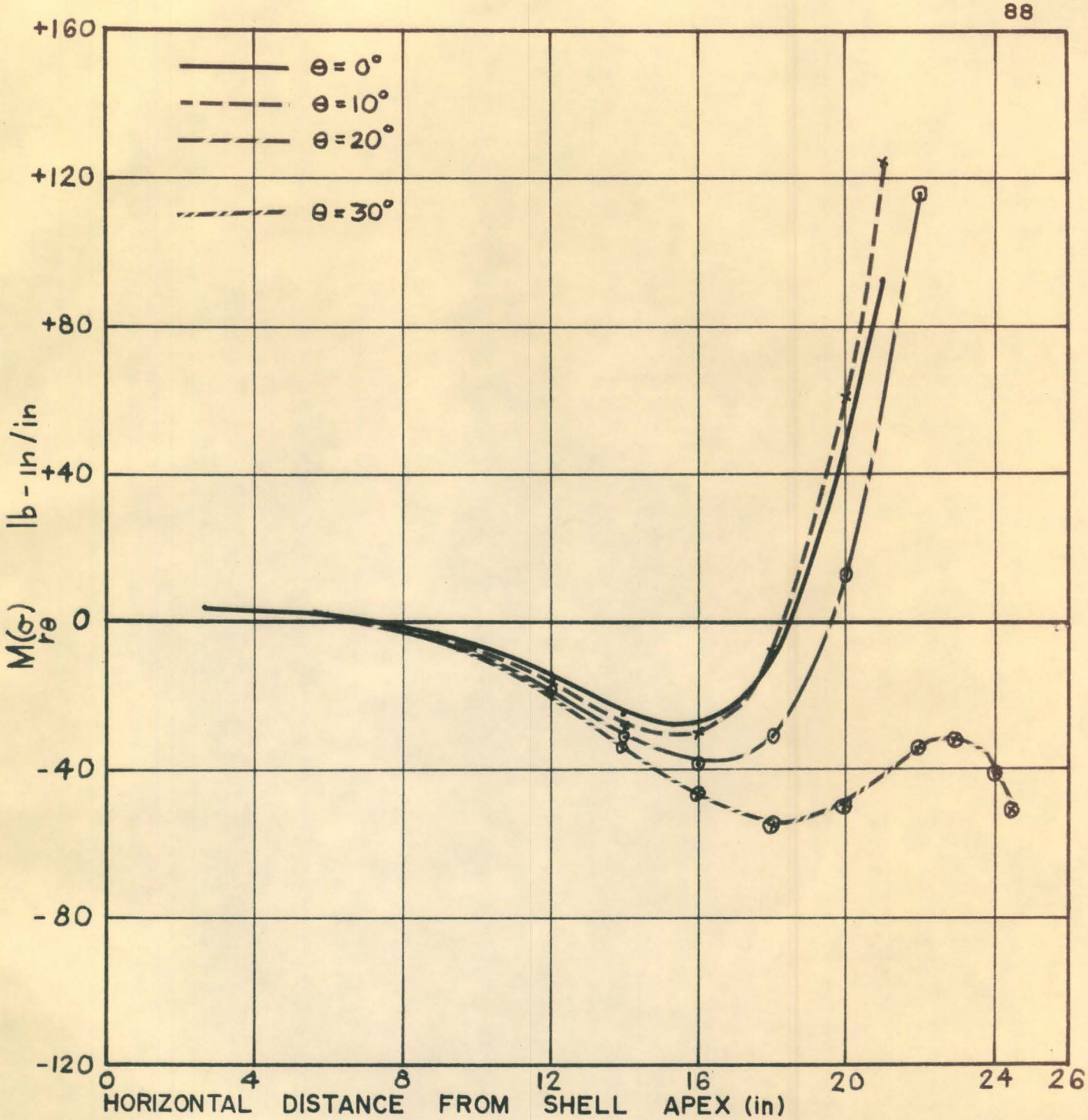

DISTRIBUTION OF STRESS COUPLE $M_{re}(\sigma)$ FOR 3 COLLOCATION POINTS $0,15,30^{\circ}$

$P_h = -20$ psi

FIGURE 41

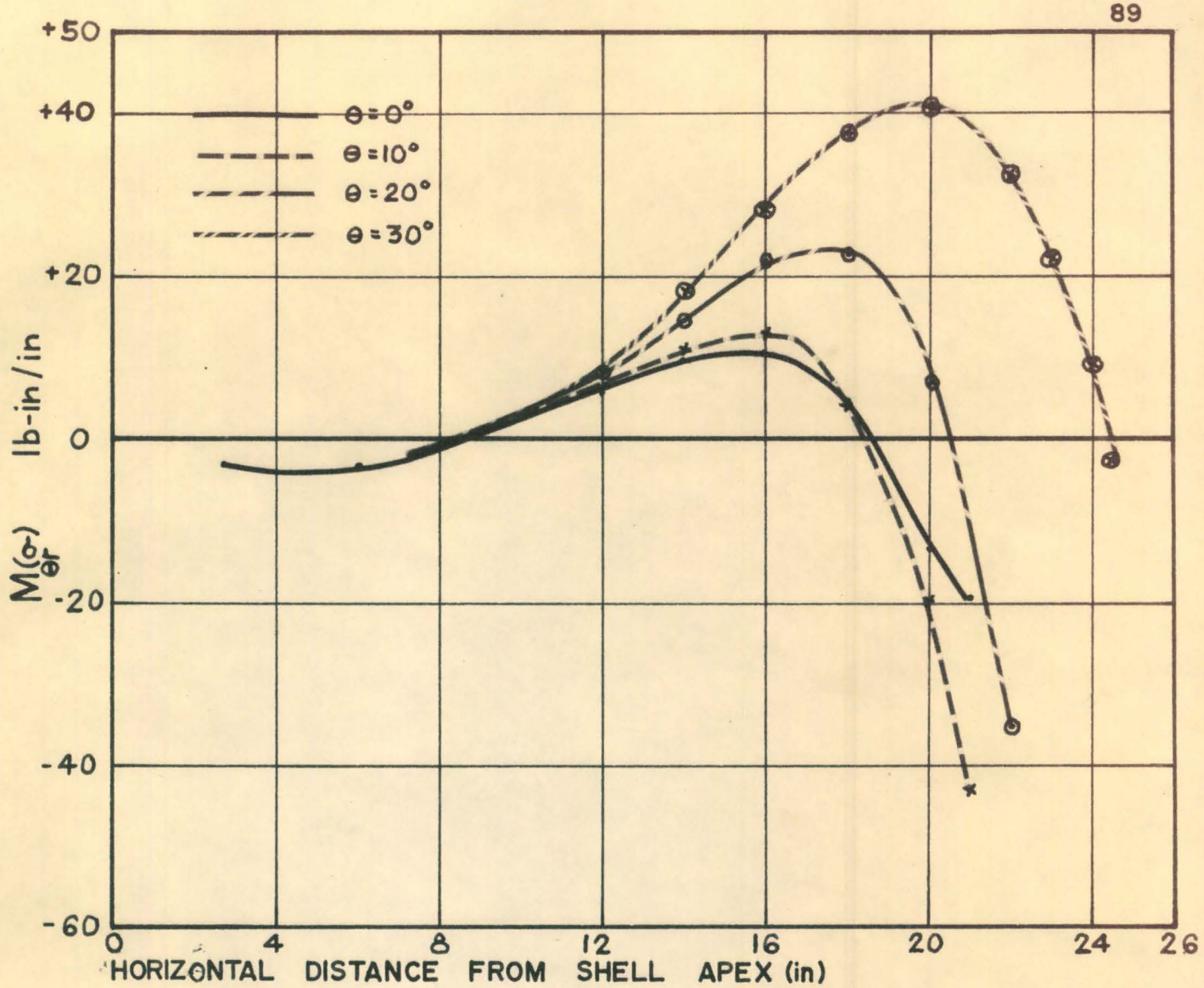

DISTRIBUTION OF STRESS COUPLE $M_{\theta r}(\sigma)$
FOR 3 COLLOCATION POINTS $0^\circ, 10^\circ, 30^\circ$
$P_n = -20$ psi

FIGURE 42

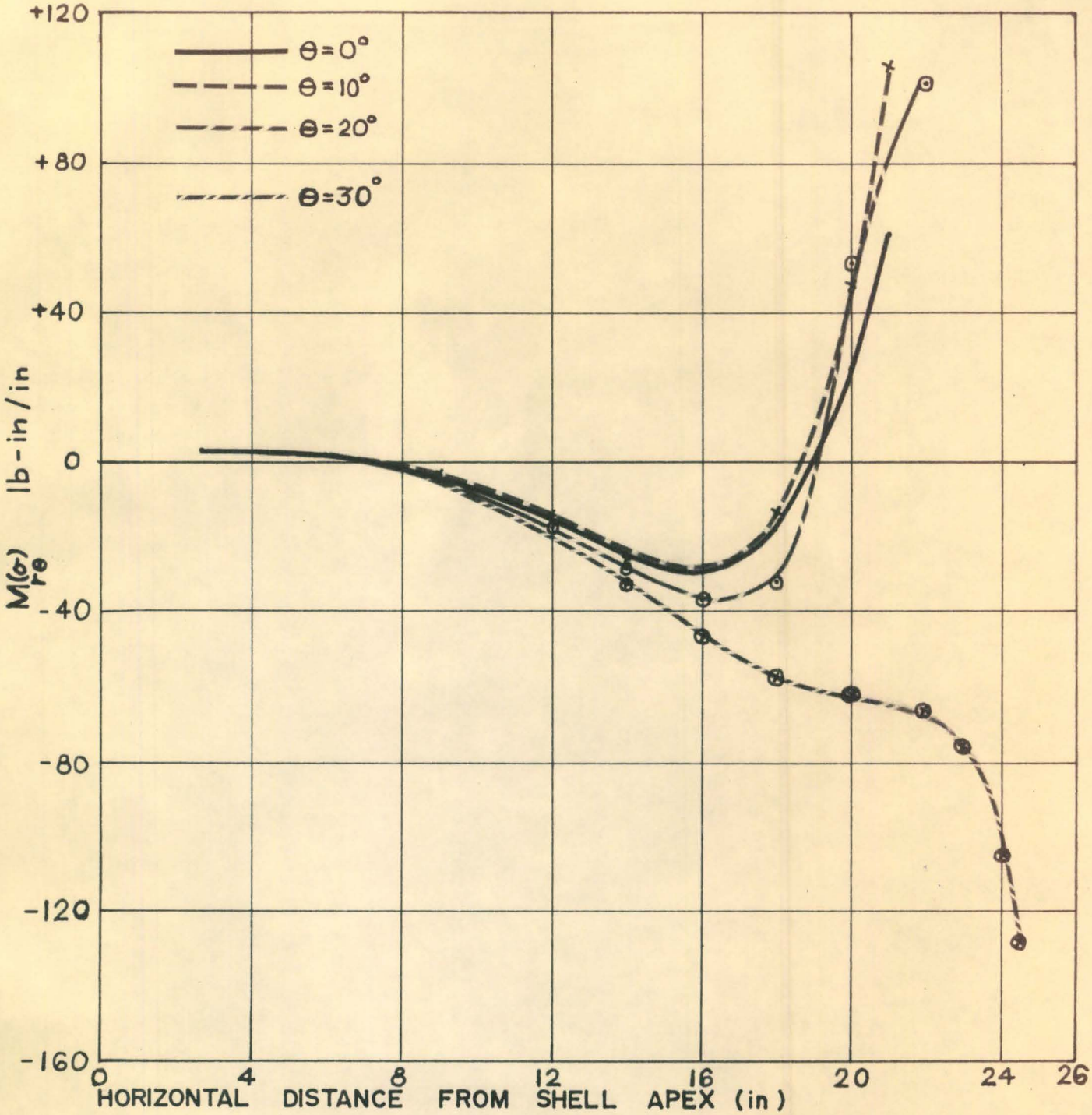

DISTRIBUTION OF STRESS COUPLE $M(\sigma)_{re}$ FOR 3 COLLOCATION POINTS 0°,15°,30° AND BOUNDARY ROTATION .0010 RADIANS

P_n =-20 psi

FIGURE 43

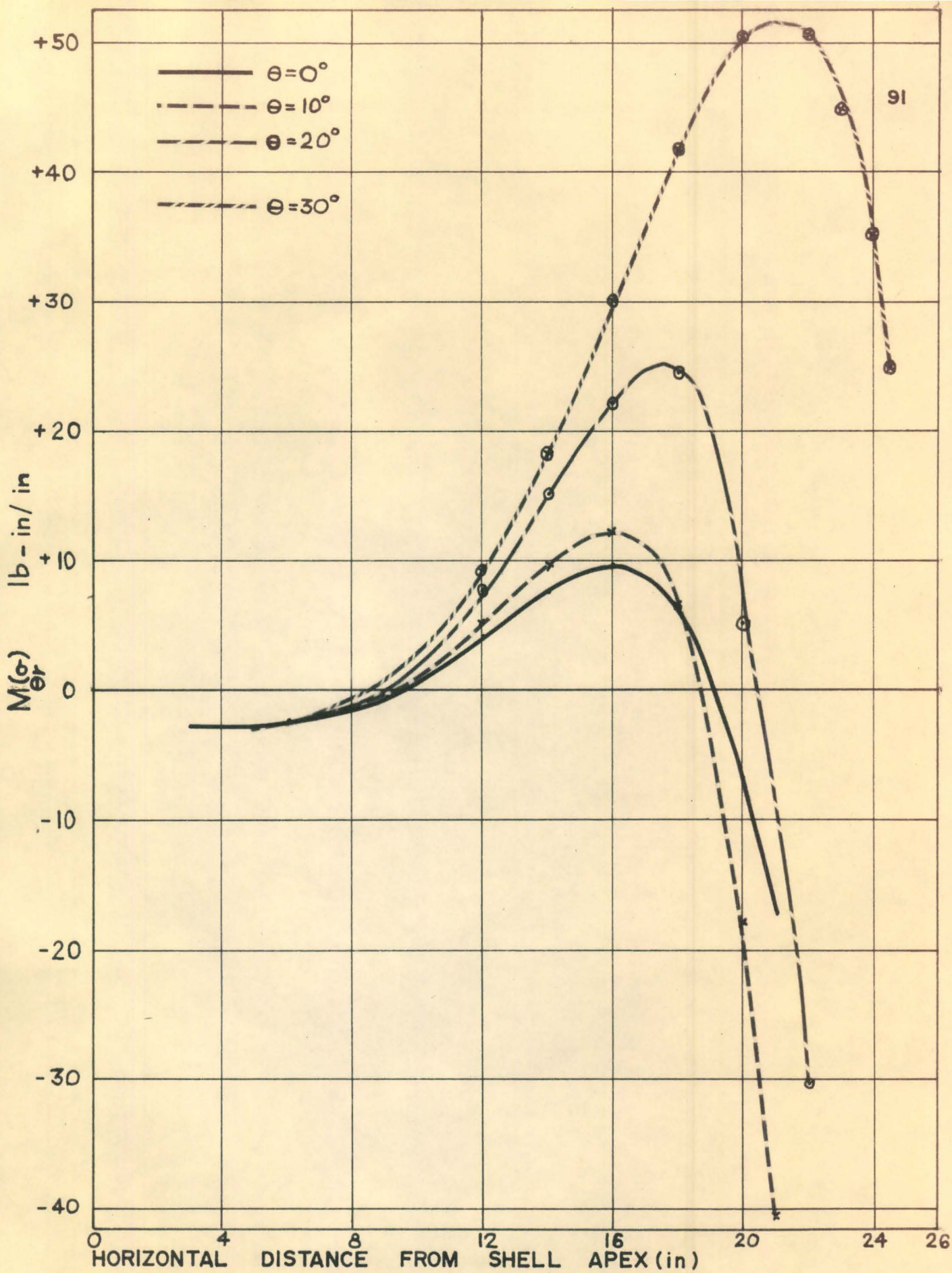

DISTRIBUTION OF STRESS COUPLE $M_{\theta r}(\sigma)$ FOR 3 COLLOCATION POINTS 0°, 15°, 30° AND BOUNDARY ROTATION .0010 RADIANS, P_h =-20 psi

FIGURE 4 4

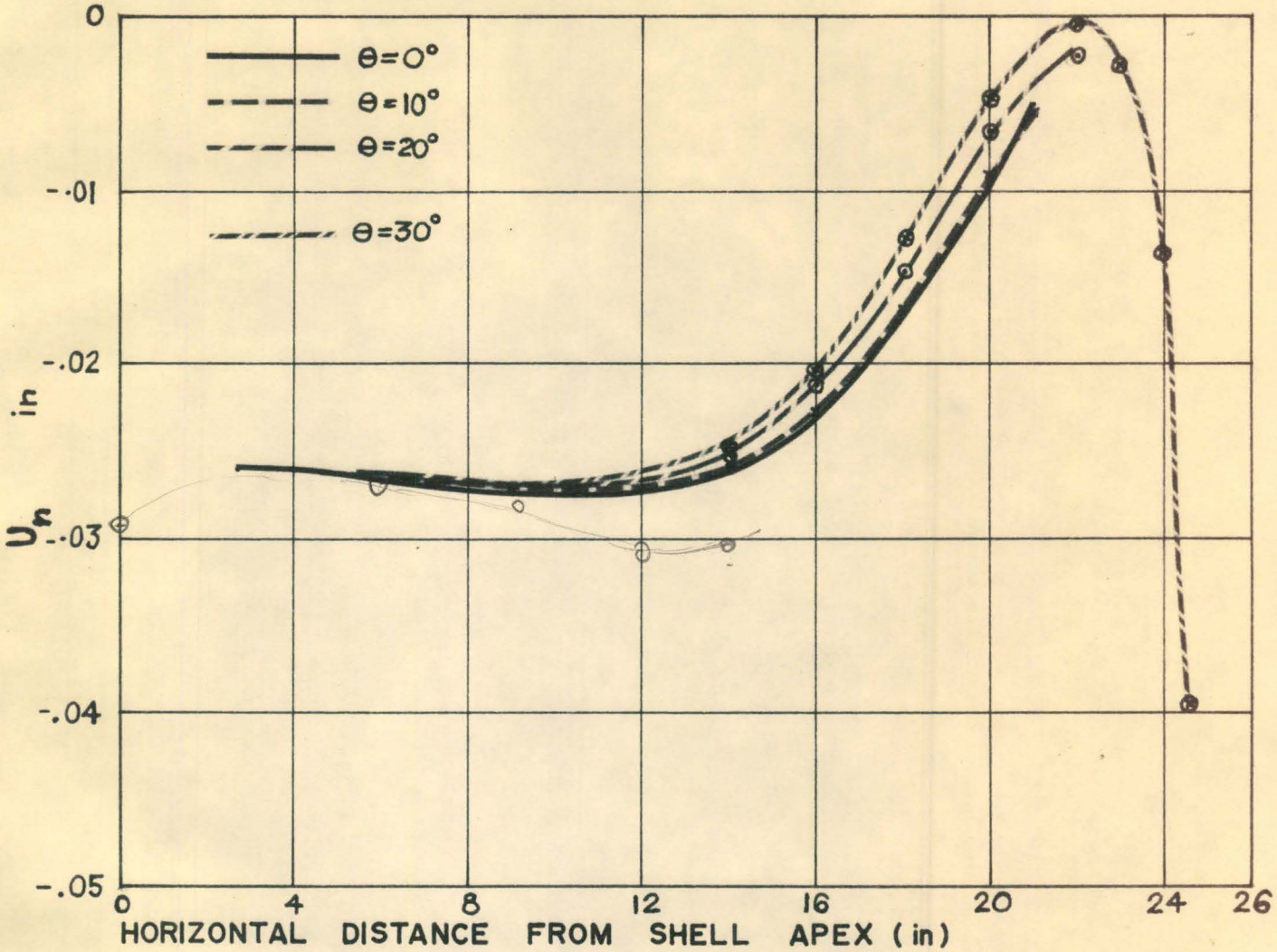

VARIATION OF NORMAL DISPLACEMENT U_n FOR 3 COLLOCATION POINTS $0°, 15°, 30°$

P_n =-20 psi

FIGURE 45

CHAPTER 5

SUMMARY

The purpose of this investigation consisted of the experimental and theoretical study of the state of stress and strain in a shallow spherical calotte shell over a hexagonal base. The effect of the rotationally periodic boundary on the stress and strain distribution in the shell, which was subjected to a rotationally symmetric applied loading, represented an integral part of this investigation. As far as it is known, no experimental study has been carried out on such a calotte shell. Moreover, the analytical solution has not been extensively studied because KELVIN Functions of higher order have not been tabulated, and computational difficulties are encountered in their evaluation. In the theoretical solution, the application of TÖLKE's Boundary Collocation Procedure for the approximate pointwise satisfaction of the support conditions for the rotationally periodic boundary of the shell, constitute an important part of the solution.

The results of this investigation can be examined in the light of the limitations of the experimental and theoretical procedure. The geometric configuration of the manufactured shell could not be brought into a perfect harmony with the mathematical configuration of the shell. The unavoidable deviations from the uniform thickness and from the spherical configuration of the shell, as well as the presence of slit corners in the shell structure, contributed to some discrepancy between

the experimental and theoretical results. Also, the theoretical criterion of zero variation in boundary rotations was not quite achieved in the experimental shell and corrections had to be introduced in the boundary value problem. The base of the assembled shell was not perfectly plane and consequently it did not receive perfectly uniform support from the rollers, therefore a completely rotationally periodic state of stress and strain could not be obtained in the experiment. The experimental shell structure was not primarily constructed for the purpose of simulating an actual structure but it rather served as a testing vehicle providing experimental results for the state of strain and stress which could be compared to corresponding theoretical results as the "actual" solution. It served as the first stage of a study on the structural behaviour of this type of shell under various boundary conditions. This work endeavoured to investigate the spherical calotte shell under such boundary conditions which inhibit boundary rotations, normal boundary displacements and horizontal reactions against the lateral movements of the boundary members. As it turned out, the boundary members did actually rotate, which had to be taken into account in the theoretical solution, and it seems that the rolling friction could have brought about a horizontal boundary force which, in all probability, might have had some effect on the experimental results. The presence of the slit in the re-entrant corners of the shell exerted an unpredictable effect on the state of strain and stress in the shell, which could not be quite adequately matched in the theoretical solution. Therefore, the experimental results were not as accurate as had initially been hoped. Better experimental results can probably be obtained for this shell if its boundary is completely clamped against lateral displacement and rotation, which represents

the second stage of this study.

This shallow spherical calotte shell over a hexagonal base with rotationally periodic boundary and subjected to rotationally symmetric normal loading tended to exhibit a rotationally periodic state of strain and stress.

The flexural strains at the boundary were of the same order of magnitude as the direct strains. The rotationally periodic disturbance of the state of strain and stress tended to attenuate with the radial distance from the shell's boundary and emerged essentially as a rotationally symmetric state of strain and stress in the proximity of the shell's apex.

The maximum measured tensile circumferential stress occurred at the re-entrant corner, where the state of stress was intensified by the presence of the slit. The resolution of strain measurements indicated that over 50% of the tensile stress at this location was caused by transverse flexure.

The limitations of the theoretical solution emanate from the finite degrees of freedom approximation inherent in the truncated series solution in the circumferential direction $\bar{e}_\theta$, and from the approximate procedure of satisfaction of the boundary conditions only at a finite number of discrete points.

The distribution of the stress resultants and stress couples exhibited satisfactory, rather than exceptional agreement in the experimental and theoretical comparisons. The largest discrepancy between theoretical and experimental results existed along the line $\theta = 30^\circ$, for which both the slit boundary in the experimental results and the sensitivity of the theoretical solution to the truncation of the series

with respect to the θ co-ordinate were the contributing factors.

This investigation indicated that an increase in the number of collocation points on the boundary does not necessarily improve the accuracy of every facet of the solution. For instance, it appeared that the location of the collocation points had as crucial an influence upon the solution as their number. The investigation seemed to assert that a variation in the location of a given number of collocation points has the least effect upon the distribution of direct stress resultants. The reduced boundary conditions imposed upon the collocation point in the re-entrant corner of the shell seemed to exert a strong influence upon the solution in general. TÖLKE's Method of Collocation in its application to this spherical calotte shell problem was quite successful, but further study is indicated in order to obtain a more definitive evaluation of the relative merits in the number and location of the boundary collocation points, which seems to be the temperamental feature of this theoretical procedure.

It is necessary to attempt to use more than four collocation points in the theoretical solution to evaluate the functional and boundary accuracy of the solution series. Also, it seems that a study of a calotte shell with completely fixed boundaries would yield better experimental and theoretical agreement.

APPENDIX A

GENERAL THEORY OF SHALLOW SHELLS

A - 1 Introduction

This section proposes to develop the fundamental equations of DONNELL, MARGUERRE, MUSHTARI and VLASOV using the direct kinematic method of analysis. The kinematic tensorial method together with its direct notation is used throughout this work, which emphasizes the intuitive physico-geometric content of the subject matter.

A - 2 Statical Equilibrium Conditions

(a) Force Equilibrium

Figure 46 illustrates the free body diagram used in the formulation of the moment and force equilibrium conditions.

The VECTORIAL force equilibrium equation for the infinitesimal shell element is

$$\sum_{i=1}^{3} \overline{F}_i(\sigma) = -\overline{F}_1(\sigma,\alpha_1)\,ds_2(\alpha_1) - \overline{F}_2(\sigma,\alpha_2)\,ds_1(\alpha_1) + \overline{F}_1(\sigma,\alpha_1+d\alpha_1)\,ds_2(\alpha_1+d\alpha_1)$$

$$+\overline{F}(\sigma,\alpha_2+d\alpha_2)\,ds_1(\alpha_2+d\alpha_2) + \overline{p}\,ds_1(\alpha_2+\tfrac{d\alpha_2}{2})\,ds_2(\alpha_1+\tfrac{d\alpha_1}{2}) = 0$$

Expanding the quantities above into TAYLOR series and supressing terms

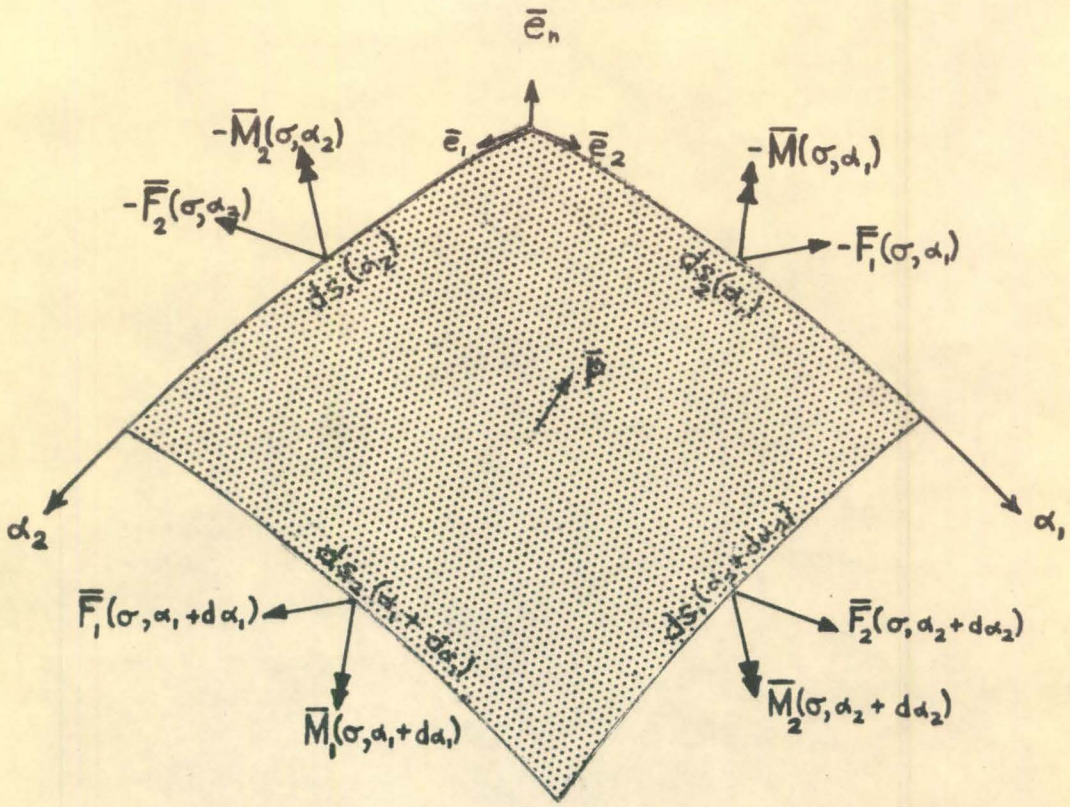

$$\bar{F}_1(\sigma) = F_{11}(\sigma)\bar{e}_1 + F_{12}(\sigma)\bar{e}_2 + F_{1n}(\sigma)\bar{e}_n$$

$$\bar{F}_2(\sigma) = F_{21}(\sigma)\bar{e}_1 + F_{22}(\sigma)\bar{e}_2 + F_{2n}(\sigma)\bar{e}_n$$

$$\bar{M}_1(\sigma) = M_{11}(\sigma)\bar{e}_1 + M_{12}(\sigma)\bar{e}_2$$

$$\bar{M}_2(\sigma) = M_{21}(\sigma)\bar{e}_1 + M_{22}(\sigma)\bar{e}_2$$

$$\bar{p} = p_1\bar{e}_1 + p_2\bar{e}_2 + p_n\bar{e}_n$$

DIFFERENTIAL SHELL ELEMENT SHOWING DIRECT AND FLEXURAL STRESS RESULTANTS

FIGURE 46

of higher order yields the direct form of the force equilibrium equation

$$\frac{\partial}{\partial\alpha_1}\left[\overline{F}_1(\sigma,\alpha_1)\,ds_2(\alpha_1)\right]d\alpha_1 + \frac{\partial}{\partial\alpha_2}\left[\overline{F}_2(\sigma,\alpha_2)\,ds_1(\alpha_2)\right]d\alpha_2 + \overline{p}\,ds_1(\alpha_1)\,ds_2(\alpha_2) = 0 \qquad (1)$$

In order to establish equivalent rectangular forms of this equation, it is necessary to resort to the theory of differential geometry of surfaces in order to establish the unit surface vectors constituting the mobile RIBAUCOUR Triad (see NOVOZHILOV in 1941). Using

$$\overline{F}_1(\sigma) = F_{11}^{(\sigma)}\overline{e}_1 + F_{12}^{(\sigma)}\overline{e}_2 + F_{1n}^{(\sigma)}\overline{e}_n$$

$$\overline{F}_2(\sigma) = F_{21}^{(\sigma)}\overline{e}_1 + F_{22}^{(\sigma)}\overline{e}_2 + F_{2n}^{(\sigma)}\overline{e}_n$$

$$\overline{p} = p_1\overline{e}_1 + p_2\overline{e}_2 + p_n\overline{e}_n$$

$$ds_1(\alpha_2) = A_1\,d\alpha_1$$

$$ds_2(\alpha_1) = A_2\,d\alpha_2$$

and the derivatives of unit vectors of the RIBAUCOUR Triad, the force equilibrium equations can be expressed in its component form

$$\frac{\partial}{\partial\alpha_1}(A_2F_{11}(\sigma)) + F_{12}(\sigma)\frac{\partial A_1}{\partial\alpha_2} + A_1A_2F_{1n}(\sigma)K_2^{(n)} + \frac{\partial}{\partial\alpha_2}(A_1F_{21}(\sigma)) - F_{22}(\sigma)\frac{\partial A_2}{\partial\alpha_1} + p_1A_1A_2 = 0 \qquad (2a)$$

$$-F_{11}(\sigma)\frac{\partial A_1}{\partial\alpha_2} + \frac{\partial}{\partial\alpha_1}(A_2F_{12}(\sigma)) + F_{21}(\sigma)\frac{\partial A_2}{\partial\alpha_1} + \frac{\partial}{\partial\alpha_2}(A_1F_{22}(\sigma)) - A_1A_2F_{2n}(\sigma)K_1^{(n)} + p_2A_1A_2 = 0 \qquad (2b)$$

$$-A_1A_2F_{11}(\sigma)K_2^{(n)} + A_1A_2F_{22}(\sigma)K_1^{(n)} + \frac{\partial}{\partial\alpha_1}(A_2F_{1n}(\sigma)) + \frac{\partial}{\partial\alpha_2}(A_1F_{2n}(\sigma)) + p_nA_1A_2 = 0 \qquad (2c)$$

(b) Moment Equilibrium

The vectorial moment equilibrium equation is

$$\sum_{i=1}^{n}\overline{M}_i(\sigma) = -\overline{M}_1(\sigma,\alpha_1)\,ds_2(\alpha_1) - \overline{M}_2(\sigma,\alpha_2)\,ds_1(\alpha_2) + \overline{M}_1(\sigma,\alpha_1+d\alpha_1)\,ds_2(\alpha_1+d\alpha_1)$$

$$+\overline{M}_2(\sigma,\alpha_2+d\alpha_2)\,ds_1(\alpha_2+d\alpha_2) + \frac{ds_1(\alpha_2)}{2}\overline{e}_1\times\left[-\overline{F}_2(\sigma,\alpha_2)\,ds_1(\alpha_2)\right] +$$

$$+\frac{ds_2(\alpha_1)}{2}\bar{e}_2 \times\left[-\bar{F}_1(\sigma,\alpha_1)\,ds_2(\alpha_1)\right]+\left(ds_1(\alpha_2)\bar{e}_1+\frac{ds_2(\alpha_2+d\alpha_2)}{2}\bar{e}_2\right)\times\left[\bar{F}_1(\sigma,\alpha_1+d\alpha_1)\,ds_2(\alpha_1+d\alpha_1)\right]$$

$$+\left(ds_2(\alpha_1)\bar{e}_2+\frac{ds_1(\alpha_2+d\alpha_2)}{2}\bar{e}_1\right)\times\left[\bar{F}_2(\sigma,\alpha_2+d\alpha_2)\,ds_1(\alpha_2+d\alpha_2)\right]$$

$$+\left(\frac{ds_1(\alpha_2)}{2}\bar{e}_1+\frac{ds_2(\alpha_1)}{2}\bar{e}_2\right)\times\left[\bar{p}\,ds_1(\alpha_2)\,ds_2(\alpha_1)\right]=0$$

Expanding this equation into TAYLOR series and neglecting terms of higher order delivers

$$\frac{\partial}{\partial\alpha_1}\left(\bar{M}_1(\sigma)A_2\,d\alpha_2\right)d\alpha_1+\frac{\partial}{\partial\alpha_2}\left(\bar{M}_2(\sigma)A_1\,d\alpha_1\right)d\alpha_2+\left[\bar{e}_2\times\bar{F}_2(\sigma)\right]A_1A_2\,d\alpha_1\,d\alpha_2$$

$$+\left[\bar{e}_1\times\bar{F}_1(\sigma)\right]A_1A_2\,d\alpha_1\,d\alpha_2=0 \qquad (3)$$

Setting

$$\bar{M}_1(\sigma)=M_{11}(\sigma)\bar{e}_1+M_{12}(\sigma)\bar{e}_2$$

$$\bar{M}_2(\sigma)=M_{21}(\sigma)\bar{e}_1+M_{22}(\sigma)\bar{e}_2$$

the equation (3) resolves into its components

$$M_{12}(\sigma)\frac{\partial A_1}{\partial\alpha_2}+\frac{\partial}{\partial\alpha_1}\left(M_{11}(\sigma)A_2\right)-M_{22}(\sigma)\frac{\partial A_2}{\partial\alpha_1}+\frac{\partial}{\partial\alpha_1}\left(M_{21}(\sigma)A_1\right)+F_{2n}(\sigma)A_1A_2=0 \qquad (4a)$$

$$\frac{\partial}{\partial\alpha_1}\left(A_2M_{12}(\sigma)\right)-M_{11}(\sigma)\frac{\partial A_1}{\partial\alpha_2}+\frac{\partial}{\partial\alpha_2}\left(A_1M_{22}(\sigma)\right)+M_{21}(\sigma)\frac{\partial A_2}{\partial\alpha_1}-F_{1n}(\sigma)A_1A_2=0 \qquad (4b)$$

$$-M_{11}(\sigma)K_2^{(n)}+M_{22}(\sigma)K_1^{(n)}-F_{21}(\sigma)+F_{12}(\sigma)=0 \qquad (4c)$$

where the middle surface curvature tensor can be given in the form

$$\bar{\bar{K}}(r_0)=\bar{\bar{K}}=\bar{e}_i\bar{K}_i=K_{ij}\,\bar{e}_i\bar{e}_j \qquad (i,j=\alpha_1,\alpha_2)$$

A - 3 Deformation of the Middle Surface of the Shell

The strain tensor for any arbitrary point in the shell can be derived using the fundamental KIRCHOFF's Hypothesis and the Direct Kinematic Deformation Theory (SCHROEDER in 1964). It is

$$\bar{\bar{\epsilon}}(\bar{r}) = \bar{\bar{\epsilon}}(\bar{r}_o+\bar{\pi}) = \left[\frac{\epsilon_{11}+\alpha_n \delta K_2^{(n)}}{1+\alpha_n K_2^{(n)}} \bar{e}_1\bar{e}_1 + \frac{1}{2}\left[(\gamma_1+\gamma_2)+\alpha_n\left(\frac{\delta K_2^{(t)}}{1-\alpha_n K_1^{(n)}} - \frac{\delta K_1^{(t)}}{1+\alpha_n K_2^{(n)}}\right)\right]\bar{e}_1\bar{e}_2 \right.$$

$$\left. + \frac{1}{2}\left[(\gamma_1+\gamma_2)+\alpha_n\left(\frac{\delta K_2^{(t)}}{1-\alpha_n K_1^{(n)}} - \frac{\delta K_1^{(t)}}{1+\alpha_n K_2^{(n)}}\right)\right]\bar{e}_2\bar{e}_1 + \frac{\epsilon_{22}-\alpha_n \delta K_1^{(n)}}{1-\alpha_n \delta K_1^{(n)}}\bar{e}_2\bar{e}_2 \right]$$

This tensor can be resolved into the middle surface strain tensor $\epsilon^{(d)}$ and the strain tensor due to flexure $\bar{\bar{\epsilon}}^{(f)}$, that is

$$\bar{\bar{\epsilon}}(\bar{r}) = \bar{\bar{\epsilon}}^{(d)} + \bar{\bar{\epsilon}}^{(f)}$$

where

$$\bar{\bar{\epsilon}}^{(d)} = \left[\frac{\epsilon_{11}}{1+\alpha_n K_2^{(n)}} \bar{e}_1\bar{e}_1 + \frac{1}{2}(\gamma_1+\gamma_2)\bar{e}_1\bar{e}_2 \right.$$

$$\left. + \frac{1}{2}(\gamma_1+\gamma_2)\bar{e}_2\bar{e}_1 + \frac{\epsilon_{22}}{1-\alpha_n K_1^{(n)}}\bar{e}_2\bar{e}_2 \right]$$

and

$$\epsilon^{(f)} = \left[\frac{\alpha_n \delta K_2^{(n)}}{1+\alpha_n K_2^{(n)}} \bar{e}_1\bar{e}_1 + \frac{\alpha_n}{2}\left(\frac{\delta K_2^{(t)}}{1-\alpha_n K_1^{(n)}} - \frac{\delta K_1^{(t)}}{1+\alpha_n K_2^{(n)}}\right)\bar{e}_1\bar{e}_2 \right.$$

$$\left. + \frac{\alpha_n}{2}\left(\frac{\delta K_2^{(t)}}{1-\alpha_n K_1^{(n)}} - \frac{\delta K_1^{(t)}}{1+\alpha_n K_2^{(n)}}\right)\bar{e}_2\bar{e}_1 + \frac{-\alpha_n \delta K_1^{(n)}}{1-\alpha_n K_1^{(n)}}\bar{e}_2\bar{e}_2 \right]$$

with

$$\epsilon_{11} = \frac{1}{A_1}\frac{\partial u_1}{\partial \alpha_1} + \frac{1}{A_1 A_2}\frac{\partial A_1}{\partial \alpha_2} + K_2^{(n)} u_n$$

$$\epsilon_{22} = \frac{1}{A_2}\frac{\partial u_2}{\partial \alpha_2} + \frac{1}{A_1 A_2}\frac{\partial A_2}{\partial \alpha_1} - K_1^{(n)} u_n$$

$$\epsilon_{12} = \frac{1}{2}(\gamma_1 + \gamma_2) = \frac{1}{2}\left(\frac{A_2}{A_1}\frac{\partial}{\partial \alpha_1}\left(\frac{u_2}{A_2}\right) + \frac{A_1}{A_2}\frac{\partial}{\partial \alpha_2}\left(\frac{u_1}{A_1}\right)\right)$$

$$\delta K_2^{(n)} = -\frac{1}{A_1}\frac{\partial}{\partial \alpha_1}\left(\frac{1}{A_1}\frac{\partial u_n}{\partial \alpha_1} - u_1 K_2^{(n)}\right) - \frac{1}{A_1 A_2}\frac{\partial A_1}{\partial \alpha_2}\left(\frac{1}{A_2}\frac{\partial u_n}{\partial \alpha_2} + u_2 K_1^{(n)}\right) = \delta K_{12}$$

$$\delta K_1^{(n)} = +\frac{1}{A_2}\frac{\partial}{\partial \alpha_2}\left(\frac{1}{A_2}\frac{\partial u_n}{\partial \alpha_2} + u_2 K_1^{(n)}\right) + \frac{1}{A_1 A_2}\frac{\partial A_2}{\partial \alpha_1}\left(\frac{1}{A_1}\frac{\partial u_n}{\partial \alpha_1} - u_1 K_2^{(n)}\right) = \delta K_{21} \qquad (5)$$

$$\delta K_1^{(t)} = \frac{1}{A_1}\frac{\partial}{\partial \alpha_1}\left(\frac{1}{A_2}\frac{\partial u_n}{\partial \alpha_2} + u_2 K_1^{(n)}\right) - \frac{1}{A_1 A_2}\frac{\partial A_1}{\partial \alpha_2}\left(\frac{1}{A_1}\frac{\partial u_n}{\partial \alpha_1} - u_1 K_2^{(n)}\right) - K_2^{(n)}\left(\frac{1}{A_1}\frac{\partial u_2}{\partial \alpha_1} - \frac{u_1}{A_1 A_2}\frac{\partial A_1}{\partial \alpha_2}\right) = \delta K_{11}$$

$$\delta K_2^{(t)} = -\frac{1}{A_2}\frac{\partial}{\partial \alpha_2}\left(\frac{1}{A_1}\frac{\partial u_n}{\partial \alpha_1} - u_1 K_2^{(n)}\right) + \frac{1}{A_1 A_2}\frac{\partial A_2}{\partial \alpha_1}\left(\frac{1}{A_2}\frac{\partial u_n}{\partial \alpha_2} + u_2 K_1^{(n)}\right) + K_1^{(n)}\left(\frac{1}{A_2}\frac{\partial u_1}{\partial \alpha_2} - \frac{1}{A_1 A_2}\frac{\partial A_2}{\partial \alpha_1}\right) = \delta K_{22}$$

$$\overline{\overline{K}} = \bar{e}_i\, \delta \bar{K}_i = \delta K_{ij} \bar{e}_i \bar{e}_j \quad (i = 1,2)$$

This tensor will be used to derive the stress resultants for the middle surface of the shell (modified to include the case of plane stress $\sigma_{nn} = 0$). The expanded strain tensor $\overline{\overline{\epsilon}}(\bar{r})$ for points which are not in the middle surface will be used to establish the compatability equations for the shell, which are subsequently reduced to the middle surface compatability condition by setting $\alpha_n = 0$.

A - 4 Compatibility Equation

The SAINT - VENANT Compatibility Equation is

$$\frac{d}{d\bar{r}} \times \bar{\bar{\epsilon}}(\bar{r}) \times \frac{d}{d\bar{r}} = 0$$

which can formally be deduced using the symbolic equation for the strain tensor

$$\bar{\bar{\epsilon}}(\bar{r}) = \frac{1}{2}\left[\frac{d\bar{u}}{d\bar{r}} + \frac{\bar{u}\,d}{d\bar{r}}\right]$$

It can be shown that the strain tensor $\bar{\bar{\epsilon}}$ which satisfies the compatability equation is a necessary and sufficient condition for a continuous displacement field $\bar{u}(\bar{r})$. The strain tensor $\bar{\bar{\epsilon}}(\bar{r})$ is used in the above compatibility relation and α_n is set equal to zero, thus generating three distinct compatibility equations for the middle surface. The compatibile deformation of any other parallel surface at $\alpha_n \bar{e}_n$ is identically satisfied due to the nature of $\bar{u}(\bar{r})$. Only the third relation constituting the $\bar{e}_n \bar{e}_n$ component of the RIEMANN - CHRISTOFFEL Curvature Tensor will be employed here. The first two equations are used to simplify the expressions for transverse shear stress resultants $F_{1n}(\sigma)$, $F_{2n}(\sigma)$. The third compatibility equation will be used to deliver the second fundamental differential equation of the fourth order for thin shallow shells. This compatibility condition becomes

$$-K_1^{(n)}\delta K_2^{(n)} - K_2^{(n)}\delta K_1^{(n)} + \frac{1}{A_1A_2}\left\{\frac{\partial}{\partial\alpha_1}\frac{1}{A_1}\left[A_2\frac{\partial\epsilon_{22}}{\partial\alpha_1} + \frac{\partial A_2}{\partial\alpha_1}(\epsilon_{22}-\epsilon_{11}) - A_1\frac{\partial\epsilon_{12}}{\partial\alpha_2} - 2\frac{\partial A_1}{\partial\alpha_2}\epsilon_{12}\right]\right.$$

$$\left. + \frac{\partial}{\partial\alpha_2}\frac{1}{A_2}\left[A_1\frac{\partial\epsilon_{11}}{\partial\alpha_2} + \frac{\partial A_1}{\partial\alpha_2}(\epsilon_{11}-\epsilon_{22}) - A_2\frac{\partial\epsilon_{12}}{\partial\alpha_1} - 2\frac{\partial A_2}{\partial\alpha_1}\epsilon_{12}\right]\right\} = 0 \qquad (6)$$

A - 5 Simplified Theory For Thin Shallow Shells by DONNELL - MUSHTARI - VLASOV

In order to derive the two fundamental fourth order differential equations for thin shallow shells, the following assumptions are made:

(1) For shallow shells $K_2^{(n)} F_{1n}(\sigma), K_1^{(n)} F_{2n}(\sigma)$ are neglected in the first two force equilibrium equations 2(a), 2(b).

(2) $F_{12}(\sigma) \doteq F_{21}(\sigma)$, i.e. $\alpha_n K_1^{(n)} << 1$, $\alpha_n K_2^{(n)} << 1$

(3) u_1, u_2 are negligibly small compared to u_n, i.e. $\bar{u} = u_n \bar{e}_n$ in the expressions for variations in curvature and in torsion.

(4) Due to rapidly changing functions, it is assumed that lower order derivatives can be neglected in comparison with higher derivatives, i.e. $\frac{\partial^2 u_n}{\partial \alpha_i^2} >> \frac{\partial u_n}{\partial \alpha_i}$

These assumptions yield simplified expressions for the components of the curvature tensor $\bar{\bar{K}} = \bar{e}_i \bar{\delta} \kappa_i = \delta \kappa_{ij} \bar{e}_i \bar{e}_j$ of the middle surface

$$
\begin{aligned}
\delta K_2^{(n)} &\doteq -\frac{1}{A_1}\frac{\partial}{\partial \alpha_1}\left(\frac{1}{A_1}\frac{\partial u_n}{\partial \alpha_1}\right) - \frac{1}{A_1 A_2^2}\frac{\partial A_1}{\partial \alpha_2}\frac{\partial u_n}{\partial \alpha_2} = \delta K_{12} \\
\delta K_1^{(n)} &\doteq +\frac{1}{A_2}\frac{\partial}{\partial \alpha_2}\left(\frac{1}{A_2}\frac{\partial u_n}{\partial \alpha_2}\right) + \frac{1}{A_1^2 A_2}\frac{\partial A_2}{\partial \alpha_1}\frac{\partial u_n}{\partial \alpha_1} = \delta K_{21} \\
\delta K_1^{(t)} &\doteq \frac{1}{A_1}\frac{\partial}{\partial \alpha_1}\left(\frac{1}{A_2}\frac{\partial u_n}{\partial \alpha_2}\right) - \frac{1}{A_1^2 A_2}\frac{\partial A_1}{\partial \alpha_2}\frac{\partial u_n}{\partial \alpha_1} = \delta K_{11} \\
\delta K_2^{(t)} &\doteq -\frac{1}{A_2}\frac{\partial}{\partial \alpha_2}\left(\frac{1}{A_1}\frac{\partial u_n}{\partial \alpha_1}\right) + \frac{1}{A_2^2 A_1}\frac{\partial A_2}{\partial \alpha_1}\frac{\partial u_n}{\partial \alpha_2} = \delta K_{22}
\end{aligned}
\qquad (7)
$$

Introducing

$$
\delta K^{(9)} = \frac{\delta K_2^{(9)} - \delta K_1^{(9)}}{2}
$$

then

$$\bar{\bar{\epsilon}}^{(f)} = \begin{bmatrix} \alpha_n \delta\kappa_2^{(n)} \bar{e}_1\bar{e}_1 & + \alpha_n \delta\kappa^{(t)} \bar{e}_1\bar{e}_2 \\ + \alpha_n \delta\kappa^{(t)} \bar{e}_2\bar{e}_1 & - \alpha_n \delta\kappa_1^{(n)} \bar{e}_2\bar{e}_2 \end{bmatrix}$$

A-6 Formulation of Fundamental Differential Equation for Thin Shallow Shells

As in the theory of plates, the mixed method used to establish the two fundamental differential equations of thin shallow shell problems consists of replacing the stress resultants and stress couples in the equilibrium equation by their equivalent expressions in terms of displacement, supplemented by the third compatibility equation expressed in terms of stress resultants and stress couples. If the simplifications accruing out of the thinness and shallowness criteria of the shell are imposed, and VLASOV's Force Function $\bar{\Phi}$, which can express the direct stress resultants $F_{ij}(\sigma)$, $(i,j=1,2)$ and approximately satisfy the force equilibrium equations in the middle surface, is introduced, the fundamental differential equations can be established as functions of u_n and $\bar{\Phi}$.

(a) First Differential Equation

The first two moment equilibrium equations 4(a), 4(b) can be solved for the transverse shear stress resultants $F_{1n}(\sigma)$, $F_{2n}(\sigma)$, and substituting for the stress couples their equivalent expressions

in terms $\delta K_1^{(n)}$, $\delta K_2^{(n)}$, $\delta K^{(t)}$, and utilizing the first two compatibility equations in the expressions for terms involving $\delta K^{(t)}$, the resulting expressions for the transverse shear stress resultants become

$$F_{1n}(\sigma) = \frac{Eh^3}{12(1-\nu^2)}\left\{\frac{1}{A_1}\frac{\partial}{\partial\alpha_1}\left(\delta K_2^{(n)} - \delta K_1^{(n)}\right) - \frac{1-\nu}{A_1 A_2} K_2^{(n)}\left(-\frac{\partial}{\partial\alpha_1}(A_2\epsilon_{22}) + \frac{\partial A_2}{\partial\alpha_1}\epsilon_{11}\right)\right\}$$

$$F_{2n}(\sigma) = \frac{Eh^3}{12(1-\nu^2)}\left\{\frac{1}{A_2}\frac{\partial}{\partial\alpha_2}\left(\delta K_2^{(n)} - \delta K_1^{(n)}\right) + \frac{1-\nu}{A_1 A_2} K_1^{(n)}\left(\frac{\partial}{\partial\alpha_1}(A_1\epsilon_{11}) - \frac{\partial A_1}{\partial\alpha_2}\epsilon_{22}\right)\right\} \qquad (8)$$

Using the Directed Derivative in the surface

$$\frac{d}{d\bar{r}_o} \equiv \bar{e}_1\frac{1}{A_1}\frac{\partial}{\partial\alpha_1} + \bar{e}_2\frac{1}{A_2}\frac{\partial}{\partial\alpha_2}$$

it can be shown that

$$\delta K_2^{(n)} - \delta K_1^{(n)} = -\left(\frac{d}{d\bar{r}_o}\cdot\frac{d}{d\bar{r}_o}\right) \qquad (9)$$

Substituting (9) into (8), expanding the last expression of (8), and using assumption (4) of the simplified theory delivers

$$F_{1n}(\sigma) \doteq -\frac{Eh^3}{12(1-\nu^2)}\frac{1}{A_1}\frac{\partial}{\partial\alpha_1}\left(\frac{d}{d\bar{r}_o}\cdot\frac{d}{d\bar{r}_o}\right)u_n$$

$$F_{2n}(\sigma) \doteq -\frac{Eh^3}{12(1-\nu^2)}\frac{1}{A_2}\frac{\partial}{\partial\alpha_2}\left(\frac{d}{d\bar{r}_o}\cdot\frac{d}{d\bar{r}_o}\right)u_n \qquad (10)$$

If relations (10) are inserted in the Force Equilibrium Equation (2c) and $F_{1n}(\sigma)K_2^{(n)}$ and $F_{2n}(\sigma)K_1^{(n)}$ are neglected in (2a), (2b)

$$-F_{11}(\sigma)K_2^{(n)}+F_{22}(\sigma)K_1^{(n)}-\frac{Eh^3}{12(1-\nu^2)}\left\{\frac{\partial}{\partial\alpha_1}\left[\frac{A_2}{A_1}\frac{\partial}{\partial\alpha_1}\left(\frac{d}{d\bar{r}_0}\cdot\frac{d}{d\bar{r}_0}\right)u_n\right]\right.$$

$$\left.+\frac{\partial}{\partial\alpha_2}\left[\frac{A_1}{A_2}\frac{\partial}{\partial\alpha_2}\left(\frac{d}{d\bar{r}_0}\cdot\frac{d}{d\bar{r}_0}\right)u_n\right]\right\}+p_n=0 \qquad (11)$$

Equation (11) can be condensed to

$$-F_{11}(\sigma)K_2^{(n)}+F_{22}(\sigma)K_1^{(n)}-\frac{Eh^3}{12(1-\nu^2)}\left(\frac{d}{d\bar{r}_0}\cdot\frac{d}{d\bar{r}_0}\right)\left(\frac{d}{d\bar{r}_0}\cdot\frac{d}{d\bar{r}_0}\right)u_n+p_n=0 \qquad (12)$$

To solve the three Force Equilibrium equations, VLASOV introduced the force function Φ such that

$$F_{11}(\sigma)=-\frac{1}{A_2}\frac{\partial}{\partial\alpha_2}\left(\frac{1}{A_2}\frac{\partial\Phi}{\partial\alpha_2}\right)-\frac{1}{A_1A_2}\frac{\partial A_2}{\partial\alpha_1}\frac{1}{A_2}\frac{\partial\Phi}{\partial\alpha_1}$$

$$F_{22}(\sigma)=-\frac{1}{A_1}\frac{\partial}{\partial\alpha_1}\left(\frac{1}{A_1}\frac{\partial\Phi}{\partial\alpha_1}\right)-\frac{1}{A_1A_2}\frac{\partial A_1}{\partial\alpha_2}\frac{1}{A_2}\frac{\partial\Phi}{\partial\alpha_2} \qquad (13)$$

$$F_{12}(\sigma)=F_{21}(\sigma)=\frac{1}{A_1A_2}\left[\frac{\partial^2\Phi}{\partial\alpha_1\partial\alpha_2}-\frac{1}{A_2}\frac{\partial A_1}{\partial\alpha_2}\frac{\partial\Phi}{\partial\alpha_1}-\frac{1}{A_2}\frac{\partial A_2}{\partial\alpha_1}\frac{\partial\Phi}{\partial\alpha_2}\right]$$

It can be shown that the first two Force Equilibrium equations are

approximately satisfied by these functions, at least to the extent consistent with terms previously discarded as negligible; the third equation of equilibrium along the normal of the shell yields the differential equation

$$\frac{Eh^3}{12(1-\nu^2)}\left[\left(\frac{d}{d\bar{r}_o}\cdot\frac{d}{d\bar{r}_o}\right)\left(\frac{d}{d\bar{r}_o}\cdot\frac{d}{d\bar{r}_o}\right)u_n\right]-\frac{1}{A_1A_2}\left[\frac{\partial}{\partial\alpha_1}\left(-K_1^{(n)}\frac{A_2}{A_1}\frac{\partial(\dots)}{\partial\alpha_1}\right)+\frac{\partial}{\partial\alpha_2}\left(K_2^{(n)}\frac{A_1}{A_2}\frac{\partial(\dots)}{\partial\alpha_2}\right)\right]\bar{\Phi}=p_n$$

Setting

$$\nabla^2\equiv\frac{d}{d\bar{r}_o}\cdot\frac{d}{d\bar{r}_o}$$

$$\nabla^4\equiv\nabla^2\,\nabla^2$$

$$\nabla_K^{\,2}\equiv\frac{1}{A_1A_2}\left\{\frac{\partial}{\partial\alpha_1}\left[-K_1^{(n)}\frac{A_2}{A_1}\frac{\partial(\dots)}{\partial\alpha_1}\right]+\frac{\partial}{\partial\alpha_2}\left[K_2^{(n)}\frac{A_1}{A_2}\frac{\partial(\dots)}{\partial\alpha_2}\right]\right.$$

Thus the fundamental differential equation becomes

$$\frac{Eh^3}{12(1-\nu^2)}\nabla^4(u_n)-\nabla_K(\bar{\Phi})=p_n \qquad (14)$$

(b) Second Differential Equation

A second relation between the same functions was obtained by VLASOV from the third condition of compatibility (GOL'DENVEIZER in 1939). Here the variations of normal curvatures $\delta K_1^{(n)}$, $\delta K_2^{(n)}$ are expressed by

(7) and the middle surface strains ϵ_{11}, ϵ_{22}, ϵ_{12} are expressed in terms of the force function $\bar{\bar{\Phi}}$. Using the stress resultant tensor

$$\bar{\bar{F}}(\sigma) = \int_{-h/2}^{+h/2} \left(2\hat{\mu}\bar{\bar{\epsilon}} + \hat{\lambda}\epsilon_I \bar{\bar{1}}\right) d\alpha_n = \left(2\hat{\mu}\bar{\bar{\epsilon}} + \hat{\lambda}\epsilon_I \bar{\bar{1}}\right) h$$

the strain-stress relation can be established in the form

$$\bar{\bar{\epsilon}} = \frac{\bar{\bar{F}}(\sigma)}{2\hat{\mu}h} - \frac{\hat{\lambda}}{2\hat{\mu}h}\left(\bar{\bar{\epsilon}} : \bar{\bar{1}}\right)\bar{\bar{1}}$$

The first invariant of the Stress Resultant Tensor is

$$F_I(\sigma) = \bar{\bar{F}}(\sigma) : \bar{\bar{1}} = h(2\hat{\mu}+3\hat{\lambda})\epsilon_I$$

from which

$$\epsilon_I = \frac{F_I(\sigma)}{h(2\hat{\mu}+3\hat{\lambda})}$$

Hence

$$\bar{\bar{\epsilon}} = \frac{\bar{\bar{F}}(\sigma)}{2\hat{\mu}h} - \frac{\lambda F_I(\sigma)}{2\hat{\mu}h(2\hat{\mu}+3\hat{\lambda})}\bar{\bar{1}}$$

This relation can be simplified by substituting for

$$\hat{\lambda} = \frac{2\hat{\mu}\nu}{1-2\nu}$$

hence

$$\bar{\bar{\epsilon}} = \frac{1}{h}\left[\frac{1}{2\hat{\mu}}\bar{\bar{F}}(\sigma) - \frac{\nu}{E}\bar{\bar{F}}(\sigma) : \bar{\bar{1}}\right]$$

Consequently

$$\epsilon_{11} = \bar{e}_1\bar{e} : \bar{\bar{\epsilon}} = \frac{1}{Eh}\left(F_{11}(\sigma) - \nu F_{22}(\sigma)\right)$$

$$\epsilon_{22} = \bar{e}_2\bar{e}_2 : \bar{\bar{\epsilon}} = \frac{1}{Eh}\left(F_{22}(\sigma) - \nu F_{11}(\sigma)\right)$$

$$\epsilon_{12} = \bar{e}_1\bar{e}_2 : \bar{\bar{\epsilon}} = \frac{1+\nu}{Eh} F_{12}(\sigma)$$

Utilizing (6) and neglecting lower order derivatives of $\underline{\Phi}$ for thin shallow shells yields the second partial differential equation of fourth order

$$Eh\nabla_K^2(u_n) - \nabla^4(\underline{\Phi}) = 0 \qquad (17)$$

The two coupled partial differential equations (14) and (17) in u_n and $\underline{\Phi}$ are used in deriving the solution for shallow calotte shells in Chapter IV.

APPENDIX B

THE BACKWARD RECURRENCE METHOD FOR COMPUTING KELVIN FUNCTIONS $\underline{BER}_n(w)$, $\underline{BEI}_n(w)$

B - 1 This method is chiefly an outline and an extension of the paper by MICHELS in 1964, whose personal advice by correspondence is acknowledged.

For the BESSEL equation

$$\frac{d^2y}{dw^2} + \frac{1}{w}\frac{dy}{dw} - \left(i + \frac{n^2}{w^2}\right)y = 0$$

McLACHLAN gives the linearly independent solutions for integer orders of n

$$y = A J_n(wi^{3/2}) + B K_n(wi^{1/2})$$

The function $J_n(wi^{3/2})$ is of importance for disturbances from the external boundary of the shell and can be expressed by

$$J_n(z) = J_n(wi^{3/2}) = ber_n(w) + i\, bei_n(w)$$

It is well known that $J_n(z)$, with z complex, satisfies the recurrence relationship

$$F_{n+1}(z) + F_{n-1}(z) = \frac{2n}{z} F_n(z)$$

If the recurrence is started from $J_o(z)$, $J_1(z)$, good accuracy is obtained

for $n \leq |z|$. However for $n > |z|$, accuracy is lost very rapidly, since $J_n(z)$ decreases exponentially in this region (forward recurrence yields accurate results for $Y_n(z)$ as this function increases exponentially for $n > |z|$.

B - 2 Statement of MILLER's Method

A scheme was devised by J. C. P. MILLER whereby the recurrence formula could be used and accuracy still maintained throughout the entire range of n values. Imposing, at some n = m, the arbitrary conditions

$$F_{m+1}(z) = 0 \qquad (1)$$

$$F_m(z) = a \qquad (2)$$

where "a" is any constant, and using the recurrence formula for increasing values of $F_m(z)$ but with decreasing integers n, a series of functions $F_n(z)$, $F_{n-1}(z)$, ... $F_o(z)$ at some $n < m$ are generated from

$$F_{n-1}(z) = \frac{2n}{z} F_n(z) - F_{n+1}(z) \ ,$$

all of which constitute constant multiples of the regular BESSEL function, i.e.

$$F_n(z) = \alpha J_n(z)$$

This relation introduces a new unknown constant α whose evaluation is a central theme of this problem. BESSEL functions of complex argument

$$F_n(z) = F_n(w i^{3/2}) = F_n\left(-\frac{1}{\sqrt{2}} w + \frac{1}{\sqrt{2}} w\right) = F_n(x+iy)$$

where

$$z = w i^{3/2} = -\frac{1}{\sqrt{2}} w + \frac{1}{\sqrt{2}} w = x + iy$$

and

$$x = -\frac{w}{\sqrt{2}} \quad , \quad y = \frac{w}{\sqrt{2}}$$

produce a recurrence relation

$$F_{n-1}(z) = \frac{2n}{x+iy} F_n(z) - F_{n+1}(z)$$

$$= \frac{2n(x-iy)}{x^2+y^2} F_n(z) - F_{n+1}(z)$$

The recurrence procedure is started on the computer by imposing the initial conditions (1), (2) and is continued until $F_o(z)$ is reached. It was necessary to resolve the complex function $F_n(z)$ into its real $\Re F_n(z)$ and imaginary $\Im F_n(z)$ components and these had to be calculated individually as the complex FORTRAN Package was not available. In the functional calculations, the value of $a = 10^{-30}$ was used throughout.

B - 3 To calculate the complex constant $\alpha = \alpha_r + i\,\alpha_i$, the known expressions for $J_n(z)$ had to be used

$$J_o(w i^{3/2}) = ber_o(w) + i\, bei_o(w)$$

then

$$\alpha = \alpha_r + i\,\alpha_i = \frac{F_o(z)}{J_o(z)} = \frac{F_o(x+iy)}{J_o(w i^{3/2})} = \frac{\Re[F_o(z)] + i\Im[F_o(z)]}{ber_o(w) + i\, bei(w)}$$

where

$$F_o(z) = \mathcal{R}[F_o(z)] + i\,\mathcal{I}[F_o(z)]$$

$$\alpha = \alpha_r + i\,\alpha_i = \left\{\frac{\mathcal{R}[F_o(z)]\,ber_o(w) + \mathcal{I}[F_o(z)]\,bei_o(w)}{ber_o(w)^2 + bei_o^2(w)}\right\} + i\left\{\frac{\mathcal{I}[F_o(z)]\,ber_o(w) - \mathcal{R}[F_o(z)]\,bei_o(w)}{ber_o^2(w) + bei_o^2(w)}\right\}$$

consequently

$$\alpha_r = \frac{\mathcal{R}[F_o(z)]\,ber_o(w) + \mathcal{I}[F_o(z)]\,bei_o(w)}{ber_o^2(w) + bei_o^2(w)}$$

$$\alpha_i = \frac{\mathcal{I}[F_o(z)]\,ber_o(w) - \mathcal{R}[F_o(z)]\,bei_o(w)}{ber_o^2(w) + bei_o^2(w)}$$

These relations give the constant values of α_r, α_i for various arguments w. Using these values, the final expressions for $ber_n(w)$, $bei_n(w)$ can be found in terms of the computed $F_n(z)$ from

$$F_n(z) = \alpha\, J_n(z)$$

$$\mathcal{R}[F_n(z)] + i\,\mathcal{I}[F_n(z)] = (\alpha_r + i\,\alpha_i)\left[ber_n(z) + i\,bei_n(z)\right]$$

Hence

$$bei_n(z) = \frac{-\alpha_i^2\,\mathcal{R}[F_n(z)] + \alpha_r\,\mathcal{I}[F_n(z)]}{\alpha_r^2 + \alpha_i^2}$$

$$ber_n(z) = \frac{\mathcal{I}[F_n(z)]}{\alpha_i} - \frac{\alpha_r}{\alpha_i}\,bei_n(z)$$

For z complex, as in this case, MICHELS states that downward recurrence

can begin anywhere in the range of integers n as long as the condition

$$\left| \frac{F_m(z)}{F_n(z)} \right| < 10^{-5}$$

is met to give eight figure accuracy in $J_n(z)$. Values for $ber_n(10)$, $bei_n(10)$, $ber_n(1)$, $bei_n(1)$, were tabulated and it was found that the above criterion could be met to give reliable functions up to order 25 if the recurrence started at $F_{33}(z)$ for any arguments in the range $1 < w < 10$. As stated earlier, attempts to tabulate higher order functions $F_n(z)$ for small arguments caused floating point overflow.

This method was used to evaluate the functions $ber_n(w)$, $bei_n(w)$ required in the calculations of the sectional resultants of the shell. It was felt that these values were reliable and reasonable for the range of arguments $1 < w < 10$ and for integer orders up to 25.

BIBLIOGRAPHY

1924 Weatherburn, C. E.
"Advanced Vector Analysis", G.Bell and Sons Ltd., London.

1925 Webb, H. A.
"Strength of Materials" by John Case, Edward Arnold and Co., London.

1933 Donnell, L.
"Stability of Thin-Walled Tubes Under Torsion" N.A.C.A. Report No. 479.

1934 Tölke, F.
"Über Spannungszustände in dünnen Rechteckplatten". Ingenieur-Archiv, vol. 5, pp. 187

1935 Dischinger, F.
"Die Rotationsschalen mit Unsymmetrischen Form und Belastung", Der Bauingenieur, vol. 16, No. 35/36 pp. 374-381, No. 37/38, pp. 393-398.

1938 Mushtari, A. KH.
"Nekotorye obobscheniya teorii tonkikh obolochek", Izvestiya Fiziko - Matematicheskovo obschestva pri Kazanskom Universitete, vol. 11, series 8.

1939 Gol'denveizer, A. L.
"Dopol'neniya i Popravki k Teorii Tonkikh Obolochek Love", Plastinki i Obolochki, Gosstroiizdat, Moscow, pp. 85-105.

Marguerre, K.
"Zur Theorie der gekrümmten Platte grosser Formänderung", Proc. 5th International Congress of Applied Mechanics, Cambridge, Mass., 1938.

Pucher, A.
"Über die Spannungsfunktion beliebig gekrümmter dunner Schalen", Proc. 5th International Congress of Applied Mechanics, Cambridge, Mass., 1938.

1939 Tölke, F.
"Zur Integration der Differentialgleichungen der drehsymmetrisch belasteten Rotationsschale bei beliebiger Wandstärke", Ingenieur Archiv, vol. 9.

1941 Novozhilov, V. V.
"Teoriya Tonkikh Obolochek", Oborongiz, Moscow.

1944 Love, A. E. H.
"A Treatise on the Mathematical Theory of Elasticity", Dover, New York.

1949 Vlasov, V. Z.
"Obshchaya teoriya obolochek i ee prilozheniya v tekhnike," Gostekhizdat, Moscow, 1949, pp. 295.

1955 Csonka, P.
"Calotte Shell over Rectangular Base", Acta Technica Acad. Scien. Hung., vol. 11, No. 3/4, pp. 427.

McLachlan, N. W.
"Bessel Function For Engineers" Oxford at the Clarendon Press, Second Edition.

1957 Csonka, P.
"On Shells Curved in Two directions", Second Symposium on Concrete Shell Roof Construction, Oslo, July 1/3, Session 11, paper No. 5.

Dwight, H. B.
"Tables of Integrals and Other Mathematical Data", Third Edition, The MacMillan Co., New York.

Oravas, G. Æ.
"Stress and Strain in Thin Shallow Spherical Calotte Shells", International Association for Bridge and Structural Engineers, Zurich.

1959 Lowell, H.
"Tables of Bessel-Kelvin Functions ber, bei, ker, kei and their derivatives for Argument Range 0(0.01) 107.50", Technical Report R - 32, National Aeronautics and Space Administration, Washington, D.C.

1964 Michels, T. E.
"The Backward Recurrence Method for Computing the Regular Bessel Function, Technical Note D - 2141, National Aeronautics and Space Administration, Washington, D.C.

1964 Schroeder, J.
"Direct Kinematic Theory of Deformation", Unpublished Lectures, McMaster University.

Young, A. and Kirk, A.
"Bessel Functions Part IV Kelvin Functions", R.S.M.T.C., vol. 10. University Press, Cambridge.